

N70-20468  
NASA-CR-108919

Final Report

For

PASSIVE SOLAR ARRAY ORIENTATION SYSTEM  
(THERMAL HELIOTROPE)

CASE FILE  
COPY

(23 Dec 1968 - 23 Sept 1969)

Contract No. NAS 5-11637  
Goddard Space Flight Center  
Contracting Officer: P. Videneks  
Technical Monitor: John Fairbanks

Prepared by

D. R. Lott, Project Leader  
R. C. Byxbee, Principal Investigator  
Electrical Power Systems  
Space Systems Division  
Lockheed Missiles & Space Company  
A Group Division of Lockheed Aircraft Corporation  
Sunnyvale, California 94088

For

Goddard Space Flight Center  
Greenbelt, Maryland 20771

Final Report

For

PASSIVE SOLAR ARRAY ORIENTATION SYSTEM  
(THERMAL HELIOTROPE)

(23 Dec 1968 – 23 Sept 1969)

Contract No. NAS 5-11637  
Goddard Space Flight Center  
Contracting Officer: P. Videneks  
Technical Monitor: John Fairbanks

Prepared by

D. R. Lott, Project Leader  
R. C. Byxbee, Principal Investigator  
Electrical Power Systems  
Space Systems Division  
Lockheed Missiles & Space Company  
A Group Division of Lockheed Aircraft Corporation  
Sunnyvale, California 94088

For

Goddard Space Flight Center  
Greenbelt, Maryland 20771



## SUMMARY

### A. OBJECTIVE

Solar array tracking systems to date have been complex electromechanical assemblies. The objective of this program was to evaluate the feasibility of simple passive tracking concepts using bimetal elements. This evaluation included an examination of the requirements for such devices, the development of thermal heliotrope concepts for selected requirements, analysis and design implementation of these concepts, and fabrication and testing of models of the preferred designs.

### B. SCOPE OF WORK

The scope of work for this contractual effort has been to study array tracking requirements for common orbits and altitudes and to devise thermal heliotrope concepts applicable to the common orbits. Modes of sun-tracking were studied which included tracking axis, direction, unidirectional or bi-directional capabilities, reset vs continuous concepts, and the necessity of single or double axis rotation. Torque requirements were determined and tracking rates at typical various altitudes plotted. The torque and rates affect design of thermal heliotropes. A thermal and mechanical analysis was performed which identified factors affecting bimetal tracker performance. Among these factors were geometric parameters of coil size and shape, along with thermal coatings and shade configurations. The preliminary analysis led to several conceptual designs. Through an iterative process, these conceptual designs established a basis for construction of four working models. The models were tested in a simulated orbital environment to prove the concepts and study operating modes. Results of the study and test phases of this effort are reported in this document.



## C. CONCLUSIONS AND RECOMMENDATIONS

The analytical work described above resulted in the development of design parameters for sizing thermal heliotrope motor and sensor elements including equations for optimizing bimetal element performance and minimizing volume and weight. A simple computer program indicates the relative merit of applying various thermal coatings on the bimetals. Construction of operating model tracking devices and subsequent testing proved feasibility of the thermal heliotrope concepts. Although the specific models were not optimized for a given tracking situation, results of the tests illustrated the areas necessary for refinement and all models operated successfully. The following items summarize some of the conclusions drawn from this work.

### Conclusions – Earth Orbiting Applications

- Counter clockwise, unidirectional tracking will satisfy the majority of earth orbit tracking rotation requirements.
- Low orbit rates associated with earth orbiting applications result in very low array inertia torque requirements for thermal trackers. The predominate torque requirement is to overcome the friction of the bearing and power transfer systems used with a specific design.
- Single-axis tracking appears more compatible than full two-axis tracking for thermal heliotropes.

### Conclusions – Thermal Heliotrope Design

- Thermal torque capacity of a bimetal helix varies directly with temperature change, element width, and the square of the element thickness. Thermal response varies directly with element thickness, a thinner coil being more responsive.
- Coil thermal response can be optimized through the use of appropriate thermal coatings. Better cooling or resetting response occurs from the device being at a high equilibrium temperature, this resulting from use of coatings that have high absorptivity and low emissivity.
- A variety of both continuous and reset thermal heliotrope trackers are feasible, based on those designs evolved in this contract.
- Where high torque requirements exist, stored energy trackers and torque multiplier concepts are available.

### Recommendations

- Based on the progress achieved in this contract, additional investigations should be conducted to optimize thermal coatings.
- Pertinent data can be obtained by performing inertia simulation and life tests.
- The work accomplished on thermal heliotropes has demonstrated their feasibility. They should next be considered for earth orbit or lunar based experiments in flight configurations.



## CONTENTS

Section	Page
SUMMARY	iii
ILLUSTRATIONS	ix
I INTRODUCTION	1
A. ABSTRACT	1
B. NOMENCLATURE	2
II TECHNICAL DISCUSSION	5
A. TRACKING REQUIREMENTS	5
1. Direction	5
2. Rate vs. Orbit	7
3. Range-Reset and Continuous Tracking	8
4. Torque and Angular Impulse	10
B. BIMETAL THEORY AND MECHANISMS	14
1. Composition of Bimetals	14
2. Principles of Operation	16
3. Bimetal Work	21
4. Coil Formulas	25
5. Specific Bimetal Types	27
C. THERMAL ANALYSIS OF BIMETAL PROPERTIES	31
1. Operating Ranges	31
2. Thermal Response	31
3. Thermal Coatings	34
D. CONCEPTS AND HARDWARE	36
1. Concepts	36
2. Auxiliary Devices	60
3. Test Specimens	64
E. DEVICE TESTING	77
1. Preliminary Testing	77
2. Final Testing	84
3. Seasonal Adjuster	86
4. Planetary Shade Tracker	87
5. Two-Coil Continuous Tracker	88
III NEW TECHNOLOGY	91



Section		Page
IV	CONCLUSIONS AND RECOMMENDATIONS	93
	A. CONCLUSIONS	93
	1. Earth Orbiting Applications	93
	2. Thermal Heliotrope Design	93
	B. RECOMMENDATIONS	94
V	BIBLIOGRAPHY, REFERENCES, AND ACKNOWLEDGEMENTS	95
	A. REFERENCES	95
	B. ACKNOWLEDGEMENTS	96
Appendix		
A	THERMAL ANALYSIS	A-1
B	ROTATIONAL INERTIAL NOMENCLATURE	B-1
C	THERMAL HELIOTROPE DEVICES (Photographs)	C-1

## ILLUSTRATIONS

Figure		Page
1	Tracking Direction for Earth Orbiting Vehicles	7
2	Orbital Rate vs Altitude	8
3	Illumination Limit Angle	9
4	Inertial Torque Requirements	11
5	Components of Bimetal Elements	15
6	Bimetal Sandwich Stress Distribution	16
7	Variation of Maximum Curvature with Modulus of Elasticity and Thickness Ratios	18
8	Variation of Deflection Rate with Temperature for Bimetals and Component Alloys	19
9	Flexivity Envelopes for Bimetals	21
10	Variation of Volume with Proportion of Free Movement and Torque or Force	22
11	Bimetal Work as Related to Load and Deflection	23
12	Bimetal Element Configurations	25
13	Sensor Coil Torque Potential for $100^{\circ}\text{F } \Delta T$ (P675-R Bimetal Material)	28
14	Bimetal Flexivity	30
15	Transient Coil Response	33
16	Bimetal Tracking Devices	37
17	Reset Tracker Concept	39
18	Improvement in Array Effectivity as a Function of Seasonal Adjustment	42
19	Seasonal Adjuster Concept	42
20	Solar Panel Area Effectivity vs Tracking Increments	44
21	Detent Concept	45
22	Brake Detent Device	47
23	Locking Ratchet Detent Device	49
24	Modified Locking Ratchet Mechanism (Internal Pivot)	51

Figure		Page
25	Modified Locking Ratchet Mechanism (Internal Pivots)	51
26	Planetary Shade Tracker	52
27	Stored Energy Device	53
28	Bidirectional Two-Coil Tracking Device	56
29	Two-Coil Continuous Tracker	57
30	Continuous Tracker Concept Configuration	59
31	Auxiliary Devices	62
32	Torque Multiplying Concepts	63
33	Helical Bimetal Coils	65
34	Stored Energy Device Components	67
35	Stored Energy Ratchet Assembly	68
36	Stored Energy Device (Test Configuration)	69
37	Seasonal Adjuster During Fabrication	71
38	Seasonal Adjuster in Test Chamber	72
39	Planetary Shade Device (Test Model)	73
40	Two-Coil Continuous Tracker	75
41	Preliminary Test Setup	78
42	Preliminary Seasonal Adjuster Tests	80
43	Vacuum Chamber Simulated Altitude	81
44	Temperature Plot for Stored Energy Device	83
45	Stored Energy Device	85
46	Seasonal Adjuster	86
47	Planetary Shade	87
48	Coil Continuous	88
49	Test Facility	89

## SECTION I

### INTRODUCTION

#### A. ABSTRACT

This document reports the procedures and results of an investigation into electrically passive sun-tracking devices. It constitutes the final report of a nine-month study to evaluate the feasibility of thermally actuated sun-seeking systems. The Lockheed document number for this report is LMSC-A963802.

Increasing power levels and mission durations have added emphasis to the static vs. tracking solar trade-off. Considerable weight and cost savings are available with tracking solar arrays in that the array size may be reduced. A non-oriented array in a tri-form configuration, for example, must be on the order of 3.7 times the area of a tracking array. This suggests penalties on the order of 270 ft<sup>2</sup> of array area and well over half a million dollars for a 1-kw array.

Solar array tracking mechanisms of the electromechanical type have been developed and used on flight vehicles. Increase in array orbit effectivity (integrated projected area over an orbit) is dramatic; however, these sun-trackers have several drawbacks. First of all, conventional electromechanical trackers are parasitic on the vehicle power system, requiring power for standby, sensing, and motor drive functions. Secondly, the complexity and high-parts count associated with these devices are unattractive. Flight history shows a series of malfunctions in sensors, relays, limit switches and motor/geartrains. High-speed rotating masses sometimes used in these devices may also introduce attitude control problems. The advantages available with tracking systems have been discounted in part by disadvantages associated with questionable long-term reliability.



Providing tracking capability without use of electrical components, extensive gear-trains, or sensing systems is of practical consideration for nearly every photovoltaic power system now being flown or considered for future vehicles. Thermally-powered trackers have been investigated for such tracking devices. One approach uses the piston-gas principle for power with bimetal sensors (Ref 1). To avoid complex linkages and gas systems, the approach taken here is use of bimetal elements for both power and sensing functions (Ref 2). The thermal heliotrope uses solar energy to heat bimetallic elements, thus producing deflection and force. A bimetal in the form of a flat-wound helical coil produces rotational motion directly and is considered for the majority of thermal tracking devices. This contract is concerned with evaluating bimetal solar-powered sun-tracker concepts. The effort consists of the following five main tasks.

- Survey general tracking requirements such as rate and torque requirements
- Study thermal heliotrope operating mechanisms and develop concepts
- Analyze thermal properties and provide conceptual designs
- Fabricate and test models in simulated orbit environments
- Document findings and recommendations

These tasks have been completed and the results are presented in the following sections.

## B. NOMENCLATURE

### Symbols

M	total mass	m	elemental mass
A	area	k	constant
Q	heat	t	total thickness
E	modulus of elasticity	q	heat flux
H	angular momentum	r	radius of curvature
$\Delta T$	temperature change	v	linear velocity
I	moment of inertia	w	coil element width
L	coil active length	$\epsilon$	emittance
F	ASTM flexivity	$\alpha$	solar absorptance
a	component thickness	$\beta$	orbit plane - solar vector angle
c	heat capacity	$\lambda$	acceleration

$\delta$	coefficient of thermal expansion	$\omega$	angular velocity
$\sigma$	Stephan-Boltzmann Constant	$\tau$	time
$\rho$	density	$\beta$	orbit plane-sun angle

### Subscripts

p	projected	c	coil
t	total	s	sink
i	initial	h	high-expansion element
f	final	l	low-expansion element
o	axis of rotation		



## SECTION II TECHNICAL DISCUSSION

### A. TRACKING REQUIREMENTS

An initial investigation during the first quarter of the contract dealt with evaluation of general tracking requirements. This study focused on the four parameters of tracking direction, tracking rate as a function of orbit altitude, rotational range requirements related to tracker type, and typical torque requirements. The scope of the contract, consistent with its funding and duration, did not allow exhaustive analysis in the four specified areas. However, valuable basic requirements data were generated which aided in the development of tracker design concepts. These data also provide a basis for experiment or flight hardware programs using thermal heliotropes.

#### 1. Direction

The question was investigated as to whether or not bidirectional or unidirectional trackers will satisfy the general orbit-tracking cases. An investigation was also conducted to examine the impact of launch base location upon tracking direction, whether the tracking system was on a vehicle launched from the Western Test Range (WTR), Vandenberg Air Force Base, or from the Eastern Test Range (ETR), Cape Kennedy.

By nature of the geography of the launch locations, specific launch constraints are associated with WTR and ETR. WTR launches are down range in southerly direction resulting in polar or near-polar orbits. The majority of satellites launched from WTR are daytime launches; however, both day and night launches were considered in the tracking direction evaluation. A uniform retrograde orbit can be achieved with WTR launches; that is, the orbit plane maintains a constant angle with the solar vector. This type of orbit is achieved by injecting into a specific inclination as a function of altitude. The SERT II vehicle will be a uniform retrograde orbit of  $\beta = 90 \text{ deg} \pm 23.50$ ,



or what is commonly called a polar twilight orbit. This is a unique and optimum orbit case where no earth shadowing occurs. The orbit plane is always near normal (within the seasonal  $\pm 23.5$  deg) to the solar vector and no major advantages accrue for solar array tracking.

Some gain may occur in power output in this type of orbit with small bidirectional roll adjustments in the array position; however, the overall array effectivity is very good and a slight array oversizing compensates for seasonal solar vector off-angles. The more predominate polar uniform retrograde orbit case is similar to NIMBUS, a near-noon orbit with a small  $\beta$  angle with the solar vector. In this type of orbit, the solar array must track in the pitch axis to remain normal to the solar vector during the illuminated portion of the orbit.

With a daylight WTR launch, looking in on the +Y side of a three-axis stabilized earth-oriented vehicle with solar arrays tracking the sun about the pitch axis, relative rotation is counterclockwise, CCW. The vehicle moves downrange into a polar-type orbit. With a nighttime WTR launch, the vehicle has changed position so that the viewer is looking in on the (-Y) side of the vehicle. Relative rotation appears to be CW; however, as viewed from the opposite or initial index side (+Y), rotation is still CCW. ETR launches are in an easterly direction. Looking down on the vehicle in its forward easterly direction, one again views the (-Y) side with relative motion CW but CCW as viewed from the initial index side. It is, therefore, demonstrated that for earth-orbiting vehicles, whether in polar or equatorial orbit, a unidirectional tracking device will satisfy the major rotational requirements. This holds true for arrays in the Y-Y or pitch axis (Ref Fig. 1).

The fact of unidirectional CCW tracking greatly simplifies requirements for the tracking system design engineer. The continuous tracking models built and tested during the course of the contract, were based on unidirectional CCW tracking.

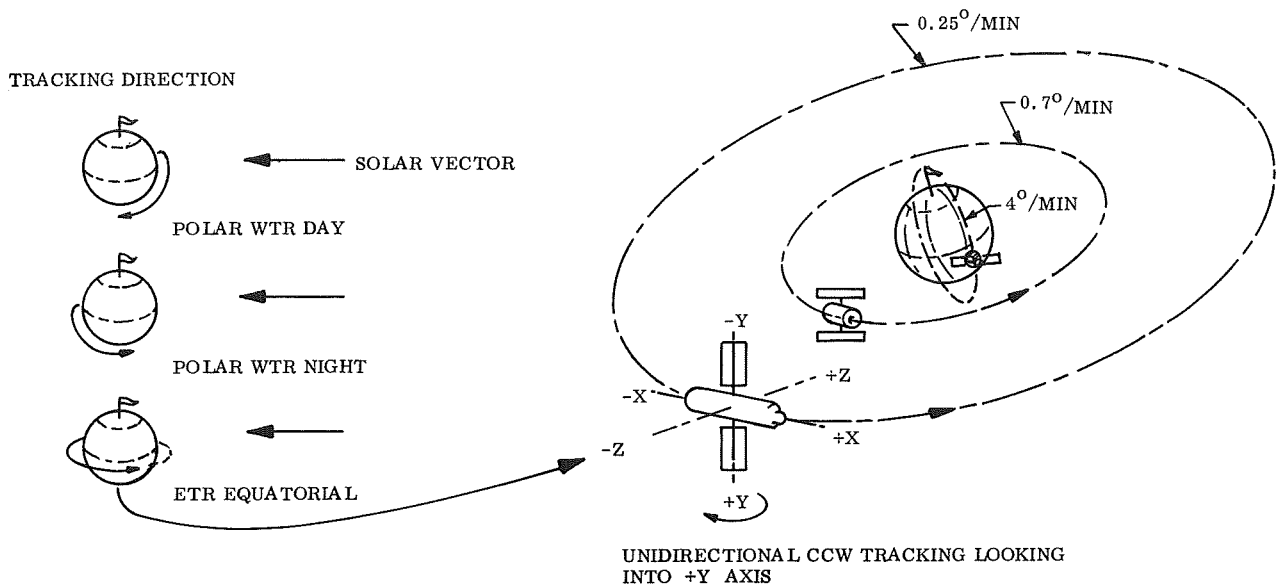


Fig. 1 Tracking Direction for Earth Orbiting Vehicles

## 2. Rate vs. Orbit

The orbital rate expressed in degrees per minute of required tracking rotation depends on the vehicle altitude. For earth-orbiting vehicles, the altitude range has varied predominately between 200 nm and synchronous. Correspondingly, the rotational rate is 4 deg/minute and .25 deg/minute respectively, with reference to the solar vector. Expressed in rotations per minute, 4 deg/minute is 0.011 rpm and .25 deg/minute is 0.000688 rpm.

Orbit rate vs. altitude is presented in Fig. 2 for 100 nm through synchronous, 19,323 nm.

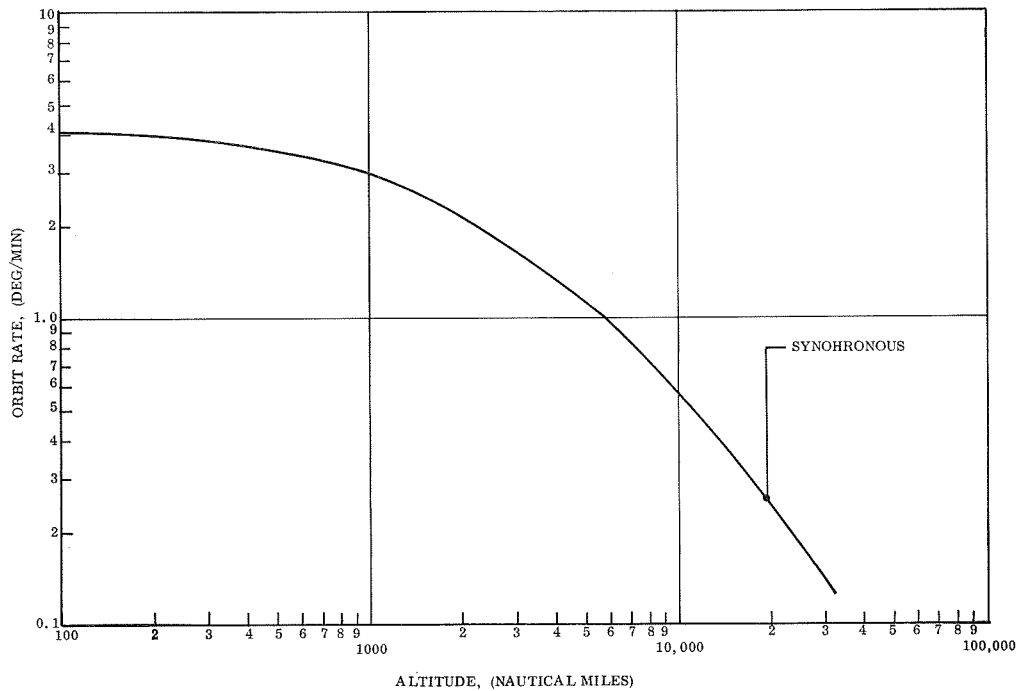


Fig. 2 Orbital Rate vs. Altitude

### 3. Range-Reset and Continuous Tracking

For a reset-type tracker, that is, a type which does not continuously commutate but counter rotates and resets once per orbit, the range or degree of tracking rotation would be a function of the sun-side duration. The sun-side duration is that portion of the orbit where the vehicle is illuminated, and this varies with altitude and the orbit plane angle with the solar vector. As an example, a vehicle at 400 nm that has a maximum  $\beta$  angle of 50 deg would benefit by tracking for the total illuminated portion of the orbit. The range is twice the illumination setback angle,  $2 \times 155$  deg or 270 deg (Ref Fig. 3). After tracking for the 270 deg, the reset tracker would have 90 deg of vehicle travel time to reset back to a fixed stop, ready for the next tracking cycle.

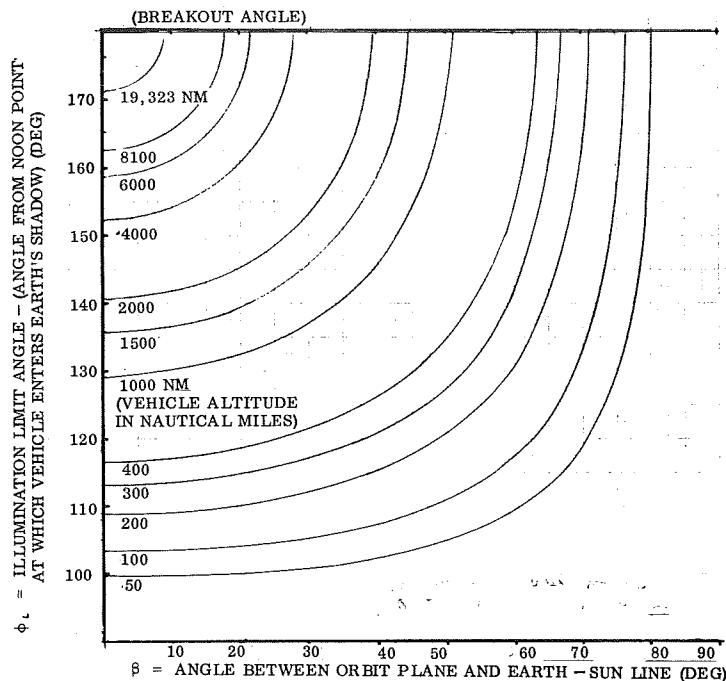


Fig. 3 Illumination Limit Angle

At synchronous altitude, using a reset tracker, it would be necessary to provide a supplementary vehicle shade which would perform the function of earth eclipse with  $\beta$  angles greater than about 8 deg. At higher  $\beta$  angles, there is less or no eclipsing; therefore, the tracker coil would not cool and reset. The vehicle shade would be sized to a maximum conservative time required to reset for the specific design. The method of power transfer for a reset-type tracker would be with the use of a flex harness. Lockheed's solar array electro-mechanical trackers have been mainly of the reset type, and the flex harnesses have functioned very satisfactorily.

For continuous thermal heliotrope trackers, it is obvious that the coil must reset in increments, thus allowing it to sequentially cool and track. There are various ways of implementing the necessary sequential incremental cooling, three of which are represented in the designs conceived and demonstrated during this contract. The selection of the range in degrees for tracking increment before coil reset is design dependent.


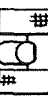
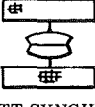


#### 4. Torque and Angular Impulse

The expression  $\Gamma = I\lambda$ , torque equals moment of inertia times angular acceleration, can be restated as  $\Gamma = I\left(\frac{\omega - \omega_0}{\tau}\right)$  in that angular acceleration  $\lambda$  can be expressed as the time rate of change of angular velocity ( $\omega$ ),  $\lambda = \frac{\omega - \omega_0}{\tau}$  where  $\omega$  is final velocity and  $\omega_0$  is initial velocity for a time of  $\tau$ . Assuming the rotational body, a solar array in this case is initially at rest,  $\omega_0$  drops out of the expression and  $\frac{\omega}{\tau}$  then becomes  $\frac{0.0011517}{\tau} \frac{\text{RAD}}{\text{sec}}$  where  $\omega$  in radians per second relates to the previously stated fastest tracking rate of 4 deg/min.

Assuming a maximum misalignment of 10 deg allowable for the array-tracking accuracy, 10 deg/4 deg min = 2.5 min could be allowed to make the alignment correction if the vehicle were not in motion while the correction was made. However, assigning an arbitrary 30 sec faster rate required to overcome the compensatory misalignment due to vehicle continuous travel, assume a maximum  $\tau$  is only 2 min or 120 sec. The initial torque expression would then be  $\Gamma = \frac{(0.0011517)}{120} = (I) (0.0000096)$ . It therefore becomes apparent that such low velocities, combined with long allowable misalignment correction times, introduce very low required values of alignment and tracking torque to overcome array inertia. The major concern then, in that required tracking torque is so low, is to minimize the friction of the bearing and power transfer techniques used in mechanizing various trackers. Actual tracking torque required to overcome the solar-array inertia is extremely small. The determining factor in torque requirements, then, is friction within the system. This is especially the case of continuous trackers which require some type of slip-ring rotary power transfer joint. Rotary-joint friction was computed for a test case to determine the order of magnitude of frictional torque. Consideration was given to a slip-ring unit with primary and capsule bearings. Bearing preloads determined frictional torque. Power brush area, number, and loading determined the drag for the slip-ring system. Signal-brush torque was also considered. The total frictional torque for a 6-power ring, 10-signal ring system applicable to a tracking solar array vehicle is about 16 in.-oz. (Ref 3). This value is well within the range of the thermal heliotrope devices considered.

The Inertial Torque Requirements Chart, Fig. 4, summarizes typical torque requirements associated with three different missions and array sizes. It also specifies estimated torque capability ranges for the tracker types developed during the contract.

CONFIGURATION	INERTIA (SLUG-FT <sup>2</sup> )	TRACKING RATE (°/MIN)	18° ORIENT TIME	REQ. TO ORIENT (IN.-OZ)	EXTERNAL TORQUE (IN.-OZ)	TOTAL TORQUE (IN.)
 200 WATT LOW ORBIT	0.29	4	180 SEC	0.00112	16	16
 600 WATT INTERMEDIATE	2.42	0.7	180 SEC	0.00925	45	45
 2000 WATT SYNCHRONOUS	31.3	0.25	180 SEC	0.1205	85	85

HELIOTROPE CAPABILITIES	TWO-COIL CONTINUOUS STORED ENERGY TRACKER RESET TRACKER	40-90 IN.-OZ 40-85 IN.-OZ 10-20 IN.-OZ
-------------------------	---	--

Fig. 4 Inertial Torque Requirements

A typical angular momentum requirement for a very accurately pointing synchronous vehicle is in the order of  $2.5 \times 10^{-3}$  ft-lb-sec. That is, the solar array tracking mechanism may impart a momentum impulse to the vehicle of this amount. Translated into oz-in. units, the value is 0.48 oz-in.-sec or about 0.5 oz-in.-sec. The total angular momentum of a body is given by (Ref 4):

$$H_o = \sum mR^2\omega + \sum mv_{oy}x - \sum mv_{ox}y \quad (1)$$

or

$$H_o = I_o\omega + \bar{x}mv_{oy} - \bar{y}mv_{ox} \quad (2)$$

The axis notation is explained in Appendix B. When the axis of rotation is fixed (pure rotation), this expression is reduced to

$$H_o = I_o \omega \quad (3)$$

The relation between the angular momentum of a body and the applied moments is obtained from the rotational equation of motion. The sum of the moments of all forces about o is

$$\sum M_o = I_o \lambda = I_o \frac{d\omega}{d\tau} \quad (4)$$

$$\sum M_o = \frac{d}{d\tau} (I_o \omega) \quad (5)$$

This means that the resultant moment about the fixed axis of pure rotation equals the time rate of change of angular momentum about the respective axis. This relation holds during the entire time of motion and may be integrated to give

$$\int M_o d\tau = I_o \omega - I_o \omega_o = I_o (\Delta \omega) \quad (6)$$

Thus, the total angular impulse equals the corresponding net change in angular momentum. A similar situation holds true for rotation about an axis through the center of mass so that

$$\text{impulse} = \bar{I} (\Delta \omega) (\text{ft-lb-sec}^2) \frac{\text{rad}}{\text{sec}} = \text{ft-lb-sec} \quad (7)$$

(where  $\bar{I}$  is the moment of inertia about the center of mass), or alternatively for constant  $\Gamma$  application,

$$\text{impulse} = \Gamma (\Delta t) \quad (8)$$

Conservation of momentum requires that when there are no externally applied moments on a system about a fixed axis (gas jets, etc.), the angular momentum of each part may change, but the total angular momentum of the system about this axis is conserved. Thus, every change in solar array momentum is transmitted to the vehicle and must be absorbed by the attitude control system. For the case in point, with a low allowable impulse input, the permissible change in angular rate (for constant  $I$ ) is very low. For example, a pair of  $10\text{-ft}^2$  solar panels at  $1.1\text{ lb/ft}^2$  have an  $I = 0.5\text{ slug-ft}^2$ . An allowable impulse of  $2.5 \times 10^{-3}\text{ ft-lb-sec}$  means that the maximum rotational speed from initial rest is about  $17.2\text{ deg/min}$ . This rate is more than adequate for tracking in the fastest possible orbit, but individual increments of incremental tracking devices may naturally occur at a higher rate. It may be seen then that incremental tracking devices may require governing to prevent excessive impulse input to the vehicle. This governing may be accomplished by means of a mechanical device or by limiting the torque capability of the tracker itself. However, it appears difficult to accurately control torque to such a low level while still having enough to compensate for friction which cannot be accurately predicted over the vehicle lifetime.

The preceding discussion has addressed itself to vehicles with extremely low impulse limitations. Many programs do not have such tight requirements, and incremental tracking is applicable. However, for those programs that do require non-incremental tracking motion, a two-coil continuous tracker has been devised and is discussed further in this report.



## B. BIMETAL THEORY AND MECHANISMS

### 1. Composition of Bimetals

The bonded material commonly used in thermostatic elements is known by several names: thermostatic metal, thermometal, thermostat bimetal, and bimetal. Bimetal is the most accepted term, although many of the subject elements are actually trimetals and some are quadrimetals. The ASTM definition of thermostat metal is: "A composite material, usually in the form of sheet or strip, comprising two or more materials of any appropriate nature, metallic or otherwise, which, by virtue of the differing expansivities of the components, tends to alter its curvature when its temperature is changed".

There is nothing new about bimetal itself, since the first patent for a brass-iron couple was awarded in 1831 (ref 5). The principal of operation was known long before and was suggested for temperature compensation in chronometers in 1766. The use of bimetals as work and torque producing devices, however, has not been exploited nearly as much as bimetal sensors. The thermal heliotrope incorporates both a sensing and work function from the same element.

A wide variety of bi- and trimetal elements are available from several domestic manufacturers. Among the producers are: Truflex (Metals and Controls Div. , Texas Instruments), WILCO (Engelhard Industries), and Chase Co. (Detroit, Mich.). Figure 5 shows a listing of some of the elements available from Texas Instruments, along with their component alloys. The elements themselves are manufactured by four main methods to form the multilayer sandwich.

- Puddle bonding consists of casting one alloy onto another heated but solid alloy.
- Hot roll bonding is a hot rolling mill operation, often at temperatures above 2000°F and moderate pressures. The material enters the mill in bar form with the edges welded to prevent contamination and separation. The actual bond is made on the first pass through the mill and improved on further passes.
- Pressure-temperature bonding is a similar operation except that the material enters the mill cold, and heat is generated by the high reduction. The bond is created in one pass and improved by a sintering operation.
- Press bonding is a high temperature and pressure static press bond.

TRUFLEX TYPE	HIGH SIDE		INTERMEDIATE		LOW SIDE	
	ALLOY	PER CENT BY THICKNESS	ALLOY	PER CENT BY THICKNESS	ALLOY	PER CENT BY THICKNESS
A1	A	55			10	45
AG1	AG	50			10	50
B1	B	50			10	50
B2	B	50			20	50
B3	B	50			30	50
B11	B	50			11	50
BN	B	50			N	50
B100R	B	28	N	44	10	28
B125R	B	34	N	32	10	34
B150R	B	36	N	28	10	36
B175R	B	39.5	N	21	10	39.5
B200R	B	42	N	16	10	42
B250R	B	44.5	N	11	10	44.5
B300R	B	47	N	6	10	47
B350R	B	48	N	4	10	48
B400R	B	49	N	2	10	49
C1	C	50			10	50
C3	C	50			30	50
C11	C	50			11	50
D560R	D	50			10	50
E1	E	50			10	50
E3	E	50			30	50
E4	E	50			40	50
E5	E	50			50	50
EN5	E	47.5	N	5	50	47.5
F1	F	63			10	37
F15R	F	5	F	80	10	15
F20R	F	5	F	60	10	35
F25R	F	10	F	50	10	40
F30R	B	20	F	40	10	40
F35R	B	24	F	36	10	40
F40R	B	29	F	31	10	40
F50R	B	25	F	25	10	50
F60R	B	32	F	18	10	50
F70R	B	34	F	16	10	50
F90R	B	38	F	12	10	50
F100R	B	40	F	10	10	50
G1	G	50			10	50
G3	G	50			30	50
G7	G	50			70	50
GA12	GA	50			12	50
GB-14	GB	50			14	50
H1	H	50			10	50
J1	J	55			10	45
J7	J	55			70	45
J8	J	55			80	45
K1	K	50			10	50
L1	L	50			10	50
M7	M	50			70	50
M8	M	50			80	50
MB18	B	47	†	†	10	47
N1	N	50			10	50
NF4	N	35	F	30	40	35
P3	P	54			30	46
P675R	P	55			10	45
P850R	P	80			10	20
PJ	P	50			J	50
R2	R	50			20	50
1513	15	50			13	50
7110	71	50			10	50

†Clad with 3% of Alloy M on HES and 3% of Alloy 80 on LES

#### ALLOY ANALYSIS

- A - 62 Cu, 38 Zn (Brass)
- AG - Pure Silver
- B - 22 Ni, 3 Cr, Bal Fe
- C - 19.4 Ni, 2.25 Cr 0.5C Bal Fe
- D - 14.65 Ni, 9.5 Mn, 5.1 Al, Bal Fe
- E - 25 Ni, 8.5 Cr, Bal Fe
- F - 98 Cu, 2 Ag
- G - 18 Ni, 11.5 Cr, Bal Fe
- GA - 18 Ni, 10 Cr, 3 Mo, Bal Fe
- GB - 19 Ni, 7 Cr, Bal Fe
- H - 14 Ni, 5 Mn, 0.5C Bal Fe
- J - 1.50 Si, 0.3 Mn, Bal Cu (Silicon Bronze)
- K - Armco Iron
- L - 25 Ni, 4 Mn, Bal Fe
- M - 18 Cr, 8 Ni, Bal Fe
- N - Pure Nickel
- P - 72 Mn, 18 Cu, 10 Ni
- R - 66.5 Ni, 1.5 Fe, 1.0 Mn 31 Cu (B Monel)
- 10 - 36 Ni, 64 Fe (Invar)
- 11 - 38.65 Ni, Bal Fe
- 12 - 31 Ni, 8 Cr, 8 Co, Bal Fe
- 13 - 32 Ni, 15 Co, 1 Mo, Bal Fe
- 14 - 38 Ni, 7 Cr, Bal Fe
- 15 - 32 Ni, 1 Co, 1 Mo, Bal Fe
- 20 - 40 Ni, Bal Fe
- 30 - 42 Ni, Bal Fe
- 40 - 45 Ni, Bal Fe
- 50 - 50 Ni, Bal Fe
- 70 - 17 Cr, Bal Fe (Type 430 stainless iron)
- 71 - 16.5 Cr, 4.5 Al, Bal Fe
- 80 - 57 Co, 9 Cr, Bal Fe

Courtesy of Metals and Controls, Inc., Division of Texas Instruments, Inc.

Fig. 5 Components of Bimetal Elements

## 2. Principles of Operation.

The principle of bimetallic deflection depends on a difference in thermal expansion coefficients between the components. For example, a basic bimetal couple is shown in Fig. 6a. The two elements are identical in size but the upper one has a coefficient of thermal expansion,  $\delta$ , larger than that of the bottom. An increase in temperature will cause both components to increase in length with the top trying to expand more than the bottom. The top component will be prevented from expanding to its free length and will be under a compressive stress developed at the bond line. Conversely, the bottom component will be stretched and will be under a tensile stress at the bond line. The two stresses are equal and uniform along the length of the components.

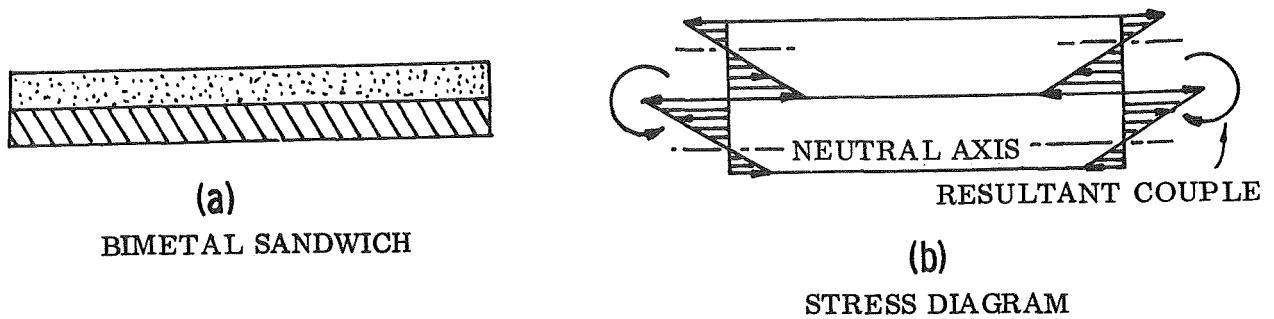


Fig. 6 Bimetal Sandwich Stress Distribution

The stress at the extreme fibers is half of the bond line stress and in the opposite direction (Fig. 6b). The high expansion component is in compression at the bond and in tension at the extreme fibers. The converse is true of the low expansion component. The neutral axis in thermal bending is one-third the distance from the extreme fiber to the bond line. The stresses may be replaced by a resultant torque at each end which tend to bend the couple into an arc of radius  $R$ . For equal component thicknesses and moduli of elasticity, the bond line stress is (Ref 5):

$$S = \frac{E}{2} (\delta_1 - \delta_2) \Delta T \quad (9)$$

Analysis on predicting bimetal deflection was performed by Timoshenko in 1925 (ref 6), who developed the basic deflection formula:

$$\frac{1}{R} = \frac{6 (\Delta\delta) (\Delta T) (1 + m)^2}{t \left[ 3 (1 + m)^2 + (1 + mn) \left( m^2 + \frac{1}{mn} \right) \right]} \quad (10)$$

where:

a = component thickness

t = total element thickness

$m = \frac{a_1}{a_2}$  = ratio of thickness

$n = \frac{E_1}{E_2}$  = ratio of moduli of elasticity

R = radius of curvature at bond line

$\Delta\delta$  = difference in component expansion coefficients

$\Delta T$  = temperature change

sub 1 = high expansion element

sub 2 = low expansion element

Timoshenko's basic formula was studied to find the optimum value of modulus of elasticity ratio for the two alloys. By setting all values in equation (10) to unity except n, the expression becomes:

$$\frac{1}{R} = \frac{24n}{(n^2 + 14n + 1)} \quad (11)$$

Differentiating  $\frac{1}{R}$  with respect to n gives a maximum value of curvature of 1.5. Dividing by 1.5 and multiplying by 100 gives the percent of maximum curvature as a function of n:

$$\% \text{ maximum curvature} = \frac{1600n}{n^2 + 14n + 1} \quad (12)$$

This expression is plotted in Figure 7a. The curve shows that for maximum deflection the modulus of elasticity ratio  $n$  should be unity; however, since the curve is relatively flat topped, deflection is not highly sensitive to small changes in  $n$ . In fact, even using  $E$  values of  $15 \times 10^6$  psi and  $30 \times 10^6$  psi degrades the maximum curvature only 3 percent.

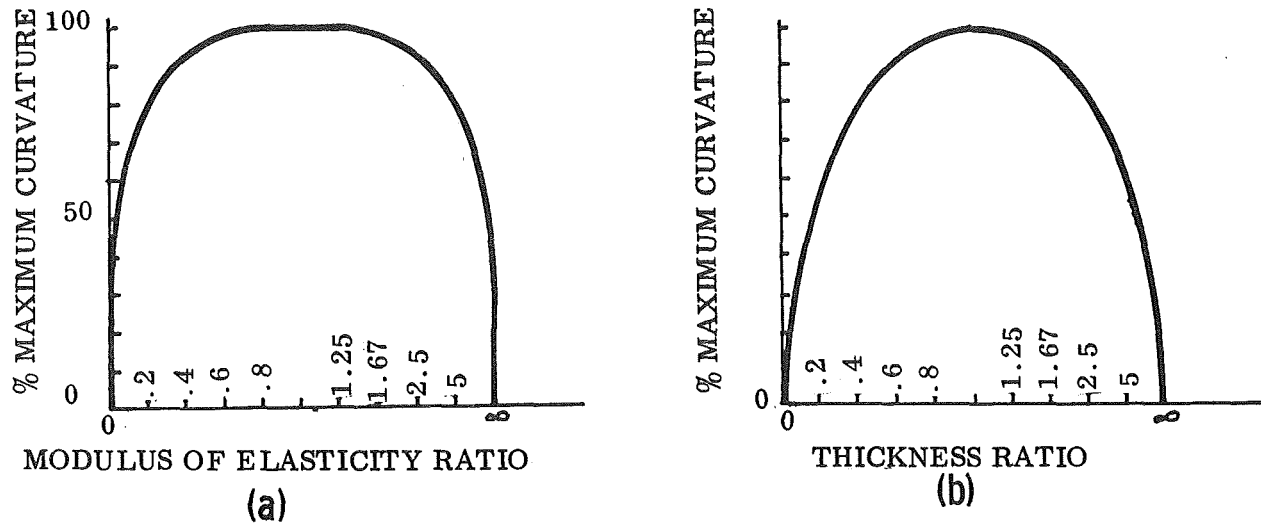


Fig. 7 Variation of Maximum Curvature with Modulus of Elasticity and Thickness Ratios

An optimum thickness ratio value,  $m$ , may also be determined in much the same way. All values in Timoshenko's basic formula (10) are set to unity except  $m$  yielding:

$$\frac{1}{R} = \frac{6m}{1 + m^2} \quad (13)$$

Manipulating as before,

$$\% \text{ maximum curvature} = \frac{400m}{(1 + m^2)} \quad (14)$$

This expression is plotted in Fig. 7b. Unlike the previous case, this curve has a relatively sharp peak at  $m = 1$  indicating the importance of accurate control of thickness ratios.

Again by manipulating (10) the relationship between  $n$  and  $m$  are obtained:

$$m = \sqrt{n} \quad (15)$$

or

$$\frac{a_1}{a_2} = \left( \frac{E_1}{E_2} \right)^{1/2} \quad (16)$$

Thus by varying thickness of the constituent alloys in proportion to the square roots of their moduli of elasticity, an optimum bimetal couple can be manufactured. The variation of thickness in commercial bimetals is illustrated in Fig. 5.

Timoshenko's basic formula assumes linearity of the difference in coefficients of expansion of the bimetal alloys. The so-called linear coefficient of expansion,  $\delta$ , is not actually linear over a broad temperature range. Figure 8 illustrates this point.

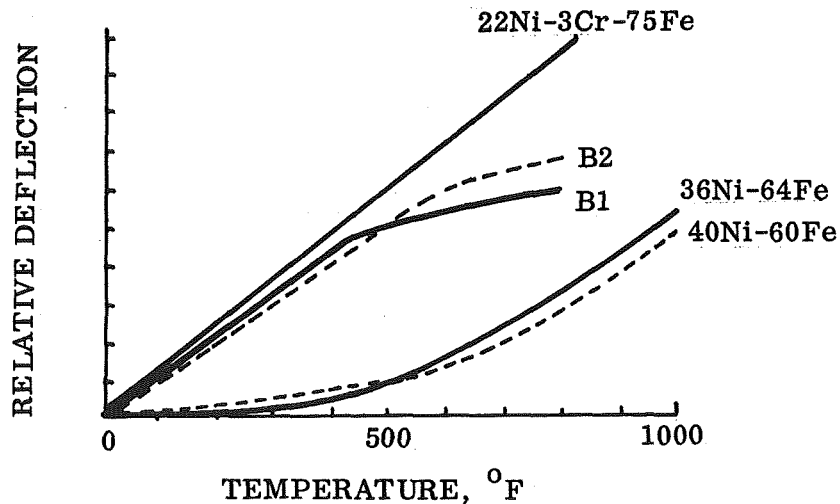


Fig. 8 Variation of Deflection Rate with Temperature for Bimetals and component alloys

The plot is arbitrarily taken from 0°F to show drop in bimetal deflection rate at increased temperatures. The 22 Ni-3 Cr-75 Fe alloy has essentially linear relative expansion in the temperature range shown; however, most alloys do not, as illustrated by the 36 Ni-64 Fe (Invar) curve. Bonding these two alloys together forms a bimetal

with deflection curve B1 that loses linearity at about 400°F. In nickel-iron alloys the temperature at which the inflection point occurs (point at which the expansion rate starts to increase) increases with alloys over about 36 Ni. Also, with higher Ni alloys, the low temperature expansion is greater. This phenomenon is shown by comparing the 36 Ni and 40 Ni alloy curves in Fig. 8. The result of these factors is a crossing of the curves, as shown. A similar crossing is evident when the alloys are bonded to a linear alloy, as shown by bimetal curves B1 and B2.

To allow for temperature induced variations in  $\delta$  and thus  $\Delta\delta$ , the ASTM term Flexivity,  $F$ , is used. It is defined as the "change in curvature of the longitudinal centerline of the specimen per unit temperature change for unit thickness" (Ref 7) or:

$$F = \frac{\frac{1}{R_1} - \frac{1}{R_2}}{T_2 - T_1} t \quad (17)$$

where the subscripts refer to initial and final temperatures.

Substituting definitions of  $\frac{1}{R}$  from Timoshenko gives

$$F = \frac{3 (\Delta\delta)}{2} \quad (18)$$

Bimetal manufacturers often supply plots of flexibility vs. temperature for any particular type of bimetal and use the flexivity term directly in their deflection formulas for specific shapes. These plots are determined empirically and apply to trimetal systems also. Figure 9 shows the envelope of flexivity curves for most bimetal elements.

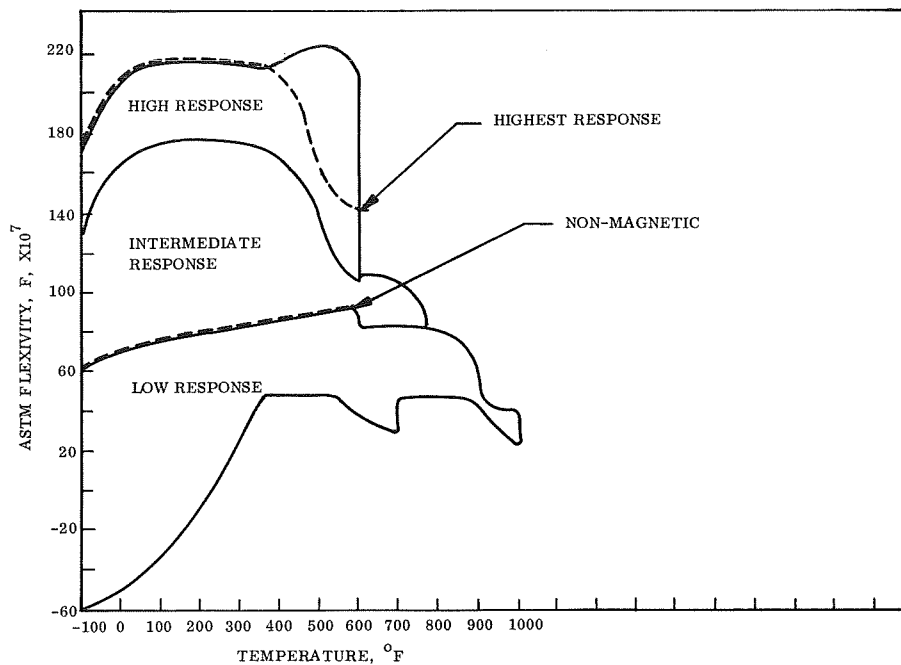


Fig. 9 Flexivity Envelopes for Bimetals

### 3. Bimetal Work

Bimetal suppliers recommend use of half the bimetal temperature change to produce deflection and half to produce force or torque. This insures a minimum volume bimetal element and hence minimum weight. Figure 10 shows the variation of element volume with deflection to force ratio. As in the case of the modulus of elasticity ratio previously discussed, the optimum ratio is on a relatively flat portion of the curve, making volume insensitive to small changes in ratio. It was also found that the weight of the actual bimetal element in a tracking system most often is a small part of the total system weight, so volume penalties are not of major consideration here. To give an indication of the order of magnitude of the weights we are discussing, a bimetal tracker element would rarely, if ever, weigh more than half a pound.



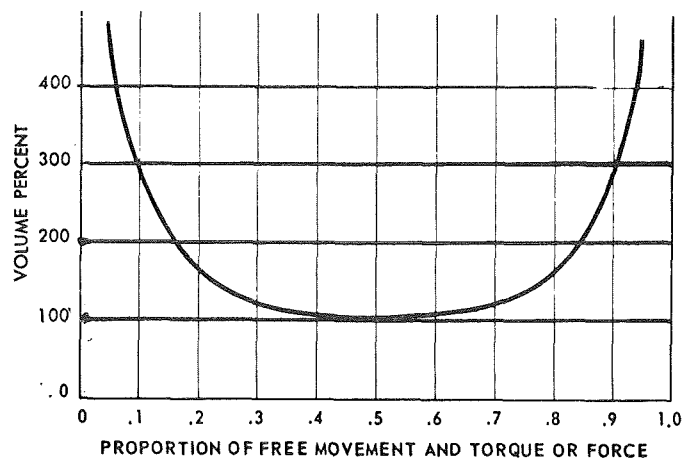


Fig. 10 Variation of Volume With Proportion of Free Movement and Torque or Force

Optimizing available work for bimetals is of some interest in tracking device design. Mechanisms consisting of slow or snap action elements can be compared for work producing capability. Work, of course, is force through a distance and a large value is desirable. Figure 11 is a plot of load vs deflection for bimetal elements in general. Three work cases exist related to this curve. If a bimetal develops a load and then displaces (overcoming a detent or snap device operation), the work path is OCE. Conversely, if an element deflects and then produces a force with no further movement, the path is OGE. A constant-rate spring load produces a work path of OF. The area under these paths is work, and it is evident that maximum ideal work is obtained by operating at a specific deflection point of 0.5 through a rectangular path. However, by combining the above cases, a larger work area is possible, as shown by path OHK. Here, force is restrained until a detent releases at H, at which point decreasing load of friction and inertia is carried to deflection point K. It can be seen that the work indicated under this path is higher than the so-called maximum work point.

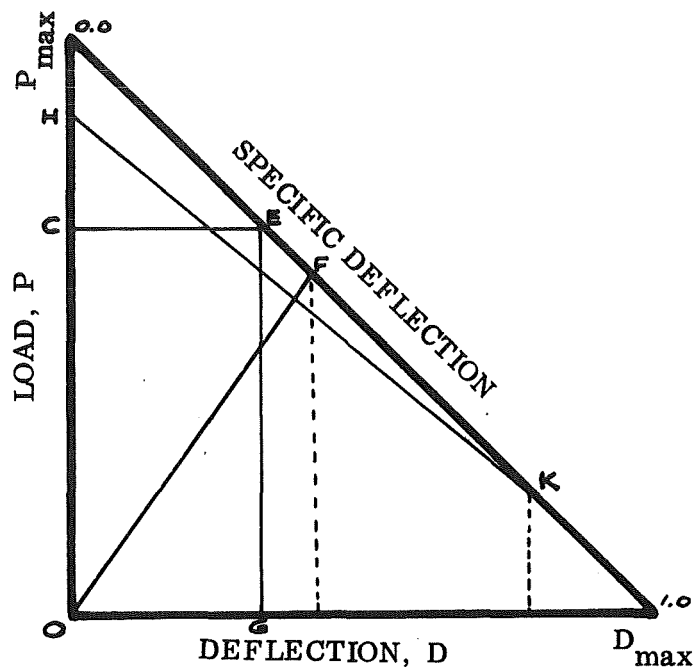


Fig. 11 Bimetal Work as Related to Load and Deflection

As delivered by the manufacturer, the bimetal element stock itself is optimized for maximum performance. The thickness ratio has been matched to modulus of elasticity ratio as previously described; however, to maximize performance of thermal heliotrope devices, tradeoffs are necessary between maximum available torque and thermal response (discussed in Thermal Analysis portion of this section). In many conventional bimetal applications the device is often designed first and the element configured to fit. This requires detailed tradeoffs to determine an element configuration that will best suit the performance requirements. In bimetal tracker design, however, the element is initially sized to satisfy torque and deflection requirements, and then the structure designed to fit the element. This greatly simplifies element selection.

For suntracking devices a high-work, rotary element is necessary. Also, maximum projected area is desirable, in that the device depends upon solar flux input for heating and radiation for cooling. It seems reasonable then, that a helical coil configuration be chosen for primary consideration on bimetal trackers. Alban (Ref 8) has shown that a coil configuration will produce approximately 54 percent more work than a

cantilever-mounted straight strip of the same volume. In addition, using a coil configuration negates the problem of converting linear to rotary motion. Adding to the effectiveness of helical coils is the fact that nearly all motion is confined to producing the desired rotating motion. For example, a rectangular cantilever-mounted strip will tend to deflect in all directions. The major curvature will occur about the width axis. Deflection about the length axis will tend to reduce the former curvature. Crimping the element will help restrain the length axis deflection and restore ideal curvature. A helical coil, however, naturally restrains the length axis deflection by means of its curved shape. Thus, no crimping is necessary to ensure maximum rotation.

Figure 12 indicates some of the available bimetal configurations supplied by manufacturers. Applied to tracking devices, the simple cantilever produces large deflections but little force. The linear motion must be converted to rotary, and available work is relatively low as explained above. Some thermal switches use simple beams of this configuration. The spiral shape is an improvement, providing rotary motion and a good packing factor, but projected area is very low. This type of actuator is often used in convective systems such as room and exhaust thermostats or automatic choke actuators. A double-wound helix is a linear device capable of large forces with small deflections. Here again, the linear motion must be converted into rotation through an additional mechanism. Snap acting disks or other snap devices are widely used as switches. The application to tracking devices is in the line of sensor elements or shade actuators and not as main drive units. The most applicable shape for tracker motor drive is the helix. Rotary motion is available with only small linear displacement. In addition a relatively large projected area and good work properties are helpful in tracker design.

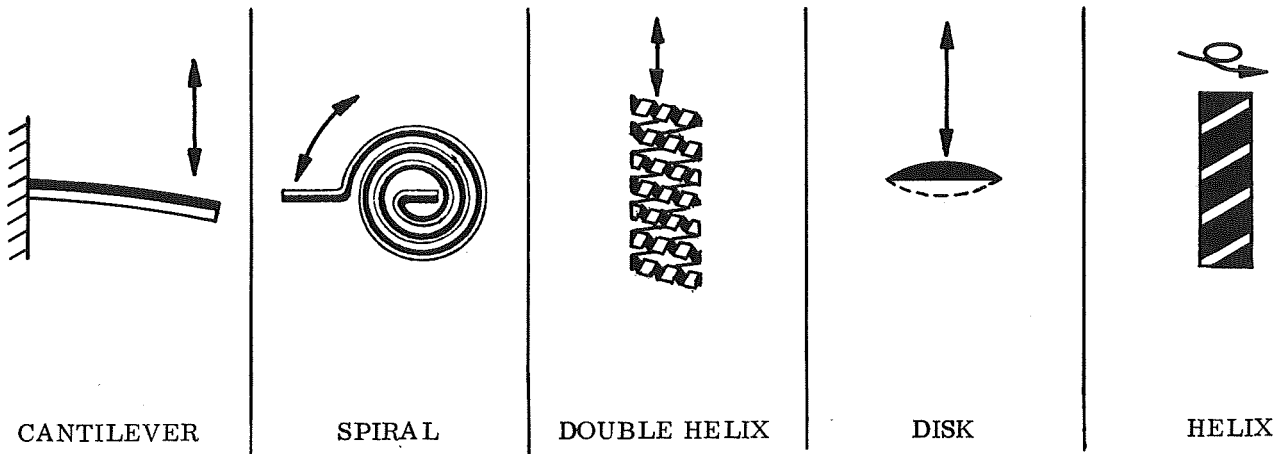


Fig. 12 Bimetal Element Configurations

#### 4. Coil Formulas

In that helical coils were selected for primary consideration on thermal sun-tracking devices, an analytical method of predicting coil performance is desirable. Bimetal manufacturers have developed empirical formulas for determining deflection and torque as functions of physical sizing and operating parameters. These formulas apply to all temperature ranges since the only temperature variable, flexivity, has a defined value for any given temperature.

$$\text{unrestrained thermal deflection} = A = \frac{67 F (\Delta T) L}{t} \quad (19)$$

$$\text{mechanical torque} = \Gamma = \frac{0.0232 EA wt^3}{L} \quad (20)$$

$$\text{thermal torque} = \Gamma = 1.55 EF (\Delta T) wt^2 \quad (21)$$

where

- A = rotation (degrees)
- F = ASTM flexivity
- $\Gamma$  = torque (in. -oz)
- E = equivalent modulus of elasticity (psi)
- $\Delta T$  = temperature change ( $^{\circ}F$ )
- w = stock width (in.)
- t = stock thickness (in.)
- L = stock length (in.)

In the thermal deflection formula, A is the angle of unrestrained rotation for a given coil subjected to  $\Delta T$ . The mechanical torque formula gives torque in in. -oz produced by rotating one end of a coil an angle of A. The thermal torque formula states the total torque available from a given coil subjected to  $\Delta T$ .

Tests on a simple helical element have confirmed the accuracy of the analytical formulas.

The value of E used in bimetal equations is an equivalent modulus of elasticity (Ref 5). The expression is:

$$E = \frac{4E_1}{t^3} \left[ (a_1 - C_1)^3 + C_1^3 + \frac{E_2}{E_1} \left\{ (a_1 + a_2 - C_1)^3 - (a_1 - C_1)^3 \right\} \right] \quad (22)$$

where

$$C_1 = \frac{E_1 a_1^2 + E_2 a_2 (2a_1 + a_2)}{2 (E_1 a_1 + E_2 t_2)} \quad (23)$$

and if

$$\frac{a_1}{a_2} = \left( \frac{E_2}{E_1} \right)^{1/2} \quad \text{for maximum deflection} \quad (16)$$

then

$$E = \frac{4E_1 a_1^3 + 4E_2 a_2^3}{t^3} \quad (24)$$

The constants in the coil equations contain the units required to balance the equations dimensionally so that torque is given in in.-oz, linear measurements in inches, and angular displacement in degrees arc. From (19, 20, 21),

$$\left\{ \frac{\text{restrained torque}}{\text{mass per degree of unrestrained deflection}} \right\} = (\text{constant}) \times (\Delta T) \quad (25)$$

For any given  $\Delta T$  (function of thermal coatings and shade elements), the restrained torque varies directly with the mass per degree of unrestrained deflection. However, it is desirable to have large values of torque and low values of mass. The related variable here is  $(\Delta T)$ , thus,  $\Delta T$  should be maximized in the design of helical elements. Note that this  $\Delta T$  is the maximum potential  $\Delta T$  from upper equilibrium temperature to lower temperature (a function of shade time and configuration). It is not the actual operating  $\Delta T$ , which is somewhat smaller.

Variation of restrained torque with mass is shown in Fig. 13. This figure is relevant for sensor-type elements where angular displacement is small. The relative mass is for a coil of unit length. It may be seen that for a given required torque several coil configurations are possible. For example, for a required sensor torque of 12.3 in.-oz coil choices include a 0.020-inch thick 0.5-inch wide element and a 0.015-inch thick element about 0.9-wide. The narrower element gives the lowest mass; however, thermal response considerations would probably dictate use of the thinner element. Since the total coil mass is relatively small, the thermal considerations predominate.

## 5. Specific Bimetal Types

Models fabricated on this contract incorporate a high activity bimetal sandwich. Truflex 675-R (trade name for Texas Instrument Inc. bimetal series) is the highest

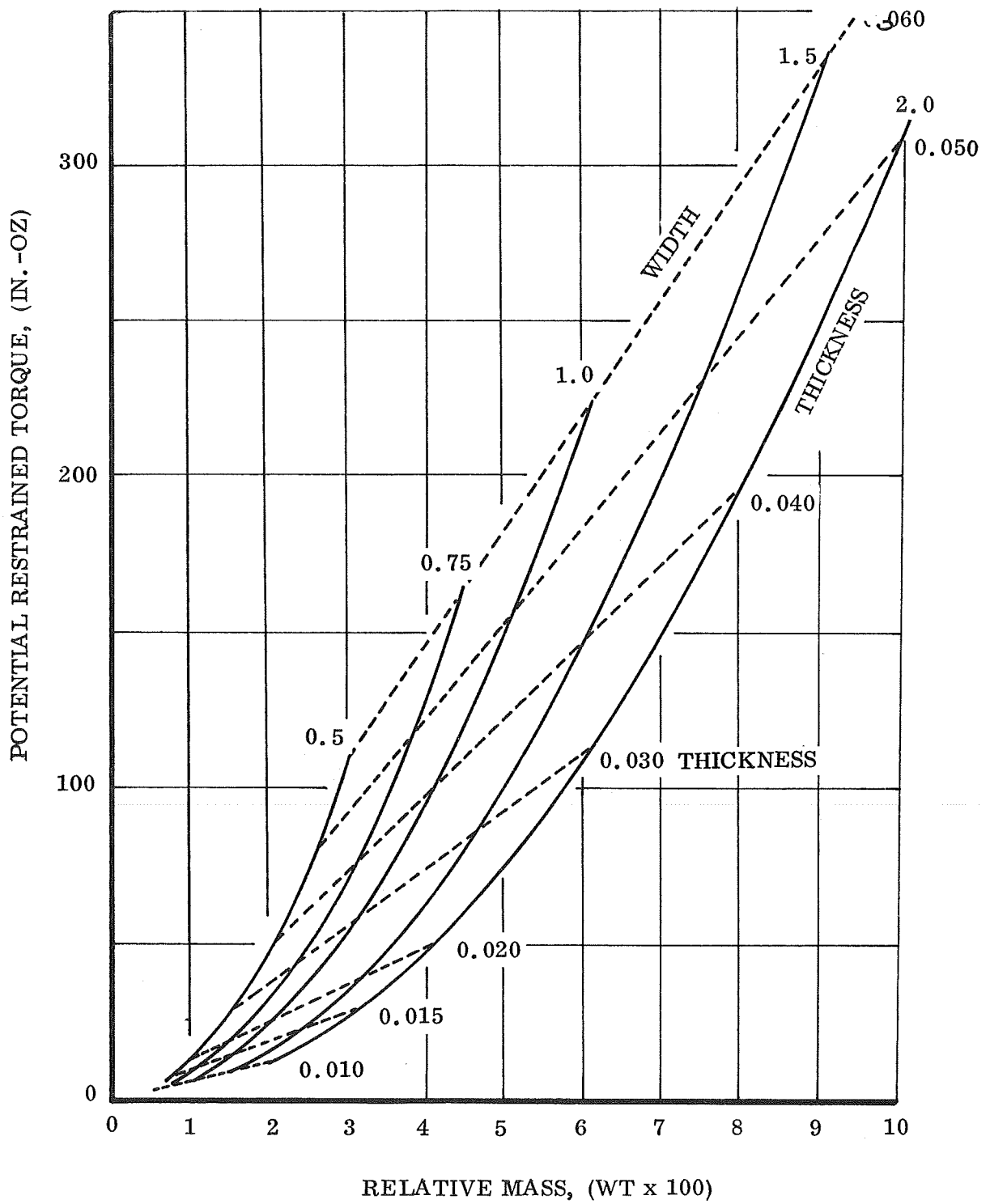


Fig. 13 Sensor Coil Torque Potential for 100°F  $\Delta T$  (P675-R Bimetal Material)

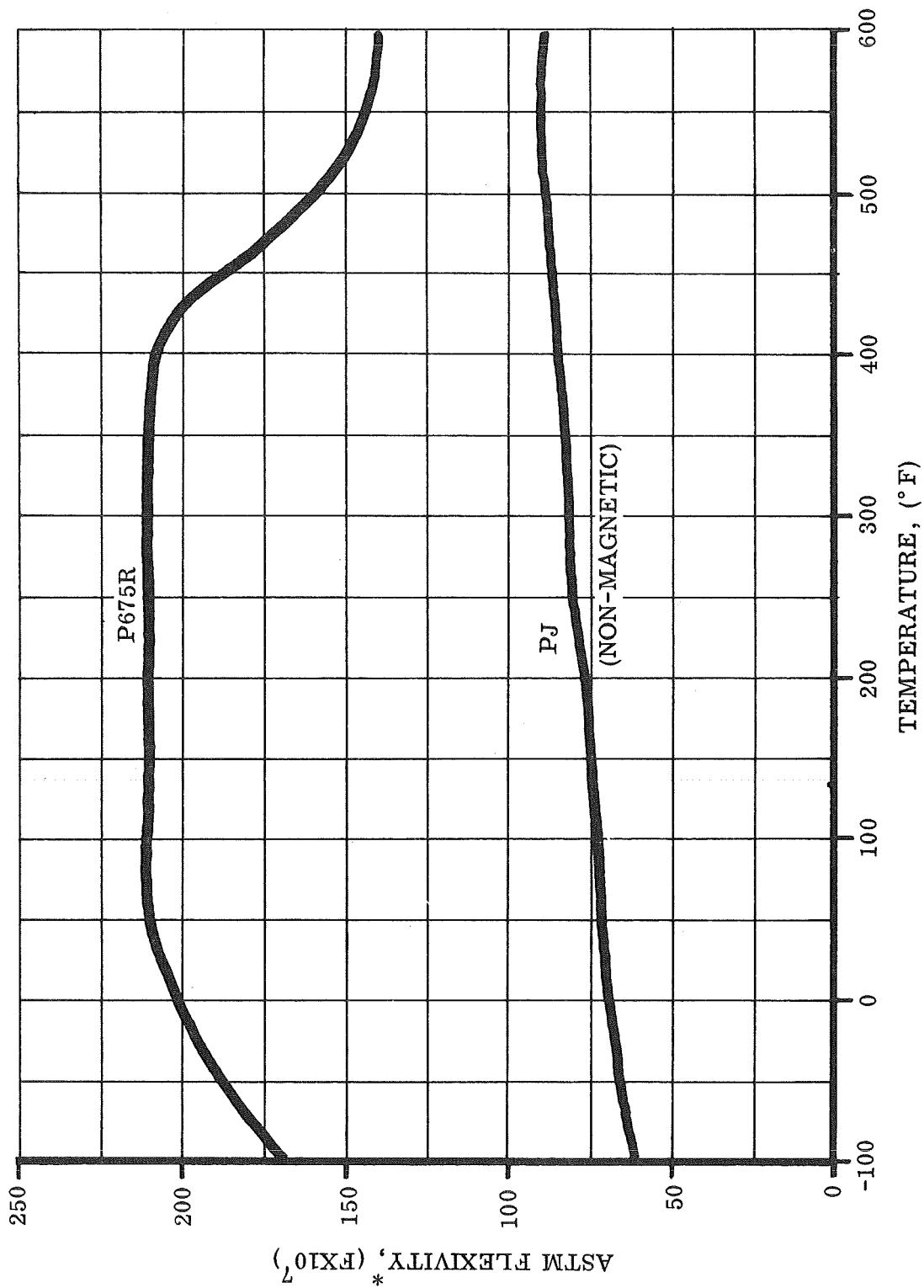
flexivity bimetal material available. It consists of two alloys; the high-expansion component, which makes up 55-percent of the total sandwich thickness, is 72 Mn-18 Cu-10 Ni. The other alloy is 36 Ni-64 Fe (Invar). The component thickness ratio is optimized to produce the maximum deflection possible according to the governing relation,

$$\frac{a_1}{a_2} = \left( \frac{E_2}{E_1} \right)^{1/2} \quad (16)$$

The equivalent modulus of elasticity (E) of this material is  $19.0 \times 10^6$  psi, and the density is 0.28 lb/in.<sup>3</sup> with an electrical resistivity of 675 ohms/cm at 75°F. The P675-R is the most active bimetal and is also the most economical. Figure 14 shows a plot of ASTM flexivity for the element. The method of test for flexivity of thermostat metals is given in the 1961 Book of ASTM Standards, Part 3 (B106). Maximum sensitivity temperature range is 0° to 400°F, with a useful deflection temperature range of -100° to 500°F. Thermal heliotrope devices operate well within these limits. The maximum recommended temperature is 600°F, but most uses are much below this value. Bimetal elements are very fatigue resistant, as witnessed by the heat riser valve in almost any automobile engine. In addition, low temperature liquid nitrogen dip tests were performed on a sample coil. Twenty cycles to LN temperature produced no damage or permanent deformation.

Figure 14 also shows a flexivity curve for PJ bimetal material. Although the flexivity is low, the material is essentially non-magnetic and fails to show any induced magnetism with magnetizing forces of up to 250 oersteds (Ref 9). Its component materials are 72 Mn-18 Cu-10 Ni for the high-expansion element and 1.5 Si-0.3 Mn-98.2 Cu (Silicon Bronze) for the low-expansion element. Equivalent modulus of elasticity is  $17 \times 10^6$  psi, which is the same as the component alloys, and density is 0.030 lb/in.<sup>3</sup>. The P675-R elements used on the conceptual models were given a 50-percent physical reduction in manufacture to obtain the desired spring properties. The range of Vickers hardness is 190-240 for the high-expansion component and 210-260 for the low-expansion element. Also, the material was chemically etched (designated LES etch by the manufacturer) to increase emissive properties and clean surface micropores of oils and impurities obtained in the manufacturing rolling operation.





\*ASTM STANDARDS, 1961, PART 3 (B106)

Fig. 14 Bimetal Flexivity

## C. THERMAL ANALYSIS OF BIMETAL PROPERTIES

### 1. Operating Ranges

The bimetal material used in thermal tracker design typically has a useful temperature range of  $-100^{\circ}\text{F}$  to  $+500^{\circ}\text{F}$  with a maximum temperature of  $+600^{\circ}\text{F}$ . As previously noted, samples of bimetal were arbitrarily subjected to  $500+^{\circ}\text{F}$  and  $\text{LN}_2$  dips in an attempt to reveal a failure mode for the material. No failures or degradation were uncovered. At very low temperatures, however, the coefficients of thermal expansion of the component alloys approach each other, becoming the same at zero absolute. Thus, flexibility is reduced at very low temperatures. It is desirable then to operate thermal tracking devices within a reasonable temperature range so that actual tracking work is accomplished in the  $-100^{\circ}\text{F}$  to  $+500^{\circ}\text{F}$  zone.

### 2. Thermal Response

Utilization of helical bimetal coils in sun-tracking systems involves radiative heating and cooling of the coil material to produce temperature changes necessary for tracking motions. It is desirable in most cases to have a relatively high thermal response coil, that is, one which will heat and cool quickly. To this end, an analysis of thermal performance was performed.

Thermal mass is directly proportional to stock thickness,  $t$ :

$$M = \text{coil mass} = wL\rho$$

$$A_t = \text{total area} = wL \text{ (one side)}$$

$$A_p = \text{projected area} = \frac{wL}{\pi} \text{ (coil configuration)}$$

$$\text{thermal mass} = \frac{Mc}{A_t} = \frac{wtL\rho c}{wL} = \rho c(t)$$

Thermal response of a helical coil element, then, is affected by only one sizing factor — thickness. Stock width, length, and winding diameter do not come into play here. It is desirable to maximize thermal response, thus a low thermal mass element is suggested. A compromise must be made, however, in that available torque is also affected by  $t$ . Thermal response varies as  $\frac{1}{t}$  and torque as  $t^2$ .

In addition to physical sizing, thermal response can be controlled by variations in thermal coatings. The most direct approach for obtaining a qualitative feel for the effect of thermal coatings on coil cooling response is through actual testing. Secondly, a simplified thermal model may be formed for analysis. By using the basic radiative and transient heat transfer formulas and making simplifying assumptions, a method of predicting coil response time was obtained. Previous non-contractural tests performed at LMSC on a reset type bimetal tracking device indicated that the simplified equations were sufficiently accurate to obtain reasonable values of angular temperature response, cooling rate, and torque. It was found that analytical substitution of the helical coil geometry by a cylinder of the same surface area provided a reasonable approximation of exposed surface areas. Additional assumptions of unity view factors and a zero sink were made in final analytical work, since the resulting calculations agreed closely with test data.

It was desired to obtain a basis for comparing thermal coatings so that bimetal coil response could be optimized. The result of such an analysis is a first-order determination of thermal coating effects. In this light, a short computer program was written to study the effect of surface thermal properties on idealized bimetal coil cooling response. The equations used and results are presented in Appendix A. Cooling times were printed out for a matrix of  $\alpha$  and  $\epsilon$  values. Values are calculated as a function of coil element thickness and temperature drop from the upper equilibrium temperature.

Figure 15 is a plot of cooling time versus desired temperature drop for various thermal properties. This particular plot is for a 0.020-inch thick coil but relates proportionally to a coil of any thickness. An important trend is identified with this data. Minimum cooling times are associated with choosing a low value of  $\epsilon$  and high value of  $\alpha$ . The high ratio of  $\frac{\alpha}{\epsilon}$  is not necessarily the direct criterion but rather the specific values themselves. One would normally associate rapid cooling with high  $\epsilon$  values, but this is not the case here. The high  $\alpha$  and low  $\epsilon$  in this case leads to a high equilibrium temperature, and the large difference between this initial temperature and the sink over shadows the low  $\epsilon$  effects.

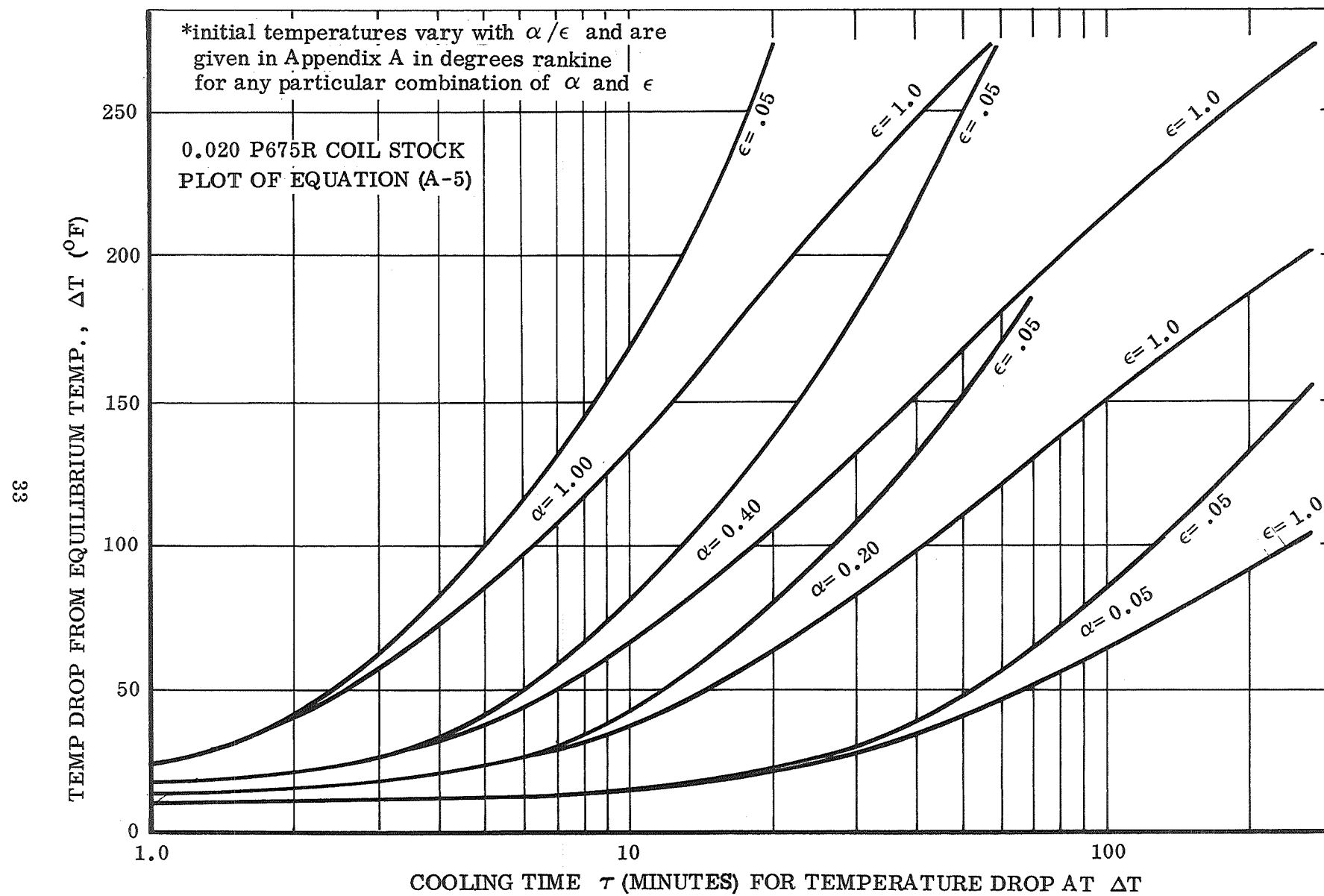


Fig. 15 Transient Coil Response

The identification of this trend is important in the design of devices in which the coil approaches its upper equilibrium temperature. A coil which provides work in a given temperature range (such as the stored energy device sensor coil), however, must be sized for its specific operating range. The fact still remains that the best cooling response for any coil is obtained by operating the unit at a high rather than a lower temperature. In addition, as previously mentioned, at very low temperature the coefficients of thermal expansion of the bimetal components approach the same value; hence, the flexivity is reduced. The reduced flexivity necessitates a greater temperature change for the same amount of work and hence longer heating and cooling times.

### 3. THERMAL COATINGS

A selective acidic oxidation of the bimetal components (a Lockheed-developed oxidation process) allowed formation of a thin oxide layer with predictable thermal properties. The layer is dark in appearance and controlled by a timed soak in the oxidizing medium, followed by immediate flush. Dip times of several minutes produced extremely durable surface layers. During the process, absorptance increases more rapidly than emittance; thus, by relating dip time to pre-tested sample properties, a given ratio may be obtained. Typical absorptance values obtained with this process were 0.88 to 0.93 with corresponding emittance values of 0.30 to 0.65. This coating treatment was used on both coils of the stored energy device. No degradation of surface properties was noticed before, during, or after preliminary testing. The metallic coating has the advantage of being thin and thermally conductive, thus preventing a significant thermal resistance between the element and environmental sink.

The seasonal adjuster coils were coated with 3M black velvet, number 161-C10. This coating has an absorptance approaching 0.95 and an emittance of over 0.90. It is applied over MIL-P-8585A zinc chromate primer and baked dry. The coating provides an upper equilibrium temperature of less than 100°F but is sufficient for seasonal adjustment devices. These coils were not treated with the LES etch (A Texas Instrument etch process), but no coating failure occurred. The slotted shade mechanism on the stored energy tracker was coated with a low-absorptance, high-emittance coating to provide cool surface temperatures, good temperatures, and good radiative

cooling of the sensor coil. White Thermatrol (2A-100) silicone paint was used which has typical absorptance and emittance values of 0.16 and 0.95, respectively. This is a flight-proven material which is highly resistant to ultra-violet, low-energy electron and thermal cycling degradation. It has an elastomeric surface, which is easily repaired in case of damage. The surface may pick up a slight electrostatic charge in ground handling, which is sufficient to attract dust particles; however, cleaning is easy with Freon TWD and distilled water. Freon TWD is a mixture of Freon TF (Dupont) and a Dupont detergent (TWD-602). The mixture will remove water soluble salts as well as oils.

## D. CONCEPTS AND HARDWARE

This section discusses the development of bimetal concepts in three main categories:

1. Concepts – Basic ideas and applications for trackers
2. Test Specimens – Units fabricated for test
3. Auxiliary Devices – Tracker Subassemblies

### 1. Concepts

During this program a wide variety of tracking device concepts were considered ranging from wild ideas to functional concepts. Figure 16 is a modified morphological chart of the main cases evaluated. The following discussion will refer mainly to this chart as an outline flow of events.

Study of the basic bimetal theory and available work suggested the use of the helical coil shape for primary application on sun tracking devices. The helix has the desired rotatory motion, efficient work generation, and large projected area necessary for a radiative thermal flow.

The tracking concepts were subdivided into two basic categories – continuous and reset. The continuous devices provide constant tracking capability with no array reset functions. This, of course, necessitates the use of a rotary power transfer joint such as slip rings or rotary transformers. The array is not directly attached to the bimetal coil but rather, it is attached through a ratchet interface which allows coil reset without resetting the entire array. The reset devices, on the other hand, rely on a flexible harness for power transfer from the solar array to the vehicle. The array then, must reset 360 deg for every 360 deg of tracking or once per orbit revolution. It should be noted here that array reset is not the same as coil reset. The bimetal cannot provide continuous rotation since it does not have an infinite temperature increase. The coil must heat and cool in cycles transferring motion through a ratchet device in order to provide unidirectional motion. The cooling mode of the bimetal coil is called coil reset.

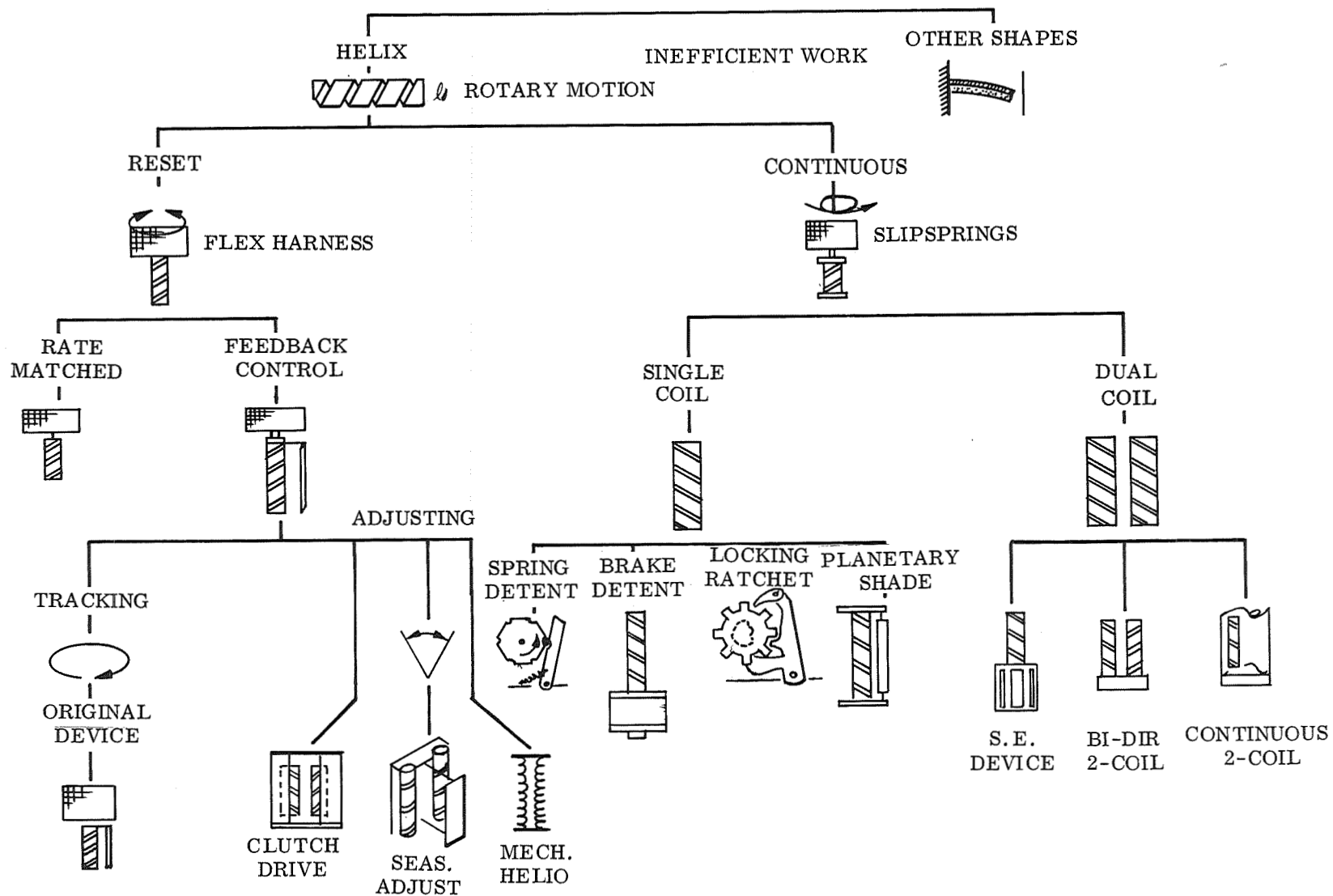


Fig. 16 Bimetal Tracking Devices



Continuous ( $360^\circ$  +) tracking units are further subdivided into single and multiple coil devices. Typically, single coil devices must compromise available tracking torque for coil thermal response. Multiple coils provide for distributing coil work over more coil area or separating motor (torque) and sensing functions entirely. Several reset and continuous concepts were analyzed and are outlined below.

a. Reset Concepts - Trackers. Reset type devices typically would use a flexible power transfer harness

- A Rate Matched device could in theory be built to handle a pitch tracking solar array on an orbiting vehicle. The coil would be mounted to the array on one end and the vehicle on the other. The thermal mass of the coil would have to be large so that direct solar heat would provide a rotation rate to exactly match the orbital rate. This becomes an impossible task in that the required coil would reset too slowly for any practical application. It is obvious that some type of feedback system is necessary so that the coil will actively track the sun. This feedback control is part of every thermal tracker, whether the device is used for orbit seasonal adjustments or actual pitch axis tracking.

- The Feedback Reset Tracker, about which all other thermal heliotropes evolved, is the simplest device available for sun tracking. This device is especially applicable to low earth orbits in which the vehicle is shaded for a period once per orbit. The device consists basically of a bimetal element and a feedback shade system. The bimetal element is fixed to the vehicle at one end and attached to the solar array at the other. Upon solar illumination, the coil temperature increases, and a torque and rotation is induced. The free end of the coil, and hence the solar array, then turns.

The bimetal coil is sized to produce more than the required angle of turn for available temperature rise. It is evident then that rate control is necessary. This is provided by throttling the amount of solar flux reaching the coil. A small shade, attached to the solar array, provides a feedback shade. An example of the feedback principle operation is presented as follows:

In Fig. 17 the vehicle is about to enter the illuminated portion of the orbit after being eclipsed by the earth. The array is resting against a mechanical stop. As the array first enters the illuminated portion of orbit, the coil is fully exposed to solar heating (Fig. 17b). A temperature rise in the coil causes the array to rotate counter-clockwise.

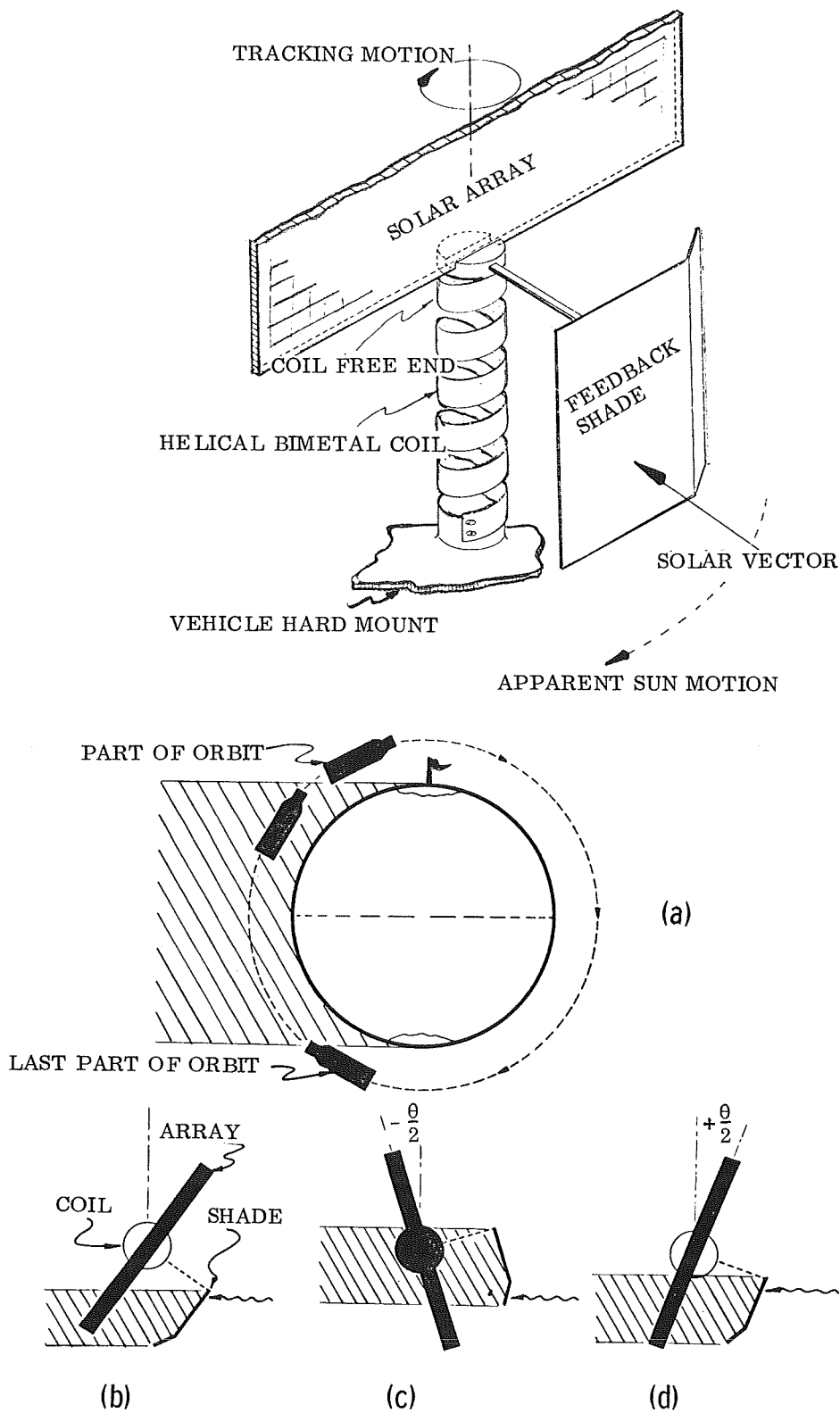


Fig. 17 Reset Tracker Concept

The array will continue to turn until the feedback shade covers most of the coil, as in Fig. 17c. At this point the array is misoriented by  $\theta/2$ <sup>1</sup>. The shade then functions throughout the illuminated portion of orbit, limiting rotation to that needed to orient the array. The "over turning" tendency built into the coil sizing for the available temperature rise is controlled by the shading function of the feedback shade. At the end of the illuminated portion of the orbit, the coil has rotated 200 or more degrees of arc and is approaching its maximum temperature. The feedback shade is positioned as shown in Fig. 17d, and the array is misoriented by  $+\theta/2$ .

At this point the vehicle enters the earth's shadow, and reset begins. The coil cools by radiation to the environment, and the entire array rests to a mechanical stop. Further coil cooling builds up a small torque restrained by the stop. The array is then ready to repeat the tracking cycle upon entering the illuminated portion of the orbit.

If the orbit is such that a sufficient earth shade period does not occur once per orbit, an auxiliary mechanical shading device may be used to provide a coil-shade reset period.

b. Reset Concepts – Adjusters. Besides pure pitch axis tracking, the reset or flex harness family of concepts may be applied to adjusting devices, that is, trackers which provide bidirectional orientation capability within given limits. These devices provide tracking in the roll axis of the vehicle and must often be capable of bidirectional tracking in the range of  $\pm 60$  deg. In many low-altitude, earth-orbiting missions it is not feasible to use a continuously tracking array because of propulsion weight penalties associated with drag makeup. In these cases the arrays are deployed in the pitch-roll plane so that the array leading edges present a minimum frontal profile to the line of flight. Small incremental changes in the array position about the roll axis of the vehicle, alpha angle adjustments, can dramatically improve array output by repositioning the array. Figure 18 illustrates the results of a study to determine the necessity of these seasonal adjustments. This particular study was for a low orbit case of about 150 nm. The effectivity curves will shift upward with increasing altitude.

<sup>1</sup>  $\theta$  is the angle of array rotation between fully shaded and fully illuminated coil modes and is a function of shade configuration:

$$\theta = \arctan \left( \frac{\text{bimetal coil diameter}}{\text{distance from shade to coil}} \right)$$

Maximum array misorientation is  $\theta/2$ .

- The Clutch Drive Adjuster was the first concept explored in this realm. This idea was first considered by LMSC in earlier inhouse work but not developed. It was found that friction or magnetic clutching of drive components was needlessly complex.
- The Seasonal Adjuster was an offshoot of the previous concept. A conceptual sketch of the seasonal adjuster is shown in Fig. 19. Solar flux passing on either side of the adjustment shade activates one of the adjustment helices, and position correction takes place. This adjustment would occur as the vehicle passes through the ecliptic plane at a frequency dependent upon the daily progression or retrogression in the orbit plane angle and the position of the operational range shade. Rotation or adjustment of the array is effected by illumination of a CW or CCW coil causing it to expand, walk an engagement gear into a fixed sun gear, and rotate the drive assembly and the array. As the coil cools, it counter-rotates and moves the engagement gear away from the sun gear. Thus, the non-working or non-illuminated coil is always disengaged except when it has a specific correction function to perform. When the assembly is properly oriented, both coils are at rest and disengaged. This type of tracker could be applied to a synchronous equatorial array to adjust the array within the  $\pm 23.5^\circ$  seasonal change from winter solstice to summer solstice. This would keep the array in the more optimum equinox position.

There are also a variety of lunar orbiting and lunar surface solar photovoltaic power applications where a bidirectional incremental adjustment tracker of the Seasonal Adjuster type could be used to great advantage. The inherent simplicity, reliability, and almost unlimited life would make the device ideal for remote unattended lunar surface photovoltaic power systems. This device was chosen for evaluation through fabrication and testing of a model.

- The Mechanical Heliotrope was the last adjusting concept explored. This concept was an effort to synthesize the common sunflower. An elementary desk top demonstration was performed using three strings of bimetals arranged in a triangle. The strings consisted of bimetal strips in semi-circular sections fastened in series with the low expansion element concave and pointed radially outward. A shade at the top of the device simulated the face of the "sunflower" or solar array active area. Tests with a sun gun showed that the upper face did indeed follow the incoming source of illumination. This device would have limited use for orbiting vehicles, but possible application

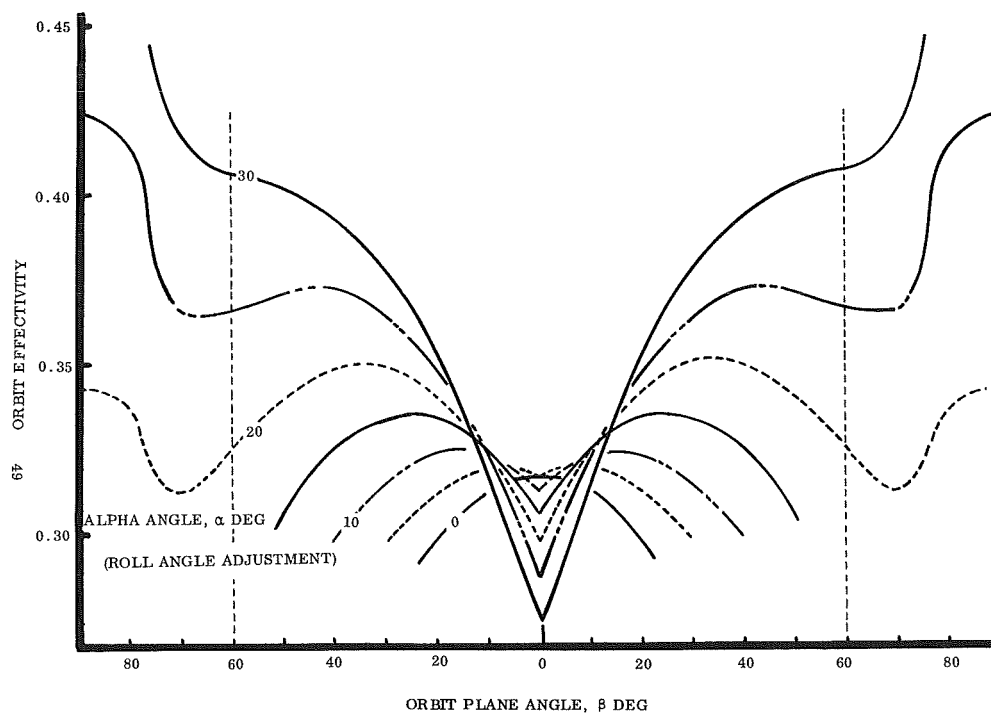


Fig. 18 Improvement in Array Effectivity as a Function of Seasonal Adjustments

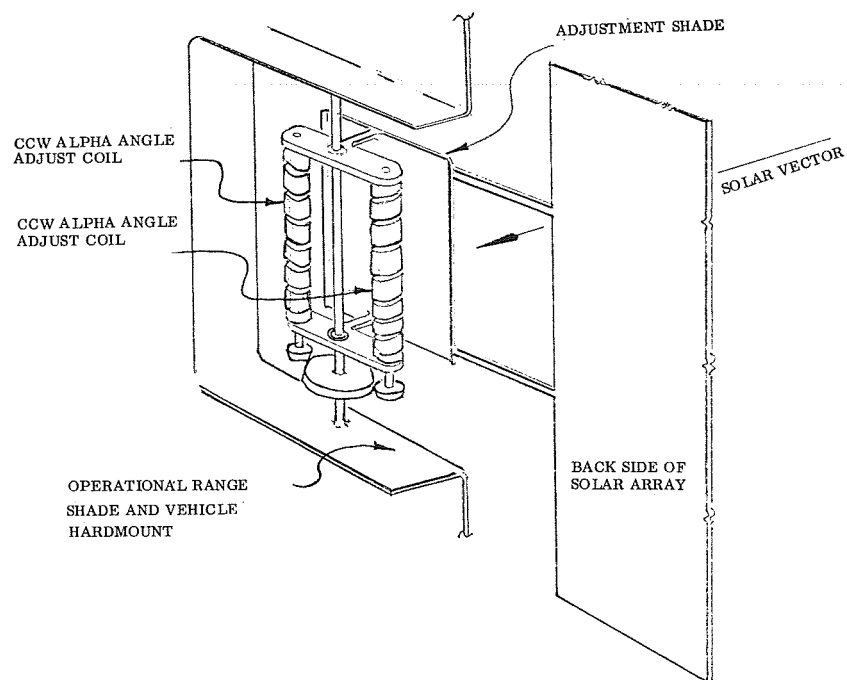


Fig. 19 Seasonal Adjuster Concept

for a lunar based sun seeking device. The particular model demonstrated had rather flimsy coils and little structural stability. Heavier coils and structural guides would aid this problem at the expense of thermal response time.

c. Continuous Concepts – Single Coil. To provide a rapid coil reset function in continuous tracking concepts an incremental action is used. This allows the bimetal coil to be shaded quickly with respect to the tracking rate thus maximizing cooling (coil reset) response.

Effective tracking may be accomplished incrementally. Figure 20 shows a plot of area effectivity vs. orbit position for various tracking increments. It is evident that the average area effectivity loss due to tracking in small increments compared to ideal tracking is very small. In an incremental device, the coil element advances and resets in increments and the array rotates unidirectionally. This type of non-array-reset device is well-suited for intermediate altitude and synchronous orbits in which a daily earth shade eclipse does not always occur. In orbits of this nature it is desirable to minimize battery cycling; therefore, a device that does not require an array reset once per orbit is required.

To explain the principle involved in incremental tracking, a schematic example of a detent device is shown in Fig. 21. One end of the bimetal coil is fixed to the vehicle. The other end of the coil drives the array and a detent wheel through a ratchet interface. A combination feedback-reset shade attached to the array provides tracking control. In the figure the array is oriented and the coil completely shaded. As the vehicle travels through its orbit path, the array and shade become slightly misoriented (the amount depends upon shade configuration). As the coil becomes partially exposed (Fig. 21b), the increase in coil temperature causes a torque increase. The array is prevented from turning by a spring-loaded detent. When the coil is nearly fully illuminated, enough torque is built up in the coil to rotate the array and detent wheel to the next detent. This may occur at 6 deg of angular misorientation, and the detents are spaced so that the next detent stop is 12 deg (in this particular example). Thus, the array rotates 12 deg of arc (Fig. 21c). In this new position, the bimetal coil is completely shaded by the reset-feedback shade for 6 deg of orbit travel.

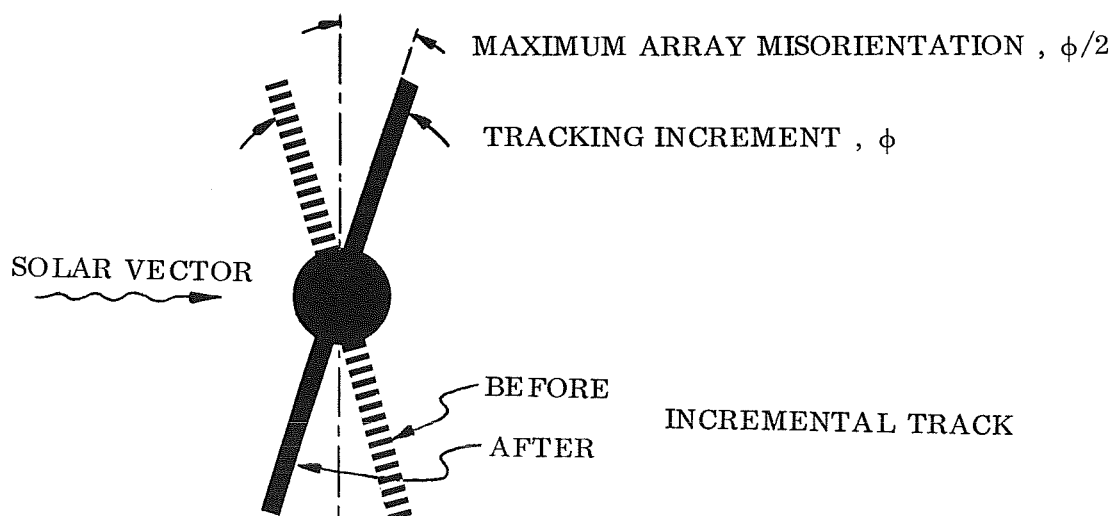
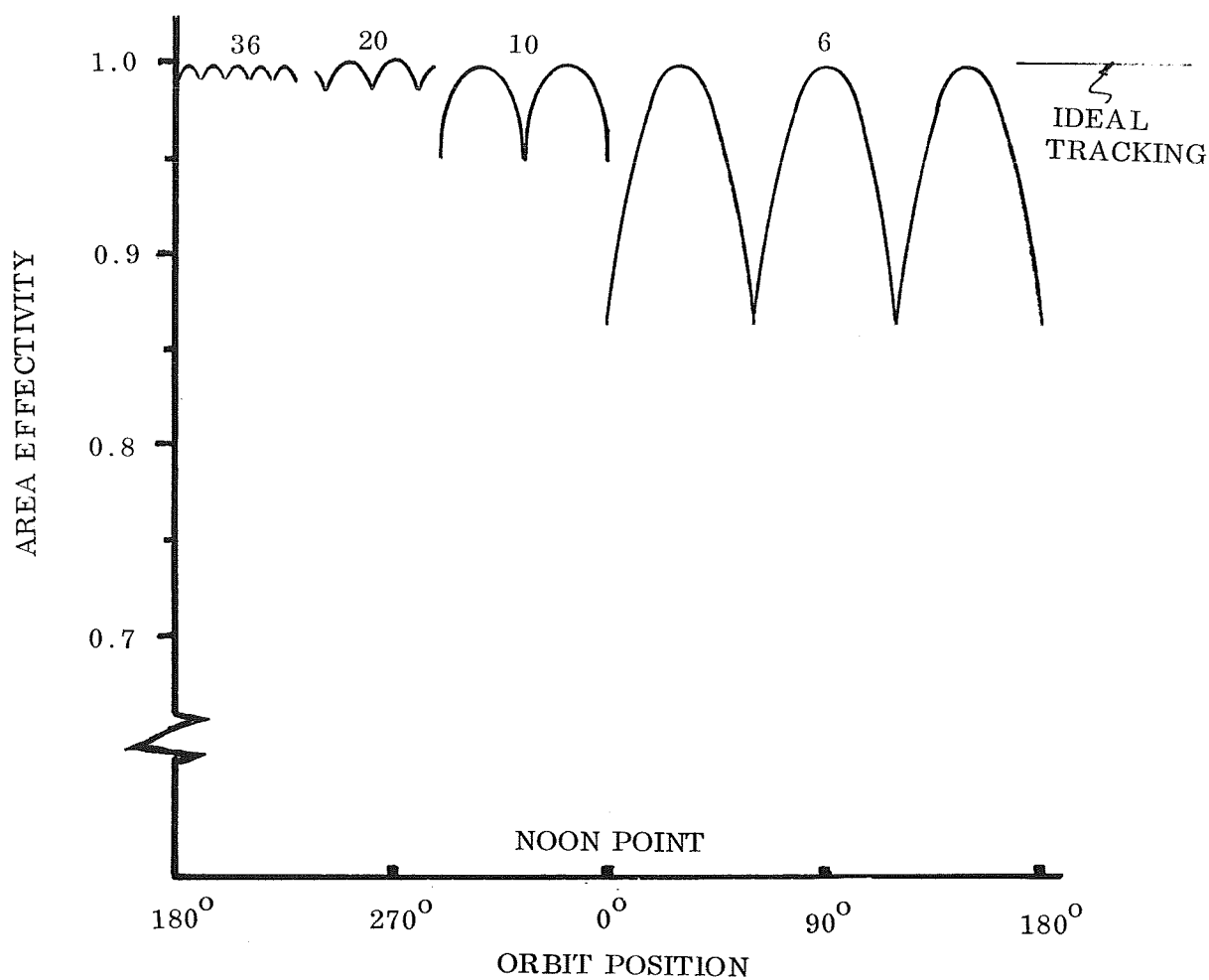


Fig. 20 Solar Panel Area Effectivity vs. Tracking Increments

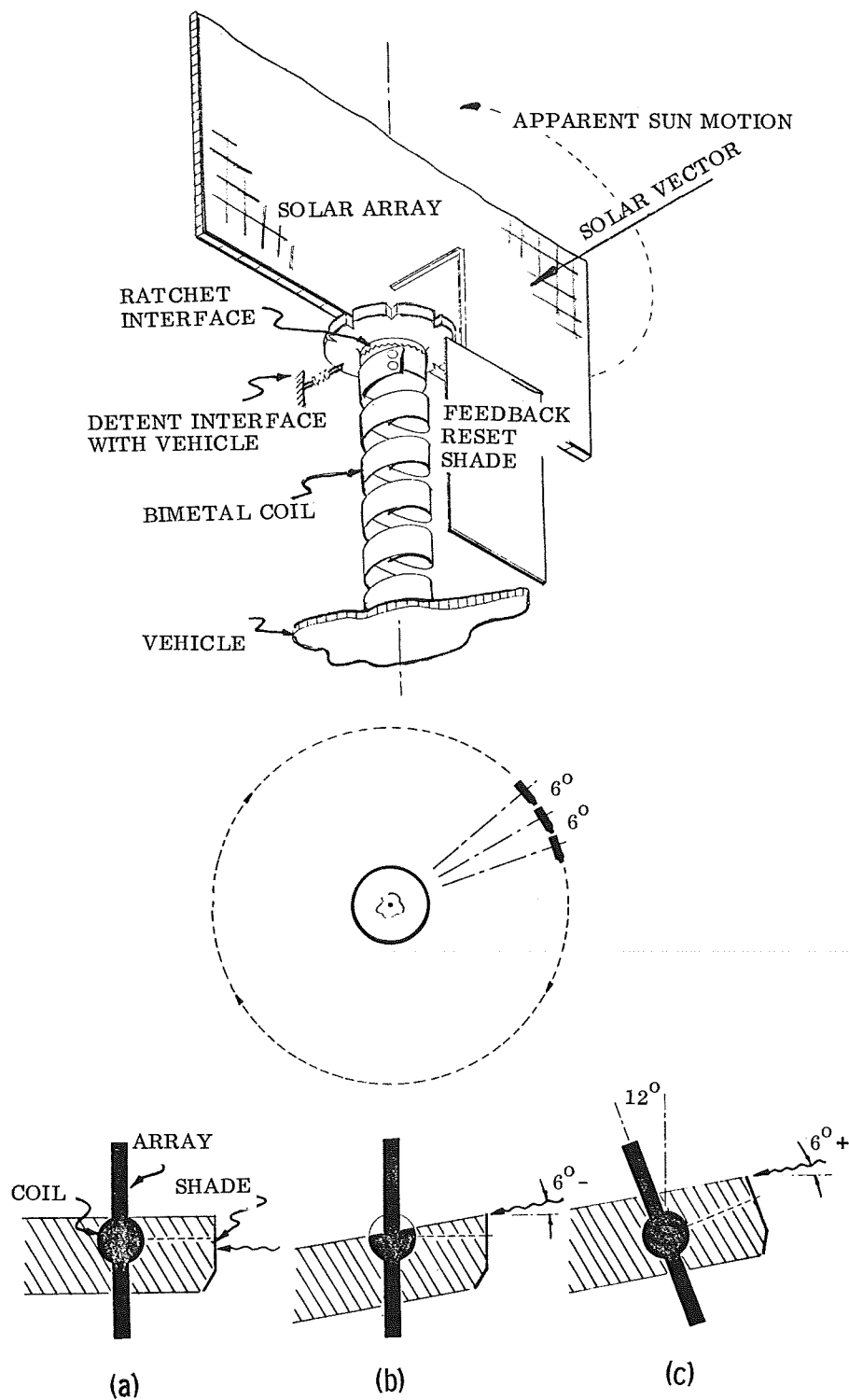


Fig. 21 Detent Concept



- The Spring Detent concept is shown schematically in Figure 21. Basically this device depends upon thermal torque built up in a bimetal coil to turn a detent wheel. The wheel is restrained by an adjustable spring-loaded detent so that it will not escape until enough torque is stored to move a complete increment to the following detent. A shade attached to the final drive is not affecting coil action during heating; however, the coil must be cooled after a tracking cycle in order to effect coil reset. There is a specific reason for the rapid incremental steps. The shade instantly is drawn in front of the coil after each incremental tracking motion, thus allowing the coil to cool. Without the rapid shading effect, the coil would reach an equilibrium temperature after which tracking would not take place.

A small desk top demonstration illustrated one major draw back to the basic spring-detent concept; the detent wheel tends to overshoot thus snapping two or more increments. Careful detent shape design and precision manufacture would help this problem, but there is still no guarantee of single increment motion.

- The Brake-Detent device was considered as a solution to the overshoot problem associated with the spring-detent unit. This concept is essentially the same except for an overshoot control brake. Escapement motion of the detent wheel actuates a cam energized friction brake which stops the drive at the following detent increment. Again, a small demonstration unit was made to demonstrate the concept. Figure 22 shows a drawing of a device incorporating the brake detent concept, which is more suited for environmental testing. This unit is enclosed except for the bimetal coil element. The outside enclosure shell may be considered to be attached to the solar array.

An explanation of operation modes follows: The base wheel and shaft are fixed to the vehicle, and the bimetal coil is fixed to the outboard end of the shaft. The other end of the coil rotates the concentric, which is restrained by a spring-loaded detent. The concentric has drive pins that mate with pins on the ratchet wheel. This wheel in turn works through a ratchet interface with the outside shell. The pins do not engage until the detent arm has been lifted fully in order to avoid excessive array misorientation. As before, misorientation of the array allows solar illumination to pass a shade (not shown but attached to the array) and heat the bimetal coil. Torque is produced until enough is stored in the coil to overcome the detent spring force. The concentric then turns an increments governed by pre-set mechanical stops and engages the ratchet wheel.

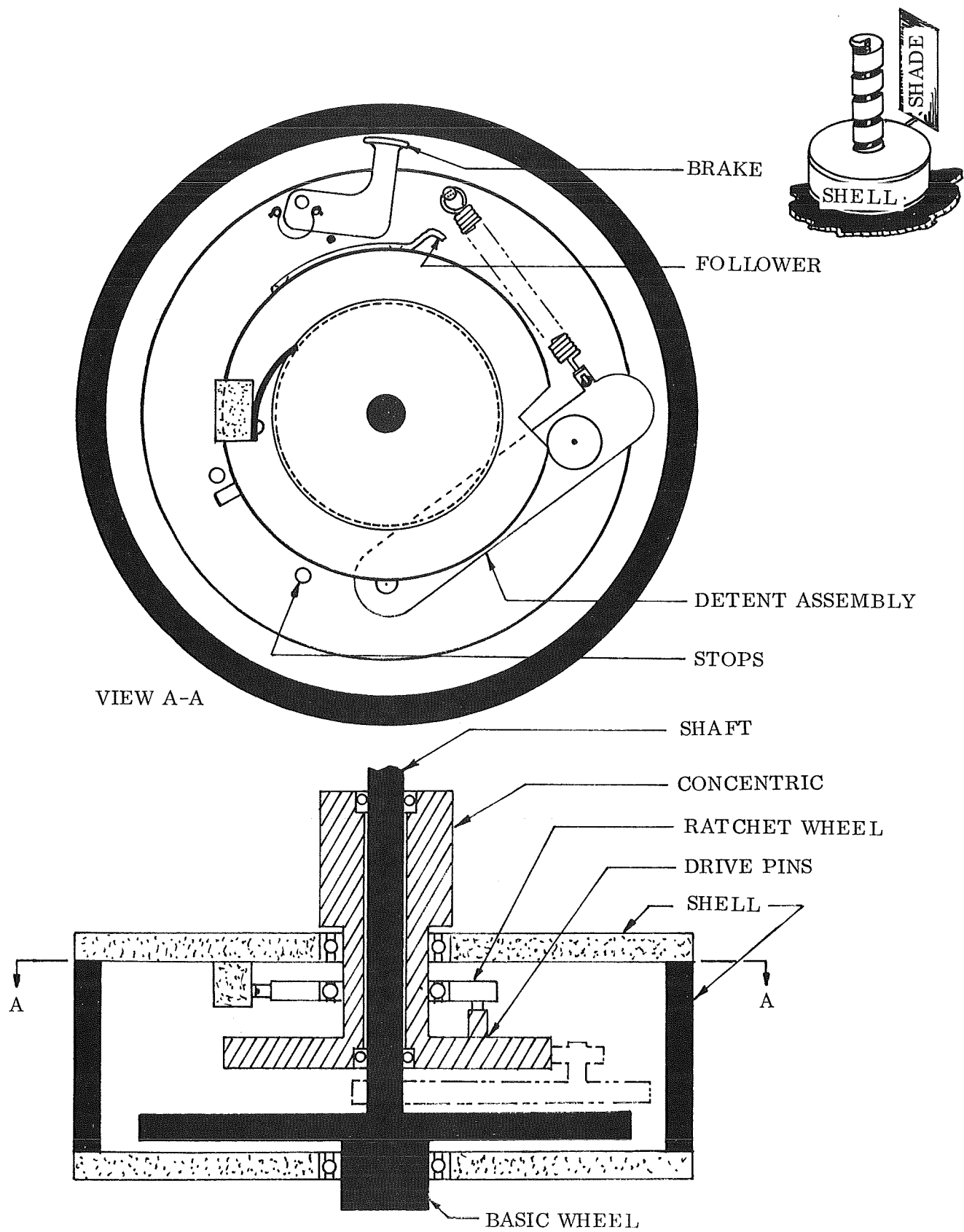


Fig. 22 Brake Detent Device

wheel. The ratchet wheel in turn rotates the outside shell (with array and shade). In the new position the coil is shaded, and reset takes place through the ratchet interface. A scheme for preventing overshooting due to system inertia incorporates the braking principle. After the concentric travels one increment, the attached spring follower activates a brake to prevent over rotation of the shell array. The array is then locked until the bimetal coil cools. It was found as suspected, that extreme accuracy and material control would be necessary to develop a brake system that would reliably stop the drive after precisely one increment of travel.

- Further refinement of detent ideas produced the Locking Ratchet concept. This unit is similar to the previous devices in that energy is built up in a bimetal element until enough torque is available to escape a detent. The detent wheel in this case, however, powers a cam and not the main drive. It contains only one detent and does not depend on accurate indexing for operation. Periodic cam motion controlled by a quickly acting shade, as previously explained, actuates a locking ratchet as illustrated in Figure 23. The cam follower operates an arm which carries a dog. Each cycle will cause the dog to move the cog wheel (main drive) a single increment. A ramp built into the arm prevents over run of the drive in a positive manner. In the figure, the shaft is integral with the vehicle interface, and one end of the coil is affixed to the outboard shaft end. The other end of the coil drives a cam and detent wheel attached to a piece part called the concentric. The concentric assembly is free to rotate about the shaft. An arm and dog assembly controls the motion of the cog wheel (to which the array is attached). The locking tooth in the arm ensures that only one increment of array travel occurs per heating cycle of the coil. The device operates as follows: Array misorientation allows coil illumination and heating as explained previously. Heating of the coil builds up cam torque which is restrained by the spring loaded detent assembly (note that the figure shows the device in a position just after an increment of tracking has taken place, and the coil has not yet cooled fully). When nearly fully illuminated, the coil produces enough torque to overcome the detent force and rotate the cam. Rotation of the cam causes the follower to actuate the attached arm/dog assembly and advance the cog-wheel one increment. The locking tooth on the arm prevents the cog-wheel from traveling more than a single increment. In this new position, the coil is shaded by a shade attached to the array-cog-wheel unit, and the coil cools. This cycle repeats for further tracking.

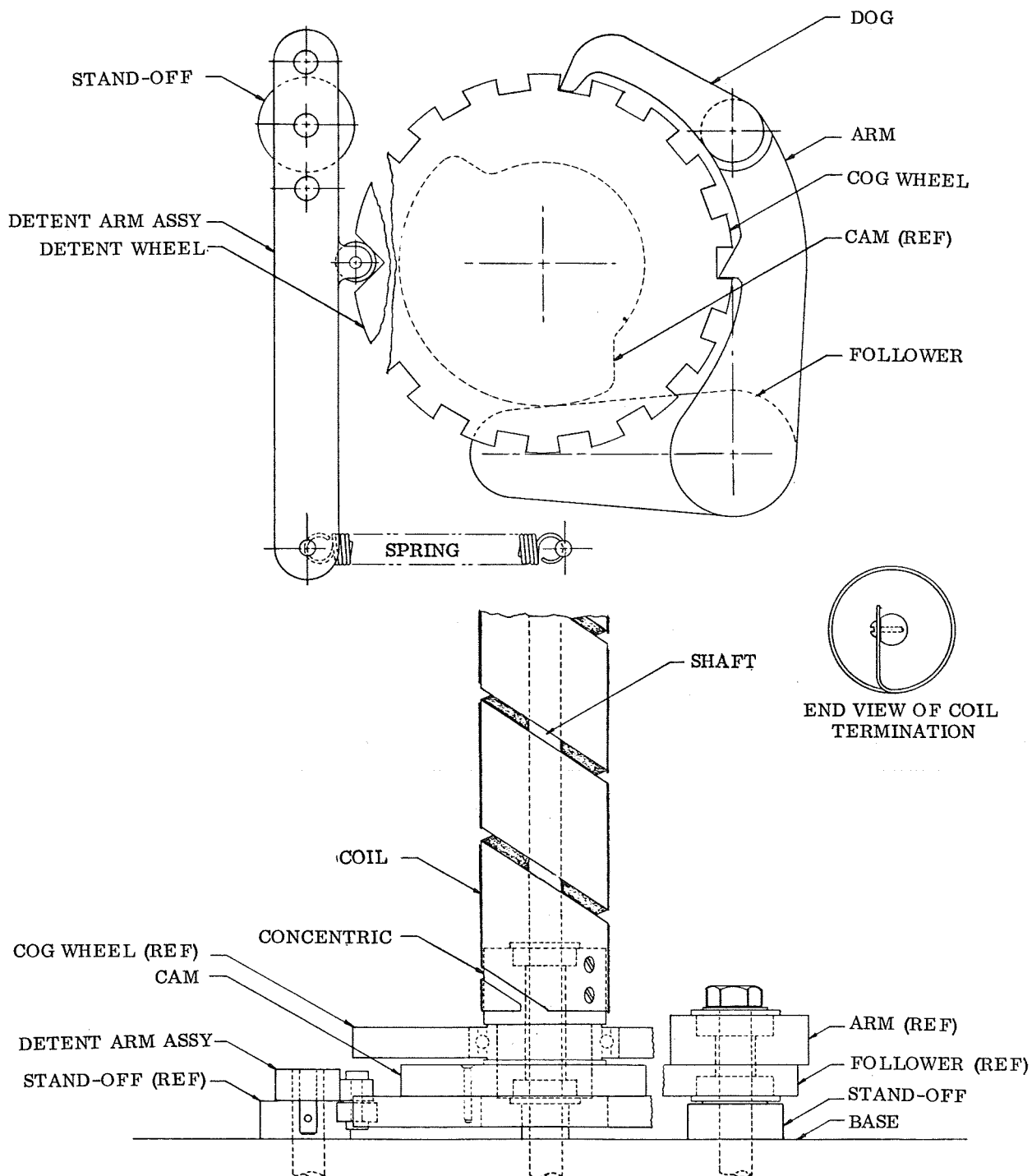


Fig. 23 Locking Ratchet Detent Device

Two modifications of this concept are shown in Figures 24 and 25. These changes provided for compaction of components into a small envelope. A cardboard mock-up of mod A showed that the mechanism would operate as planned. Although no hardware was fabricated for this particular concept it is a perfectly feasible method for indexing the main drive in a predictable fashion.

- The Planetary Shade Tracker was the final type of single coil continuous tracker investigated. The planetary shade tracker, shown in Figure 26 derives its name from the technique whereby the coil shade moves with respect to the coil. The shade is mounted on a rotating shaft which is coupled to the coil fixed end or vehicle via a small gear. The rate or times at which the shade alternately shades or allows illumination of the bimetal helical coil per 360 deg of rotation is a function of the diameters of the fixed wheel or gear and the planetary gear. It is desirable to have a large fixed gear diameter and a small planetary gear diameter to effect rapid full shading as a function of orbital rate, allowing the coil to reset so that continuous tracking can be achieved. Coil reset occurs in that the coil is ratchet-coupled to the shade assembly cage at one end. As the coil is illuminated and heated, the coil free end rotates unidirectionally at a rate faster than the orbital rate. This causes the shade cage assembly to rotate bringing the shade, which is co-planar with the array, around so that its face is directly between the sun's rays and the coil. Within the shade, reset occurs. Continued vehicle orbiting, or apparent sun displacement, again causes illumination upon the coil. This illumination is expanded because of the motion of the planetary shade. Coil rotation results and the cycle is repeated. This device was one of those chosen for fabrication and test.

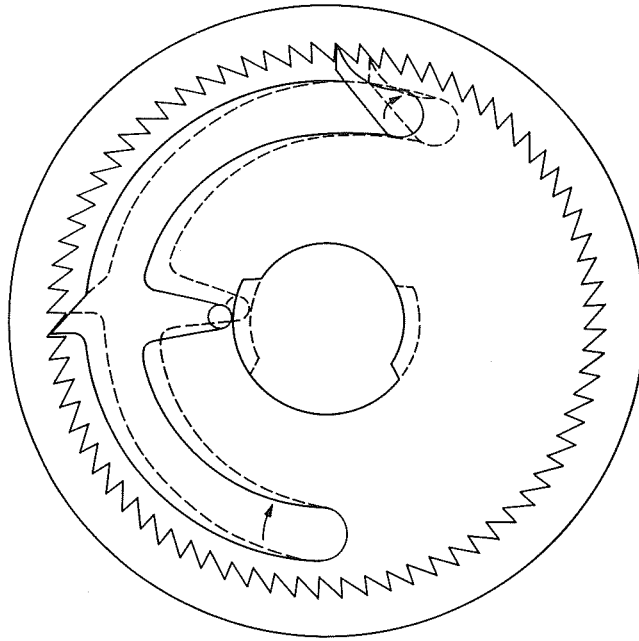


Fig. 24 Modified Locking Ratchet Mechanism (Internal Pivot)

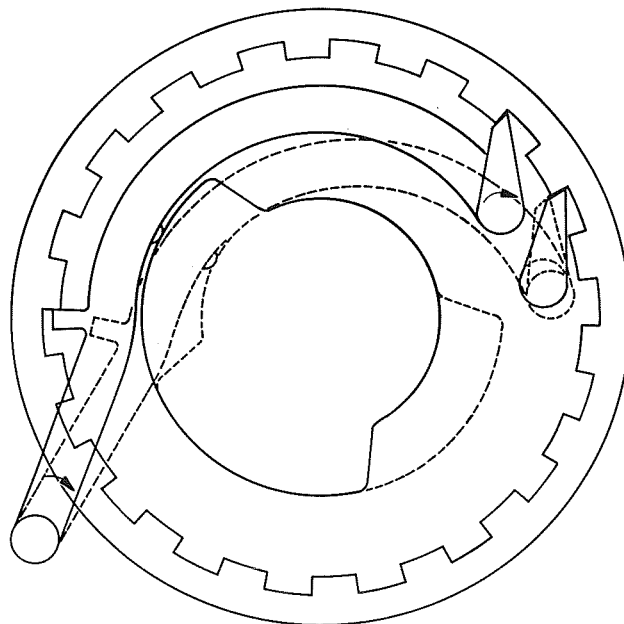


Fig. 25 Modified Locking Ratchet Mechanism (Internal Pivots)

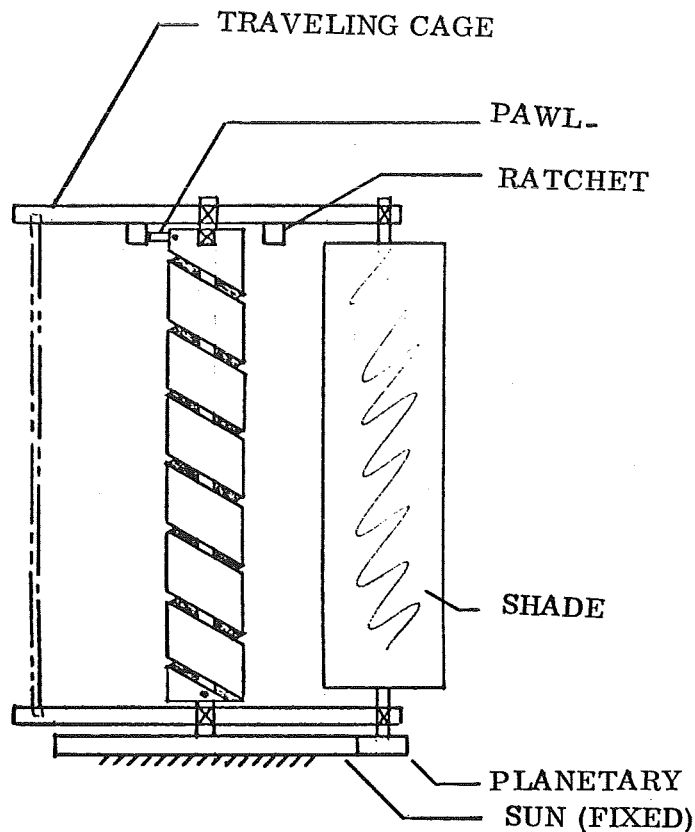


Fig. 26 Planetary Shade Tracker

d. Continuous Concepts – Multi Coil. Referring again to Figure 16, several two-coil continuous tracking concepts were explored. With the exception of the Planetary Shade device discussed previously, the preceding concepts are somewhat limited in capability in that they must have a definite heating and cooling cycle to produce motive force for each increment of tracking. If one increment of tracking does not initially orient the array and shade the coil, reset cannot take place. This problem is minimal for a no-shade orbit vehicle since after the initial revolution the tracker would begin tracking as designed. However, for the sake of reliability and versatility, a device capable of orienting a solar array from any degree of misorientation is desirable. Also, the use of multiple coils allows separation or distribution of sensing and motor functions.

- The Stored Energy Device shown schematically in Figure 27 is a tracker compatible with most orbit situations, including gross misorientation. It incorporates two coils – one for motor torque and one for the sun sensing function. In this way each coil may be optimized for its particular task instead of compromising a single coil by trying to obtain high torque and low thermal mass.

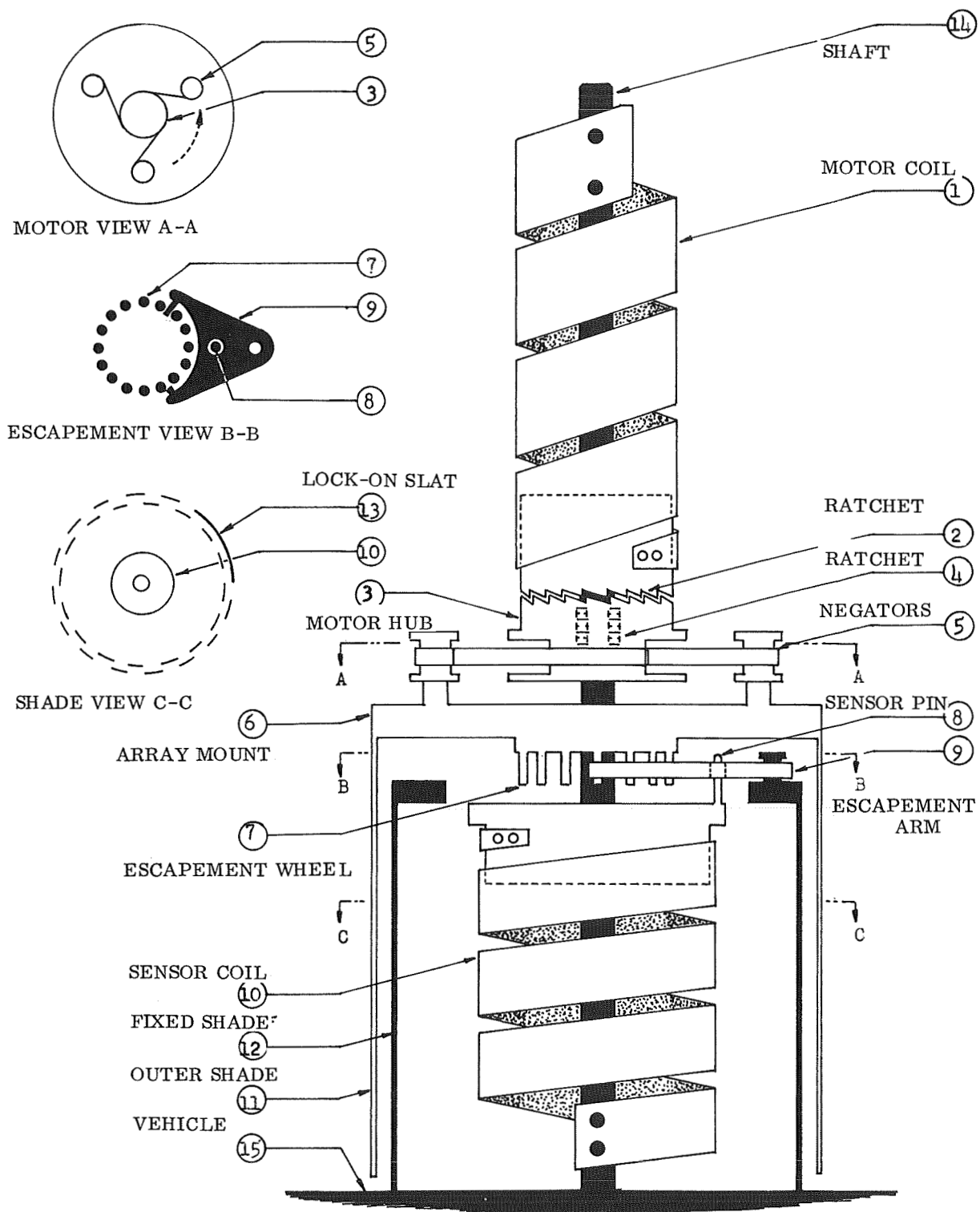


Fig. 27 Stored Energy Device



Operation of this concept is explained below (Ref. Fig. 27)

#### Energy Storage Mode

- Once per orbit, the motor coil (1) experiences a heating cycle due to solar illumination and a cooling cycle due to shading. The shading is provided by either earth eclipse or a vehicle-mounted shade.
- The heating and cooling of the motor coil produces an oscillating rotation of its free end. Note the shaft (14) is fixed to the vehicle.
- A ratchet (2) between the motor coil and the motor hub (3) allows a winding motion of the motor hub.
- Another ratchet (4) provides an interface with the shaft to allow only unidirectional rotation of the hub.
- The unidirectional rotation of the motor hub reverse winds the elements of negator springs (5) on to the hub.
- As shown in the motor view, the springs produce a constant torque on the array mount interface (6) in one direction.

#### Tracking Mode

- The solar array is attached to the array mount (6). To control rotation of the array mount, an escapement wheel (7) is used.
- The escapement arm (9) is actuated by the sensor pin (8). For each heating and cooling cycle of the sensor coil (10), the escapement slips two increments (see escapement view).
- Attached to the array mount is a slotted shade (11) concentric with another slotted shade (12) fixed to the vehicle (see shade view).
- The shades are mechanically synchronized with the escapement so that the sensor coil is alternately illuminated and shaded.
- When the slots in the shades align, the coil is illuminated. This will cause the sensor pin to actuate the escapement and allow the array to rotate one increment.
- This rotation closes the shades, and the coil begins to cool.

- When the coil cools, another escapement motion takes place and the coil again becomes illuminated with another increment of array mount and shade rotation.
- This cycle repeats until the lock-on slat (13), which is coplanar with the solar array, is normal to the sun. In this position, the sensor coil is shaded. The array remains in this position until misorientation again causes the sensor coil to become illuminated.

This concept was also chosen for further study. A model was fabricated and tested as described further in this report.

- A 2-coil Bidirectional concept was evaluated to check feasibility of a 2-coil system in a clockwise or counter-clockwise continuous tracking situation. (This situation could only exist if an orbiting vehicle did a 180-deg roll or yaw in an end-for-end spacecraft misorientation, arrays were deployed in the pitch-yaw plane, or the vehicle was in an orbit inclined to the equator and cw or ccw roll-tracking adjustments were made.) A drawing depicting this device is shown in Figure 28. In operation, the device will track in either direction in an incremental manner. The size of tracking increment is determined by the number of machined stops shown in section A-A of Figure 28. Each coil provides tracking capability in one direction. Heating of a coil stores torque similar to other detent devices until enough energy to overcome a spring follower is obtained. An increment of tracking then takes place through a controlled runaway type escapement at the top of the device. This allows a smooth increment of tracking instead of a snap motion. A single-tooth ratchet coupling at the base of each coil engages the shade assemblies after each increment of tracking so that the operating coil can cool and reset. To insure maximum heating and rates cooling, the shade system is either fully open or fully closed as controlled by the ratchet assembly.

- The 2-Coil Continuous Tracker was the final multi-coil pitch axis tracking concept evaluated. A dual-coil device was devised which provides smooth continuous tracking. Two coils are used so that they may be made of sufficient thickness to provide adequate torque capability (a high torque coil cools slowly in the reset mode, so two units are used). One coil at a time provides tracking motion while the other is cooling from a previous cycle. The device is shown schematically in Figure 29. Both coils are fastened at their outboard ends to the drive gear, which rotates about the mounting shaft on bearings. A reversing gear on each drive gear provides the correct directional

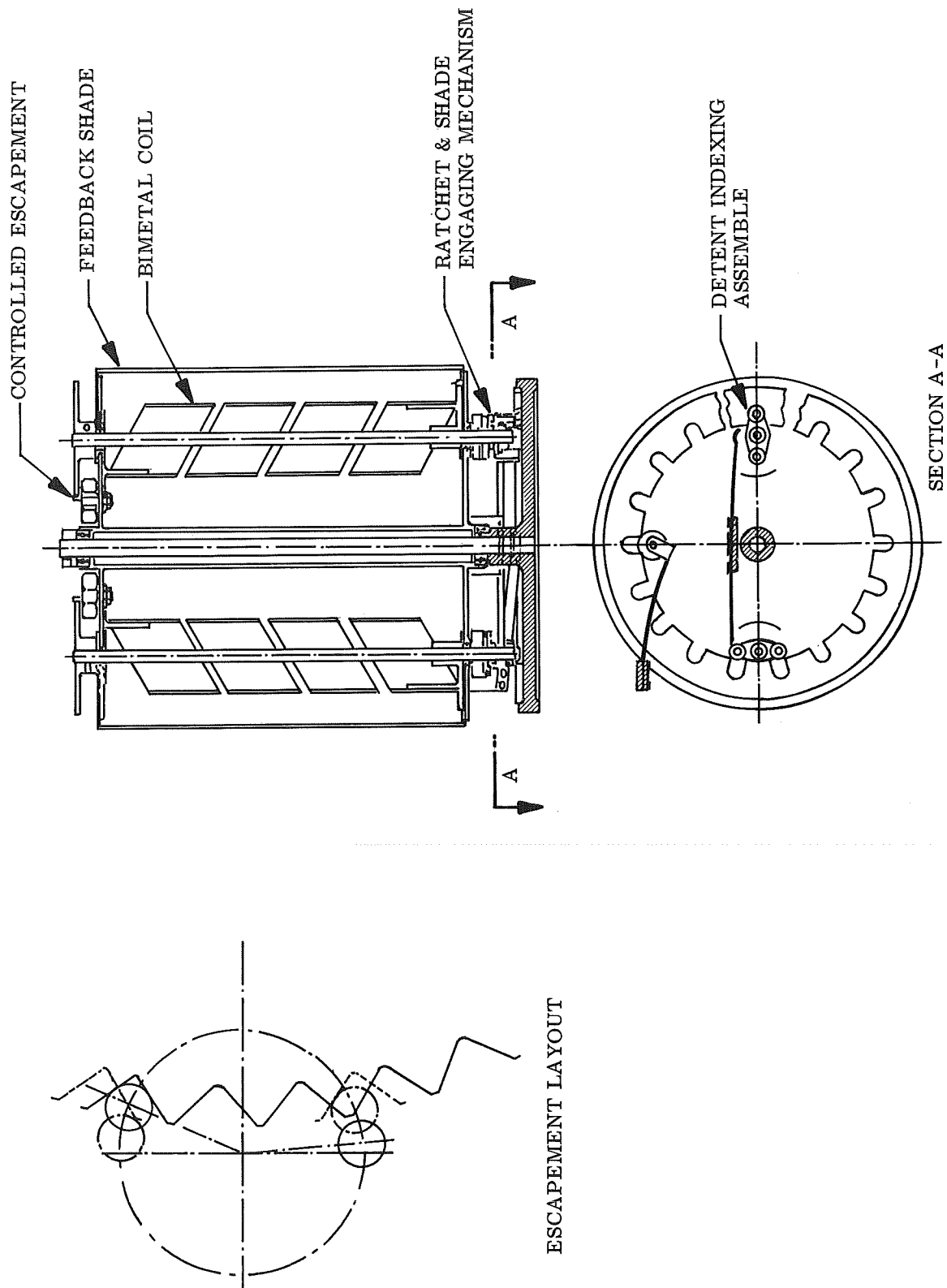


Fig. 28 Bidirectional Two-Coil Tracking Device

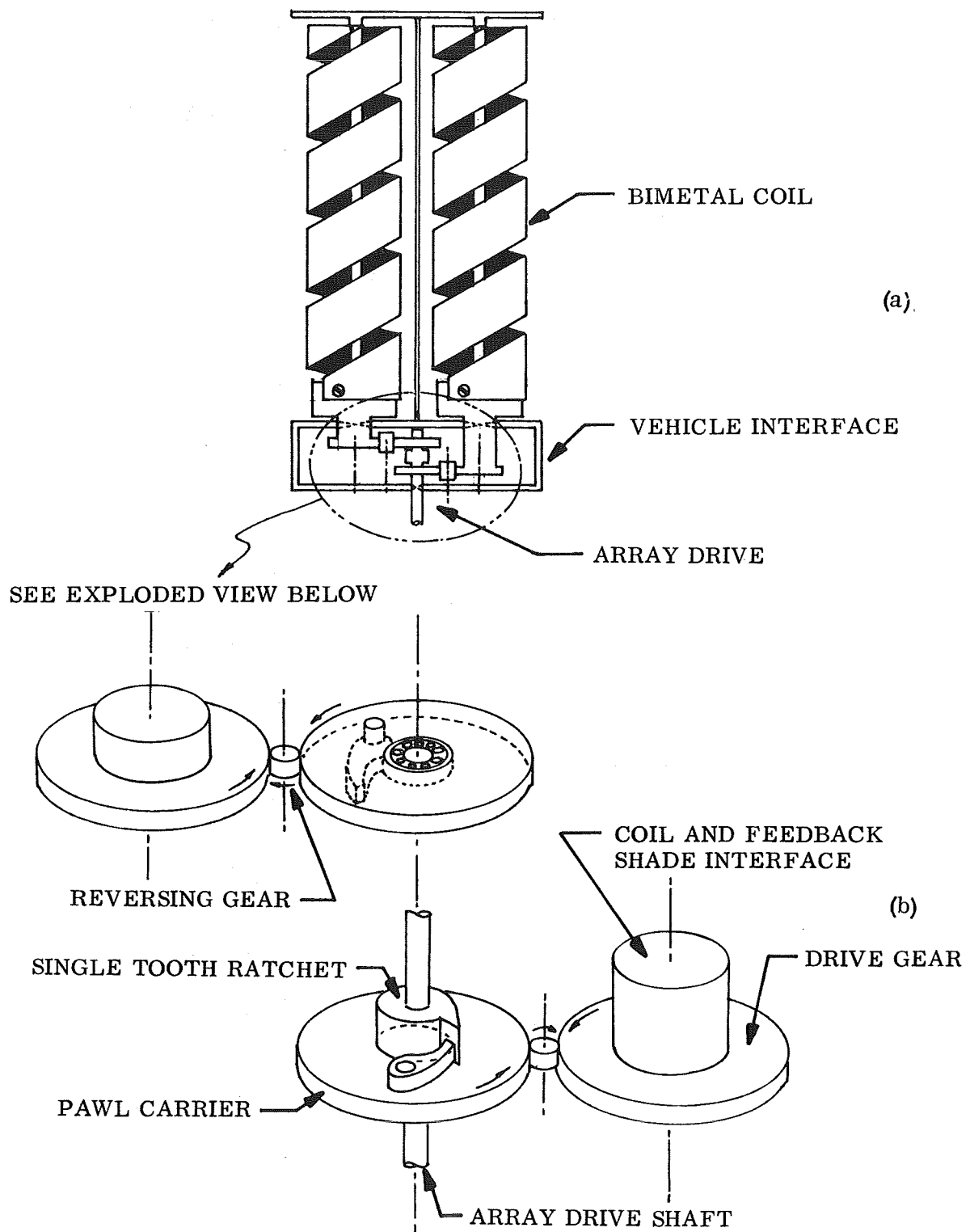


Fig. 29 Two-Coil Continuous Tracker

sense to the pawl carrier gears. Each of these gears carries a simple spring-loaded pawl which rides against a ratchet wheel. The ratchet wheel has only one tooth in order to assure positive array synchronization with the tracking coils. A sketch of the pawl/ratchet system is shown in the figure. The ratchet wheel is mounted to the array drive shaft, which turns relative to the vehicle interface. The shading arrangement is shown schematically in Figure 30. The static shade is fixed relative to the vehicle, while the feedback shades (one for each coil) rotate with the coil drive gears. The feedback shades are arbitrarily in the hot coil position.

Operation mode of the device is shown in Figure 30 and a brief explanation follows (F indicates the front coil and B is the back coil):

- (1) Coil F is hot and has finished its tracking cycle. It has reached a mechanical stop and no further rotation will occur. Coil B is cold against a stop and ready to take over the tracking action.
- (2) Coil F is becoming shaded by the static shade while coil B is becoming illuminated. Tracking by coil B has been initiated.
- (3) Tracking is being controlled entirely by coil B. Coil F begins its reset cooling cycle.
- (6) Coil B is hot and has finished tracking. The transition between coil B and coil F begins.
- (7) Coil F is tracking while coil B cools and resets.

In the transfer zones, proper alignment of shades and mechanical stops will assure a smooth transition between coils. There is no increment motion or snap action as transfer occurs, thus minimum impulse is transmitted to the spacecraft.

For synchronous application, each coil would have up to twelve hours for reset cooling. This would allow a drive coil to be sized for more than enough torque to provide tracking for most any sized array. It should be noted that the figures of the continuous tracker are conceptual sketches. This device was chosen for model fabrication and testing. Several changes were made to incorporate drive systems and compact shade outlines as will be shown in the test device section.

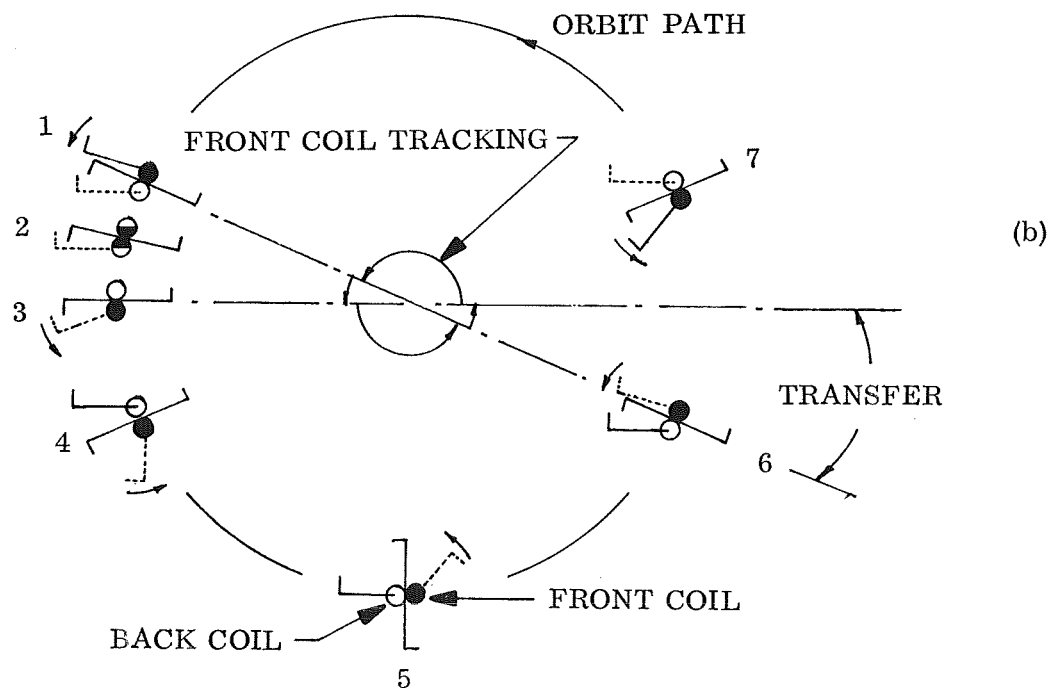
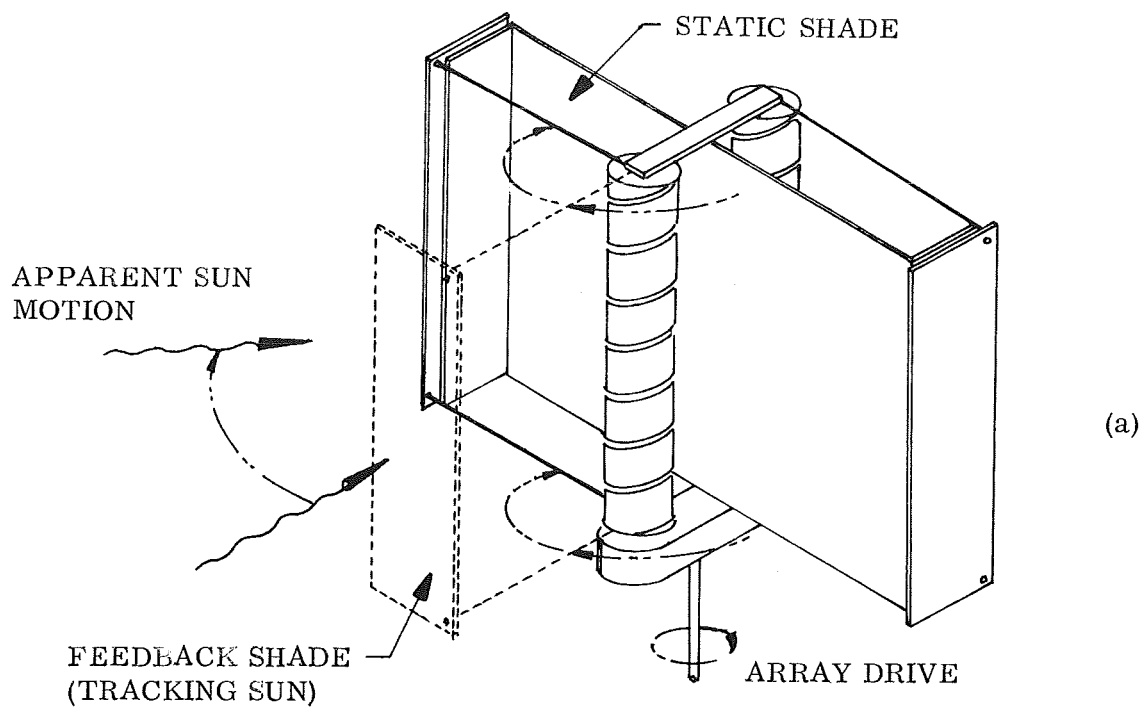


Fig. 30 Continuous Tracker Concept Configuration

## 2. Auxiliary Devices

Auxiliary devices consist of mechanical concepts associated with integrating the bimetal coil assembly into a sun-tracking device. They consist of shading devices, torque multipliers and coil types.

a. Shading and Reset Devices. Auxiliary shading and reset devices are schemes for providing the coil reset function when a natural earth eclipse does not occur. These units may be used as an addition to or as a substitution for earth eclipse. Several types of reset devices are mentioned below.

- Fixed Shade – A shade fixed to the vehicle proper will provide a daily shade period for the thermal heliotrope element. The dwell of this shade is a function of shade width and distance from the element. This type of shade is especially suited for cycling the energy storage mechanism on the unit described previously as the "stored energy device."

- Snap Acting Bimetals – Several types of snap-action devices may be fabricated utilizing bimetal elements. Snap disks provide a snap action from a cold position to a hot position, as shown in Figure 31a. The snap takes place at a given pre-set temperature. Another example of a snap bimetal is the Wilco-Taylor thermometal blade (Ref. 12) shown in Figure 31b. The blade is formed from flat stock by buckling the end section. Upon heating, the buckled section will restrain temperature deflection until enough force is developed for a snap to occur. The blade may be designed to provide an increased cold-contact-point pressure up to the point of snap by sizing the center leg so that its initial deflection is greater than that of the outer legs. By doing this, holding force of the unit is not sacrificed before snap action occurs.

- Coiled Bimetals – An auxiliary helical bimetal coil may be used to turn a shade into position by rotary motion. Energy reaching this auxiliary coil is governed by shades attached to the solar array or the vehicle. Linear motion may be achieved by winding a coil into a double helix. Motion is then in the direction of the major helix.

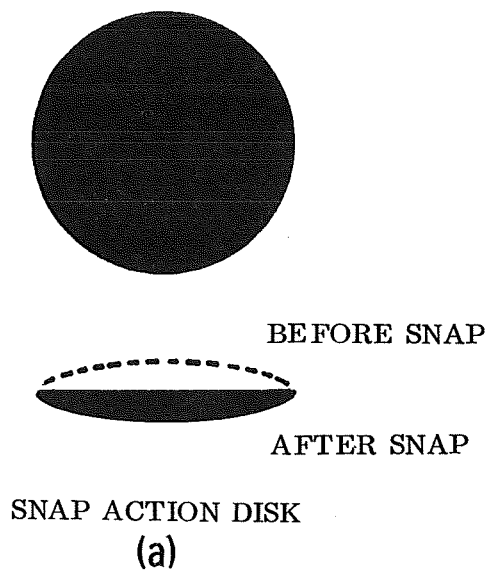
- Solenoid – An electrical solenoid may be used to actuate a coil reset shade very easily. However, even though a solenoid may be a fairly reliable device, it is the point of this study to provide completely passive (non-electrical) tracking functions.

- Slotted Shade – One of the most promising shade applications is a device that uses two concentric cylinders. Slots are opened in the cylinders at given increments as shown in Figure 31c. Rotating one cylinder one increment with respect to the other will alternately open and close the slots. This allows heating or cooling of a bimetal coil housed within the inner cylinder. This particular device is used on the "stored energy tracker" model.

- Mechanical Trip – A reset shade may be actuated as a function of solar array position with respect to the vehicle. Here, a trip on the array actuates a shade when the array achieves a given position. Multiple trips may provide a given shade time dwell.

- b. Torque Multipliers. Torque multiplication may be necessary to overcome friction associated with large solar arrays. For a given width and thickness coil, torque may be increased by either gearing down or parallel mounting of bimetal elements. Gearing down is quite straightforward. It consists of taking a coil of relatively long length (thus capable of many revolutions for available temperature change) and gearing it down by the desired torque multiplication ratio. On the overview, it might seem that in order to gear down a coil for a multiplication factor of 3:1, the coil would be three times as long as normal and have one-third the mechanical torque. This is true; however, from the bimetal equations (see the Bimetal Theory section), it may be seen that the thermal torque is independent of coil length. That is, for a given temperature rise, the restrained torque produced in a helical coil of specified width and thickness does not change with length. Hence, the gearing down approach to torque multiplication is valid. Parallel mounting of bimetal coils is another approach for increasing available tracking torque. Figure 32 shows two concepts for parallel coil drives. The first method appears to be a series configuration, in that the coils are mounted in one axis. However, each coil is grounded at one end, and the free end drives a shaft internal to the ground tube. Figure 32b shows a true parallel mounting scheme. To avoid coil shading by neighboring coils, the entire assembly rotates with the solar array. The center coil is attached to a fixed shaft and gear at the base. The free end of this coil turns an actuator arm to which the outboard coils are attached. The free ends of those coils transfer torque through gears to the fixed center unit. Therefore, all the torques generated in the coils are transferred to the array through the actuator arm. The outboard gears are twice the size of the fixed gear, since they must rotate around the





(c)

CONCENTRIC SHADES

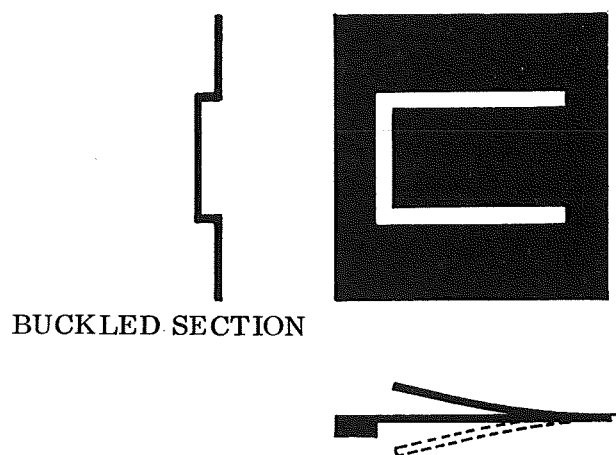
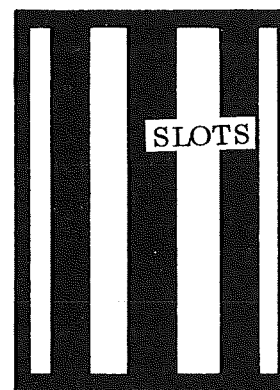
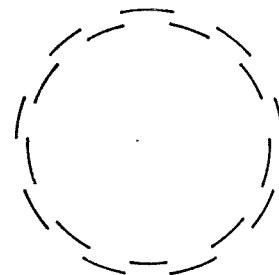


Fig. 31 Auxiliary Devices

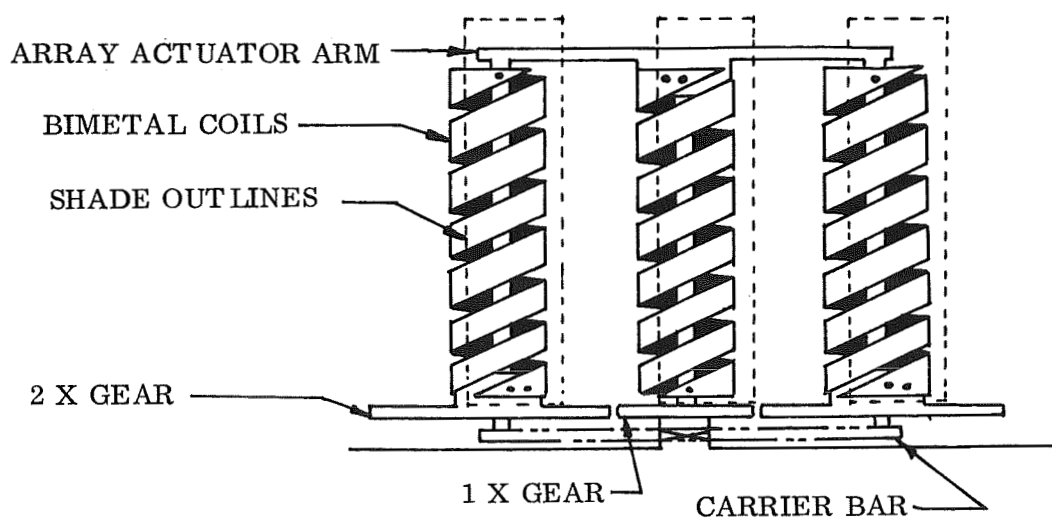
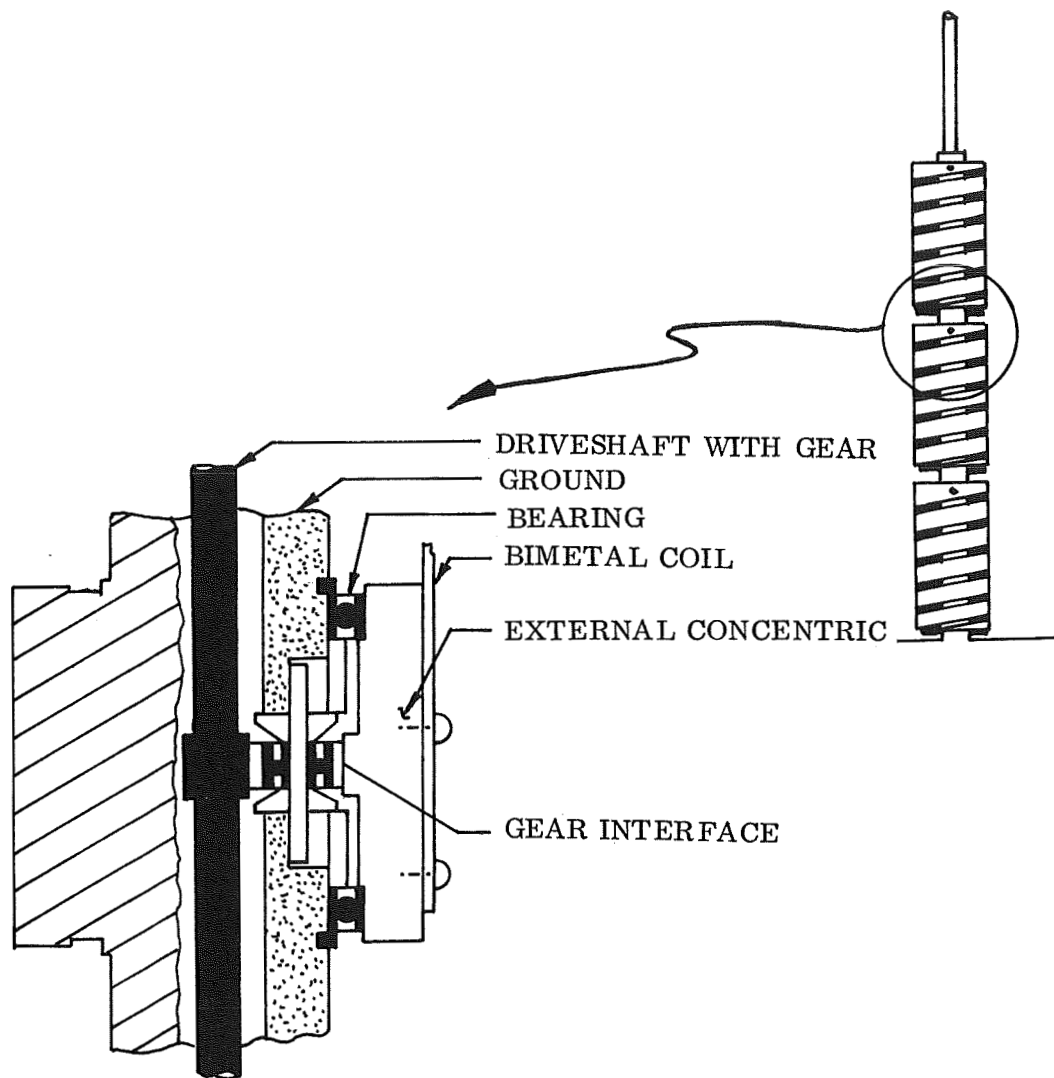


Fig. 32 Torque Multiplying Concepts

fixed unit. If they were the same size, it would take two revolutions of the outboard coils to turn the assembly one revolution about the center axis. To avoid different sized coils, the 2:1 gearing is used.

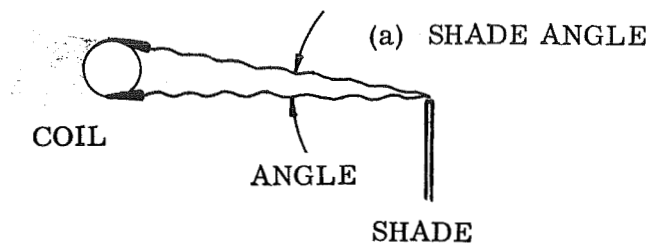
Methods of torque multiplying utilizing pinned end elements have been devised for connective heat motor systems (Ref. 10) but are not immediately applicable to radiative heating and cooling devices.

c. Coil Types. In devices incorporating a planar shading arrangement for shading a coil (like the feedback shade used on continuous devices other than the stored energy tracker), it is desirable to minimize the necessary angle of shade rotation between a fully illuminated and fully shaded mode. This angle, called the shade angle (Fig. 33a) is a function of coil diameter and shade distance from the coil  $\left( \theta = 2 \tan^{-1} \left\{ \frac{\text{coil radius}}{\text{distance from shade to coil}} \right\} \right)$ . Winding diameter can be reduced thus minimizing angle  $\theta$  without having an excessively long shade-coil distance. A small diameter helical coil, however, is not practical when using wide coil stock (a necessity for torque requirements). Winding the small diameter coil produces a high helix angle (Fig. 33b). With a high helix angle, considerable torque capability is lost due to bimetal action causing motion along the winding axis instead of around it. To avoid this situation, a zero angle "helical" coil may be formed into small diameter segments and fastened together, as shown. Thus, it is possible to wind small diameter coils of relatively large width bimetal stock without obtaining undesirable axial element expansion.

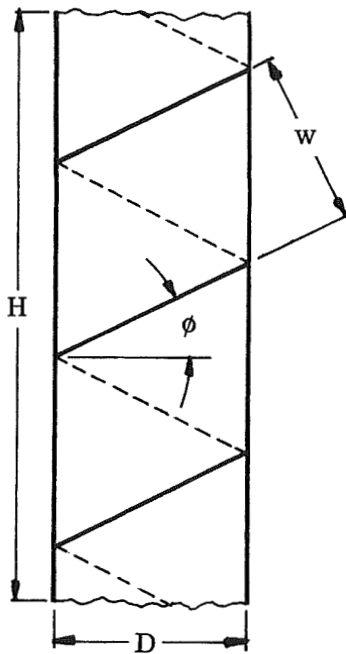
Where pure linear axial motion is desired, coils may be wound in a double helix configuration. Considerable force is available for small deflections with these coils. Area effectivity for radiative heat transfer is about 15-percent lower than for a pure helix; however, the linear force is greater. This type of coil may have application as a sensor in the triggering motion of springmotor or shade devices.

### 3. Test Specimens

Four concept test models were built. These were the a) Stored Energy Tracker, b) Seasonal Adjuster, c) Planetary Shade Tracker and d) Two-Coil Continuous Tracker. The bimetal used in all of the models was Troflex P675R with the exception of the Seasonal Adjuster which contained Wilco Morflex bimetal. Bimetal thicknesses varied



(b) CLOSED HELIX GEOMETRY



N = NUMBER OF COILS  
 L = ACTIVE LENGTH  
 w = STRIP WIDTH  
 D = COIL DIAMETER  
 H = SOLID HEIGHT  
 $\phi$  = HELIX ANGLE

$$\phi = \sin^{-1} \frac{w}{2D}$$

$$N = \frac{H}{2D \tan \phi}$$

$$H = \frac{w L}{\pi D}$$

(c) ZERO ANGLE HELIX

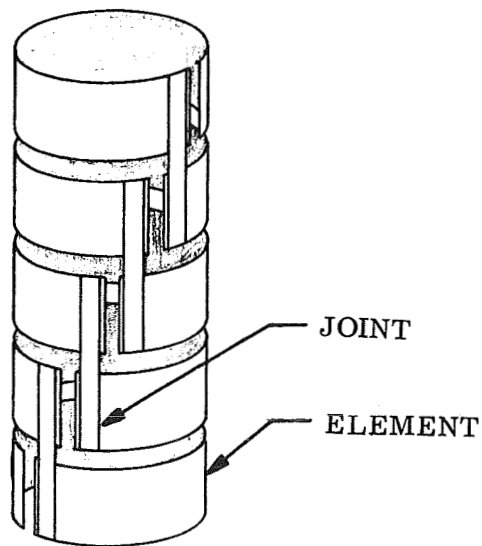


Fig. 33 Helical Bimetal Coils

from 10-mil thickness for the Stored Energy Trackers sensor coil up to 60-mil thickness for the coils on the Seasonal Adjuster. The bearings, gears, hubs and other small machine parts were purchased mainly from PIC Design Corporation, a subsidiary of Benrus. These parts were of the small precision instrument category. All bearings were cleaned with MEK and alcohol and used in a "dry" condition with one exception. It was noted that the main shade bearing on the Stored Energy Tracker was slightly rough in operation prior to the formal testing. Therefore, all the bearings in the model were treated with Dow Corning FS-1265 Hi-Vacuum lubricant prior to the test. The primary emphasis was on the tracker concept function, not on lubricant investigations. Therefore, in keeping within the scope and funding on the contract, analysis and fabrication effort on bearings and lubricants was modest.

The bimetal coils or helices were made by cold forming on a lathe arbor and subsequently stress relieved by heat treatment at 450°F for 60 minutes.

a. Stored Energy Tracker. This tracker contained more parts than the other models and also represents the most sophisticated fabrication effort. The two main parts of the concentric shade assembly were machined from single blocks of aluminum. They were primed and then coated with white Thermatrol, 2A-100 white air drying silicone paint, PB-105-101, LAC37-4294-101. The detail of the inner and outer shades prior to coating is apparent in Figure 34. This figure also shows the other disassembled components and subassemblies of this tracker. The coils were treated with the acidic oxidation treatment described in the thermal section. It is apparent that even with the thirty odd parts in the tracker, that it has an order of magnitude less parts than equivalent electro-mechanical trackers. Further detail of this tracker is given in Figure 35 showing the components of the motor coil ratchet assembly. The function of the ratchet assembly is to allow the motor coil, which is fixed at its upper termination, to rotate the motor hub, thus reverse winding the negator spring assembly once per orbit as the motor coil is alternately cooled and heated. When the escapement arm, via sensor coil assembly action, allows the outer shade to rotate, the hub/shaft ratchet also transfers the negator torque into an increment of tracking rotation ( $10^0$  in the test article). The majority of the machine parts are aluminum; the escapement wheel and escapement arm are steel. The completely assembled stored energy tracker is shown in Figure 36.

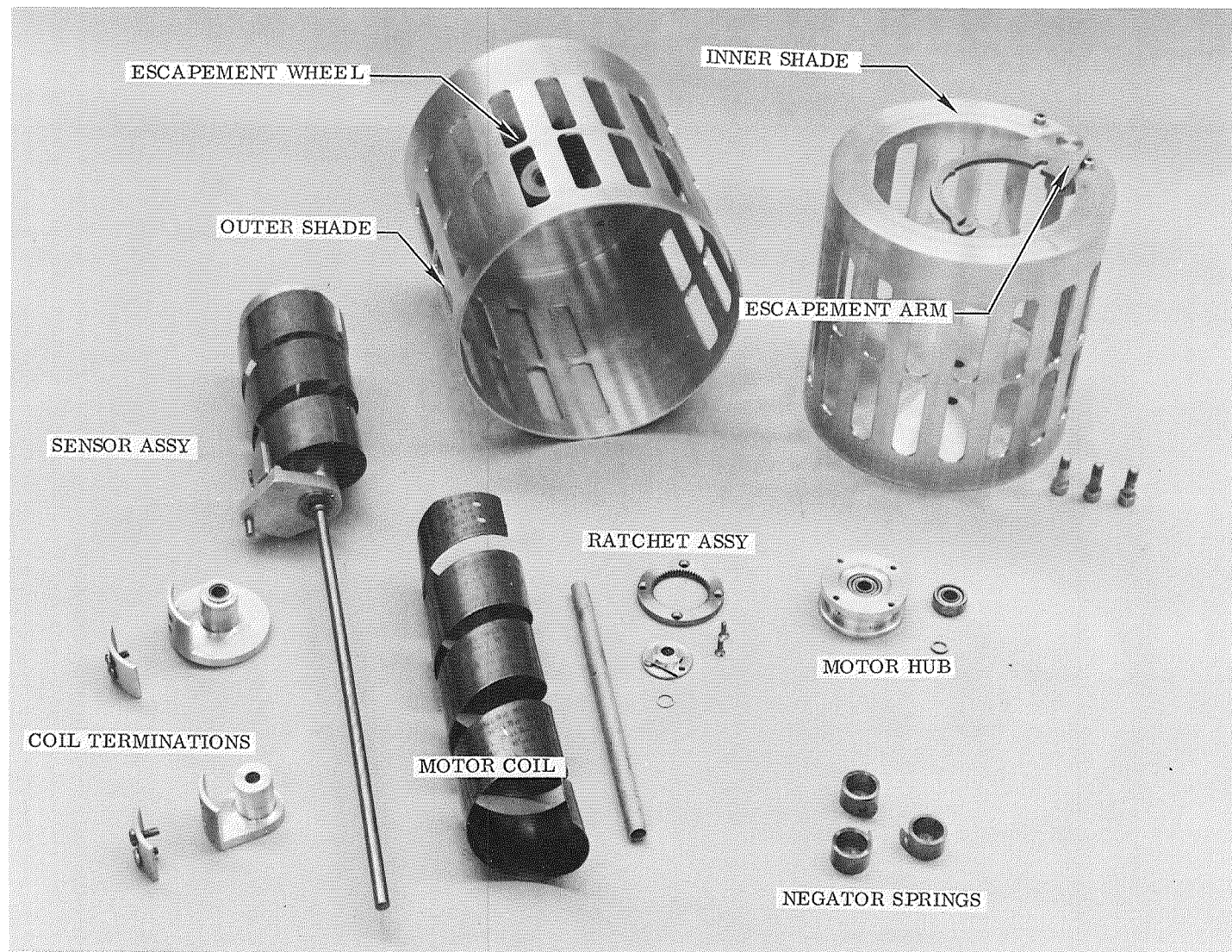


Fig. 34 Stored Energy Device Components



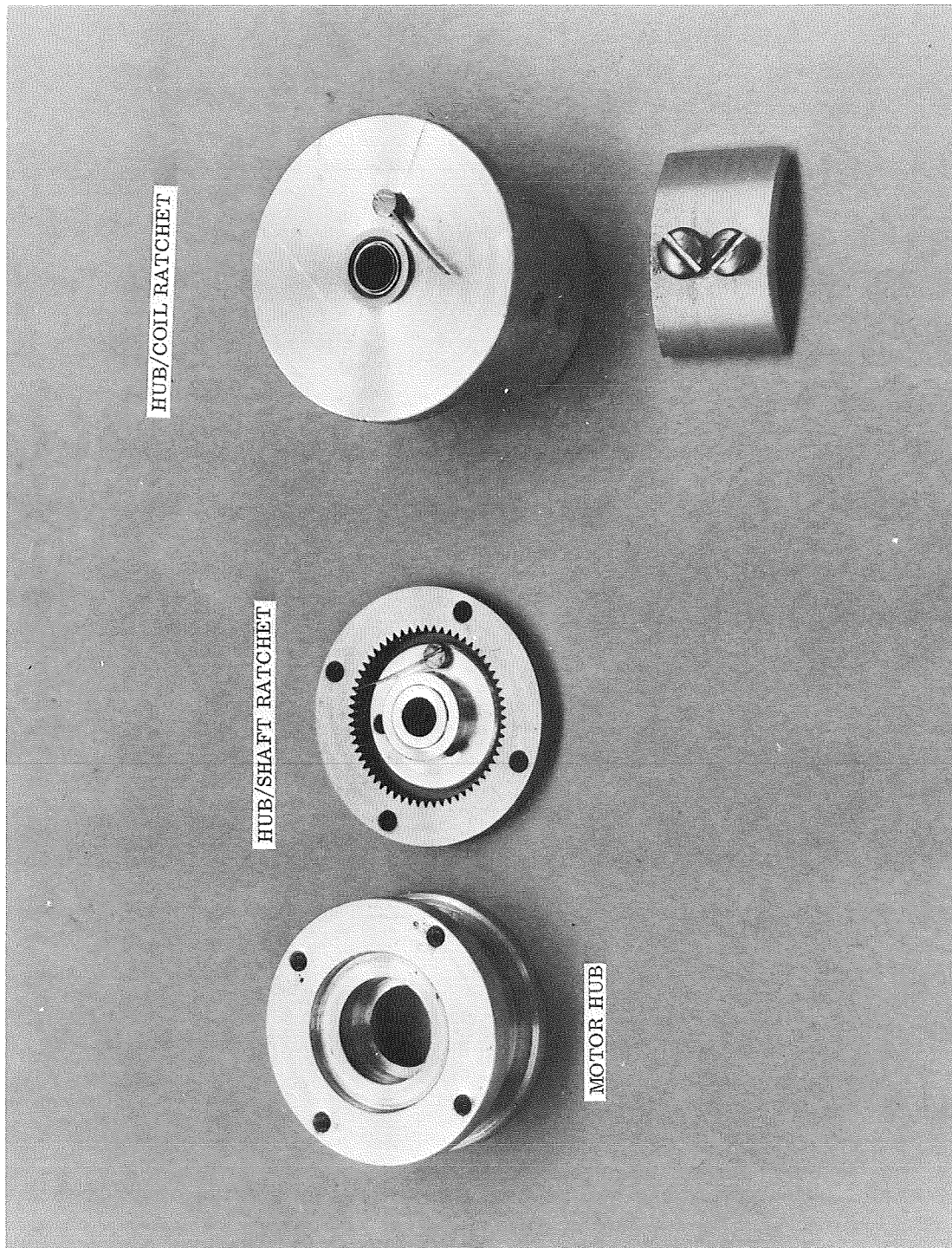


Fig. 35 Stored Energy Ratchet Assembly

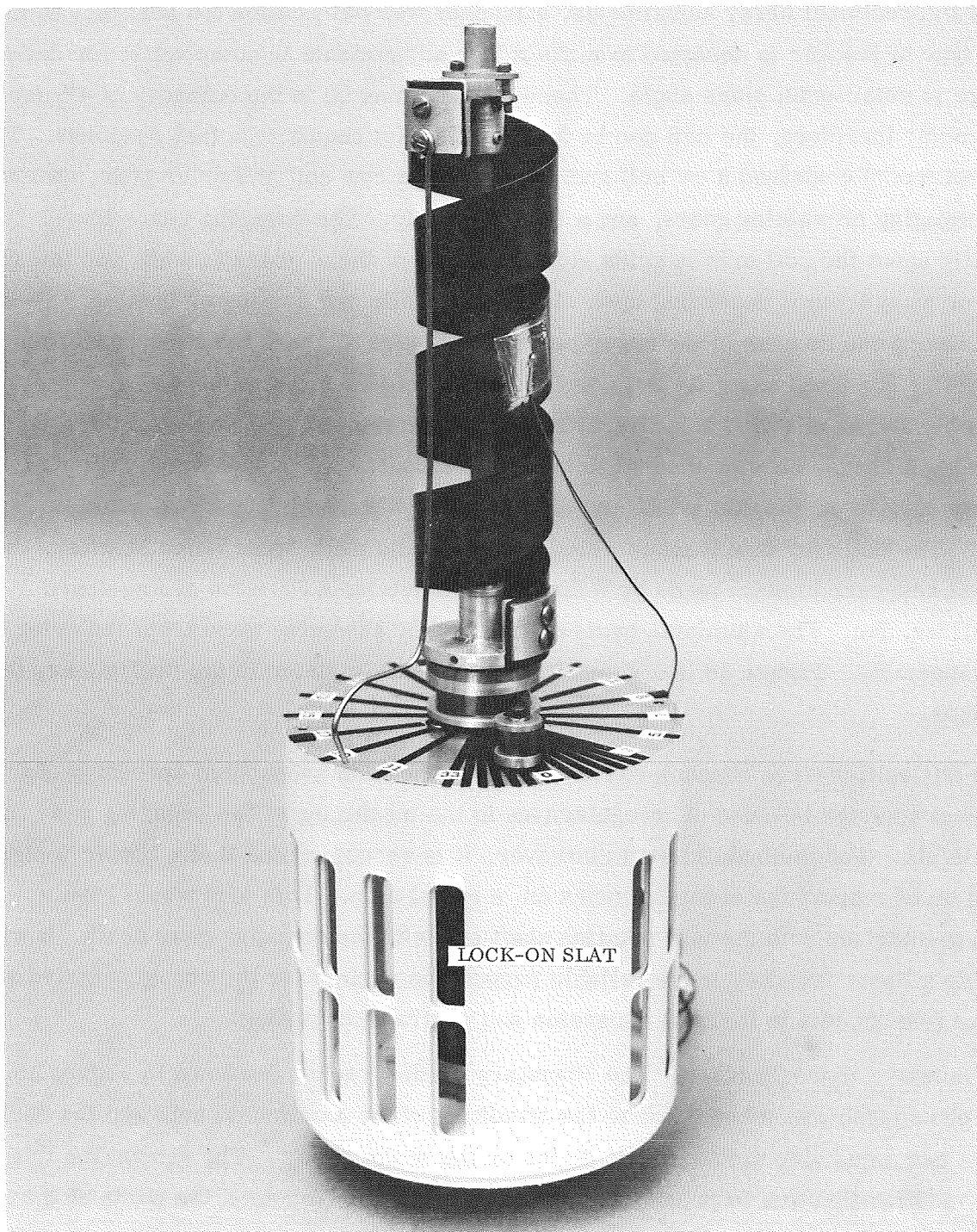


Fig. 36 Stored Energy Device (Test Configuration)



b. Seasonal Adjuster. In response to the requirement for a tracker which would make small bidirectional array adjustments, a tracker was built called the seasonal adjuster. This type of tracker is designed to make minor adjustments to compensate for daily change in polar-orbit plane angle. These changes may be in the category of  $4^{\circ}$ /day maximum; therefore, the coil can be fairly thick, not requiring a fast response. The concept model contained a cw coil and drive gear, a ccw coil and drive gear, cw and ccw engaging or walking gears, and a fixed sun gear. The engaging gears travel radially about the coil axis in guide slots which allow these gears to walk into the sun gear or away from it depending upon whether the coils are cooling or heating. These components can be seen in the upper portion of Figure 37, with the exception of the ccw coil. The fixed sun gear is locked to the vehicle such that the entire tracker assembly and an attached solar array rotate toward the solar vector until the assembly, including a shade, become normal to the solar vector. The model was built so a variety of shades, (length, width and displacement with shade supports) could be tried. The coils for this tracker were .060 thick and made from Wilco Morflex, the highest response bimetal made by Wilco Thermometals, a Division of Engelhard Industries, Inc. The aluminum parts of the tracker assembly were irridited prior to final assembly. Figure 38 is a view of the Seansonal Adjuster in the preliminary test chamber.

Some difficulties were encountered in the fabrication and subsequent operation of the seasonal adjuster because of irregularities in the machining of the engaging gear radial guide slots. The method did work; however, it is recommended that a better design would be to support the engaging gears on a radial arm. This arm would have a bearing interface with the coil rotation shaft and with the engaging gear shaft. It will provide a lower friction, more reliable suspension system for the engaging gear, and will be less subject to thermal expansion and contraction binding.

c. Planetary Shade Tracker. The Planetary Shade Tracker is shown in Figure 39. This photograph was taken prior to the irriditing of the aluminum parts and the addition of two adjustable slotted shade plates on the shade shown. The reason for this later modification was to provide the option of being able to adjust the width of the planetary shade.

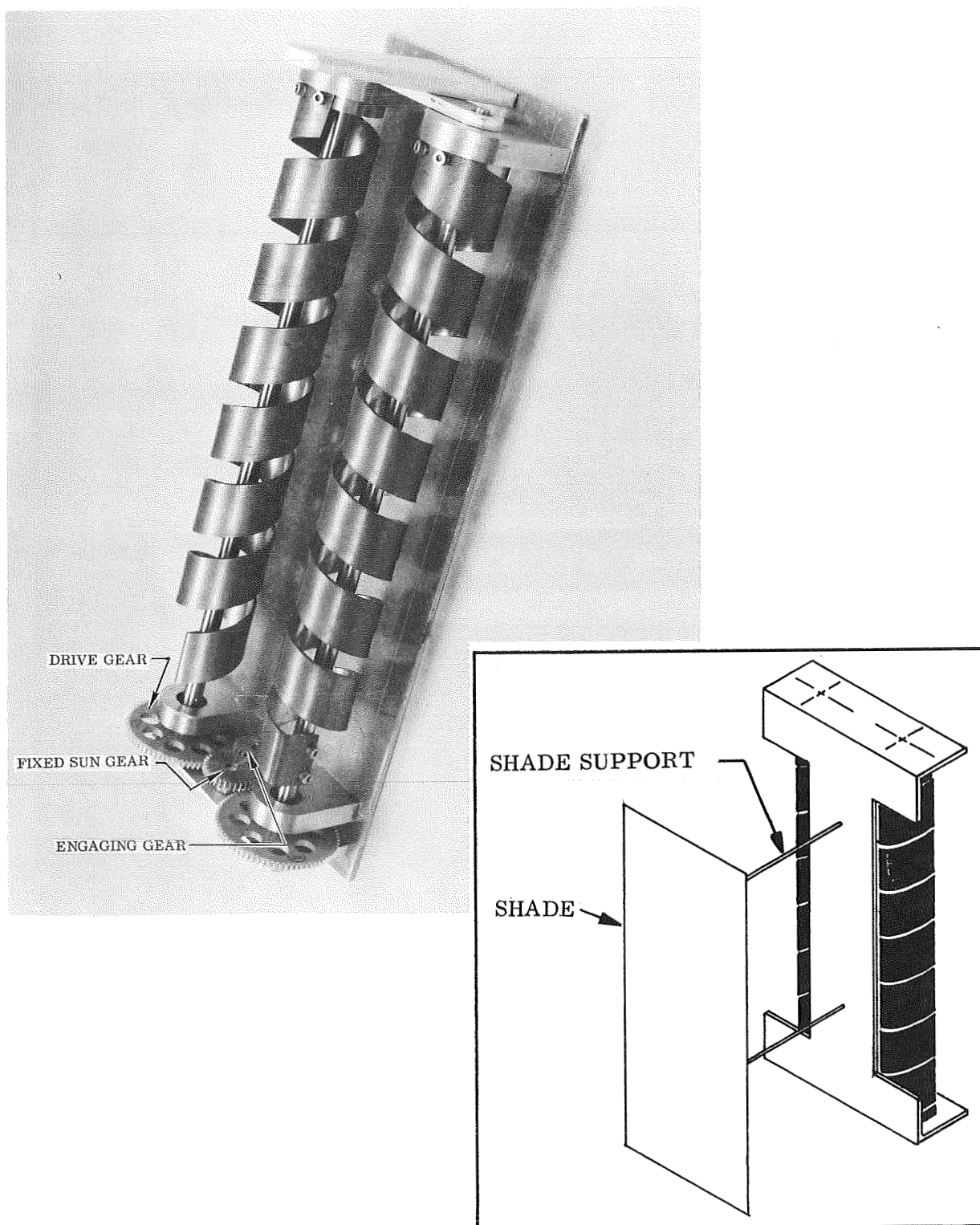


Fig. 37 Seasonal Adjuster During Fabrication

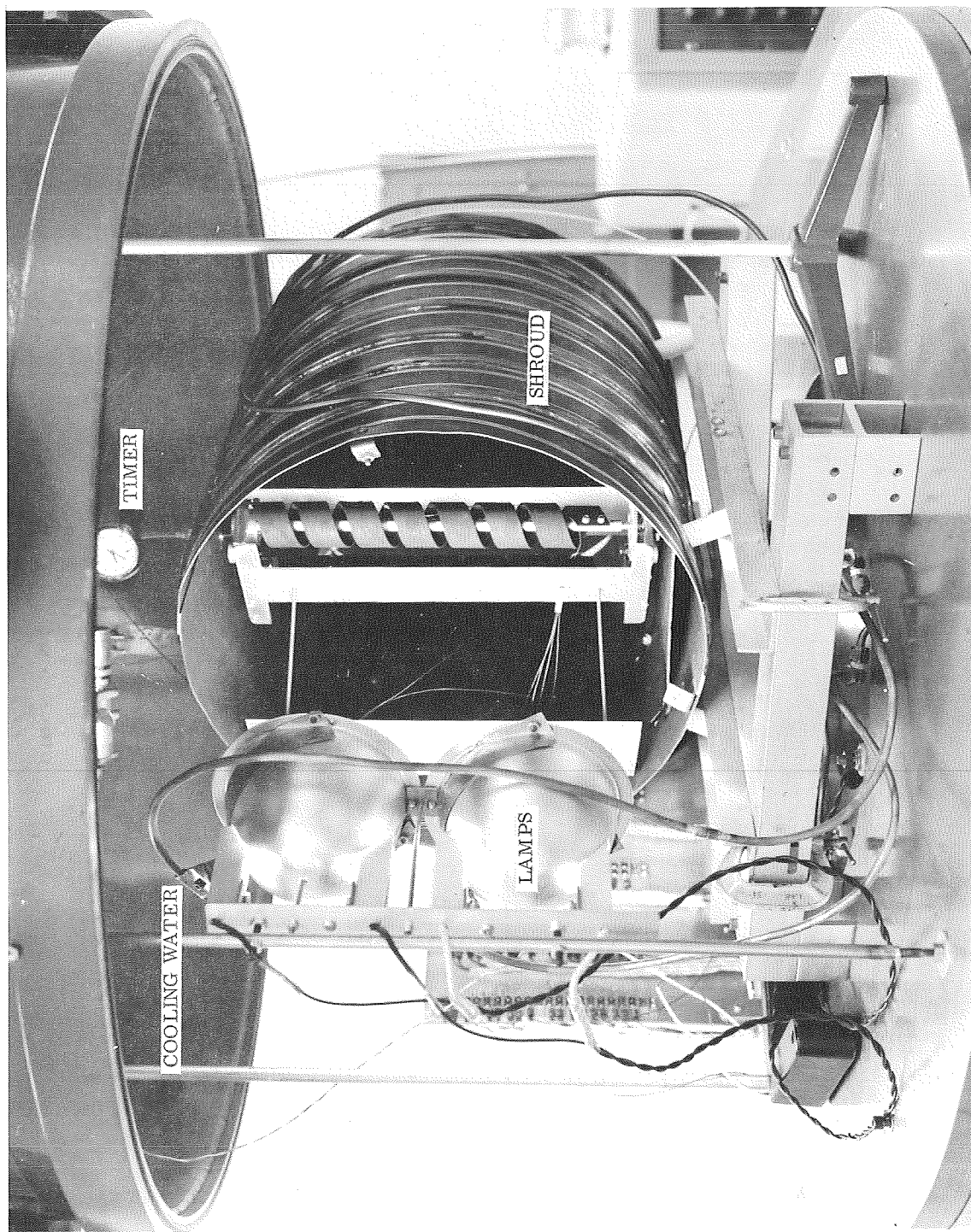


Fig. 38 Seasonal Adjuster in Test Chamber

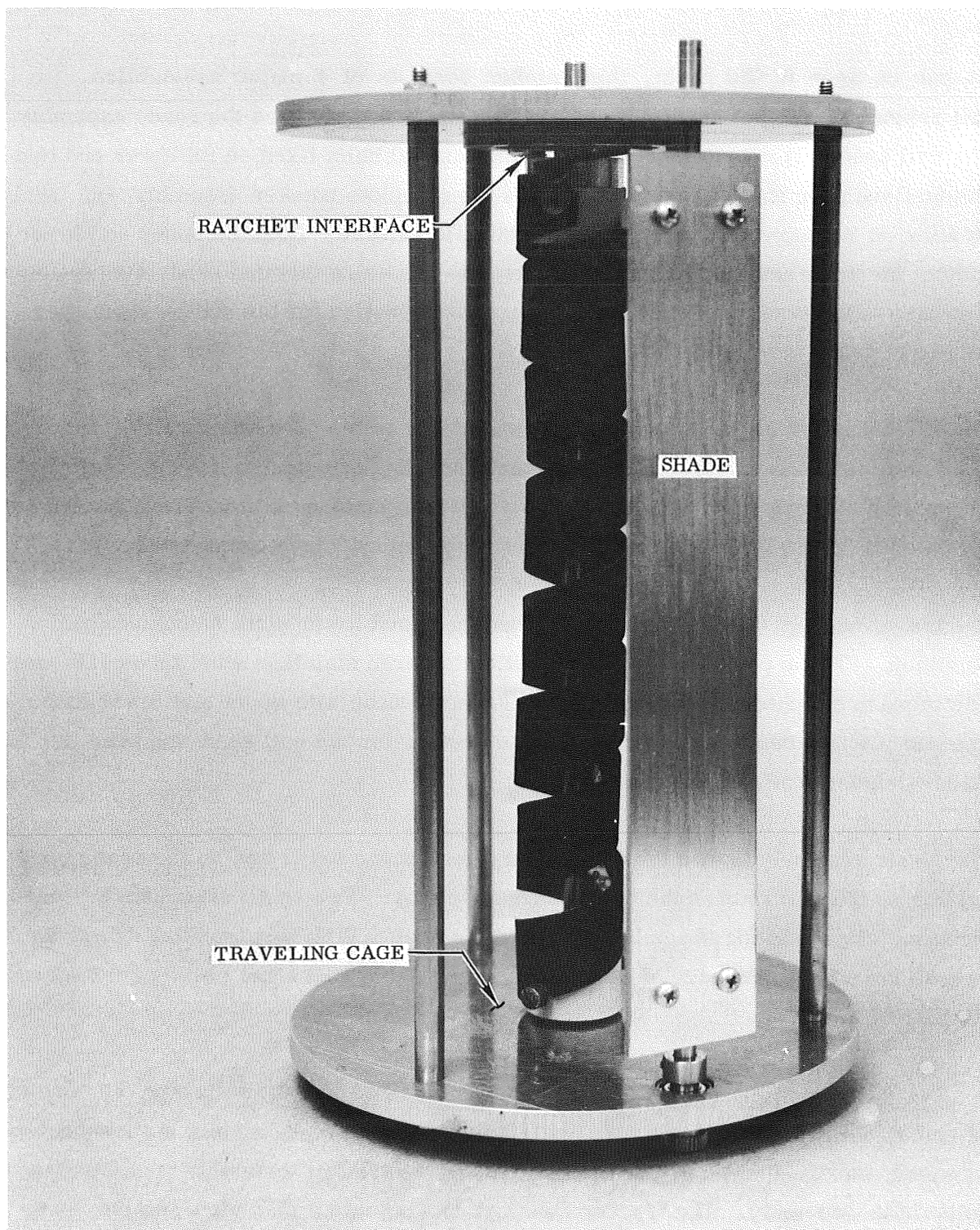


Fig. 39 Planetary Shade Device (Test Model)



As can be seen in the photo, this tracker consists of 4 major assemblies, the coil assembly, ratchet assembly, traveling cage assembly, and the shade assembly. The coil assembly consists primarily of the bimetal helix fixed on its lower end to a sun or fixed gear shaft (the center shaft of the complete tracker assembly) and freely rotating on its upper end in a bearing termination sleeve. Both the upper and lower ends of the helix are isolated with glass tape to minimize thermal conduction transients. The base of the tracker, which forms a fixed termination for the center shaft, is a large sun gear.

The ratchet assembly is mounted on the under side of the upper cage plate. It consists of an internal gear acting as a ratchet face, and appropriate spring steel ratchet fingers. For fabrication of concept models, it was more economical and timely to use internal gears in the ratchet assemblies than to machine special units.

The traveling cage assembly consists of an upper and lower plate machined from aluminum. These plates are held in position by three stainless steel tubes  $120^{\circ}$  apart. The tubes are locked in position by 8-32 threaded stock with upper and lower nuts. The end plates contain press fit bearings on center for the coil shaft and near the outer periphery for the shade assembly shaft.

The shade assembly uses a small planetary gear at the lower end so the shade plate rotates as the coil rotates the entire cage assembly. Two small aluminum threaded mounting clips held the shade base plate to the shaft. With this tracking device as well as the others, the size of commercially available gears and bearings influenced the size of the device.

d. Two-Coil Continuous Tracker. The unit fabricated, as shown in Fig. 40, contained one standard helix and one zero angle helix. The zero angle helix sprocket drive assembly was displaced farther from the top of the tracker assembly than the standard helix drive assembly. The tracker housing, looking into a plan view section, is S-shaped with oblong shaped end plates. The housing is fabricated from sheet aluminum, and the completed unit is symmetrical about a centerline with the exception of the difference in coils previously stated. The chain and sprocket drive system was selected to meet the requirement of having the array sensor rotate the same direction as the

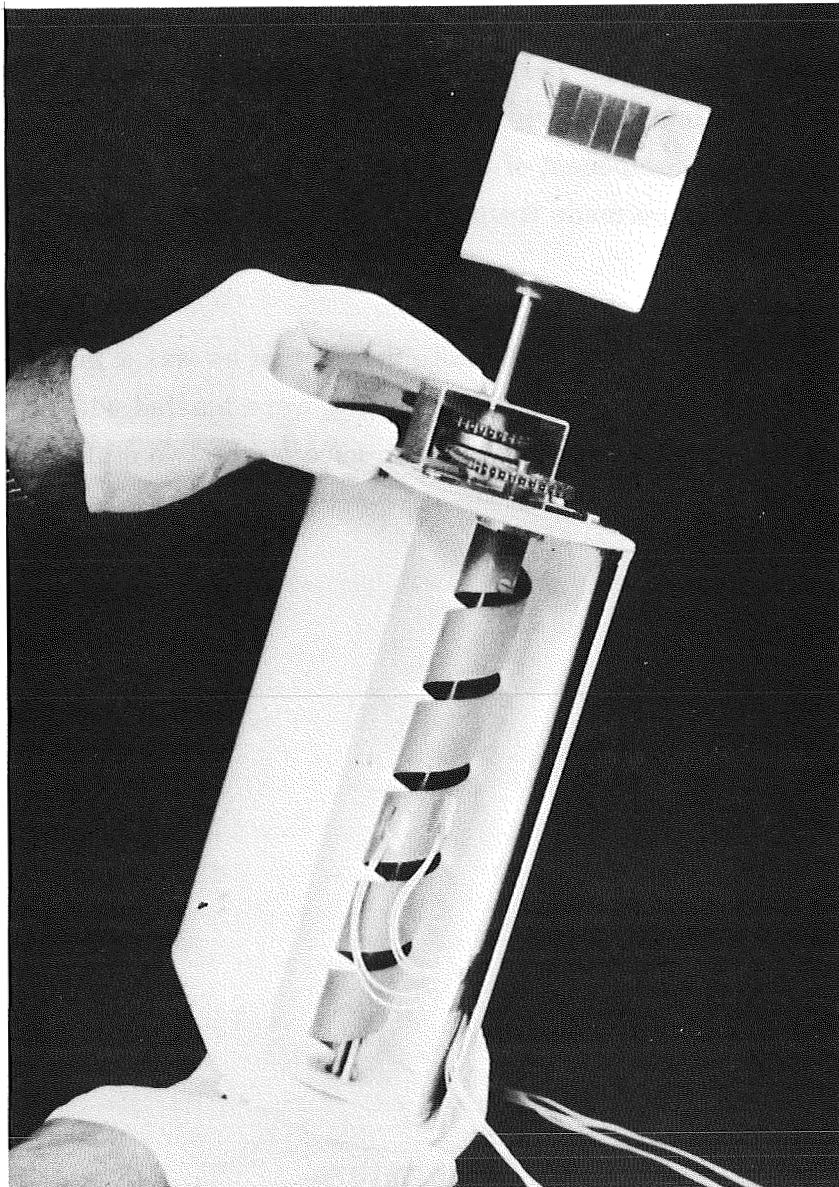


Fig. 40 2-Coil Continuous Tracker

coil free end and its feedback shade. This approach also was convenient in that the sprocket drive and driven gears could be changed to evaluate small ratio changes without affecting the distance between the gear center points. There are many moving parts in the chain so for a flight configuration it is recommended that an intermediate gear be used to affect correct rotation. The sensor or array drive shaft is bearing supported and terminates under a U-bracket in a single tooth pawl ratchet assembly. This assures that unidirectional and continuous output rotation occurs as each coil assembly is either heating and driving through the sprocket drive or cooling and resetting. The other main component of the tracker was the feedback shade. This shade is semi-cylindrical in shape made from sheet aluminum and fixed to the upper freely rotating end of the coils.

The shade assemblies are coated with white thermatrol as was a major portion of the S-housing. The concave portions of the S-housing were blasted with 2 mil glass beads to reduce reflection. This treatment was also used on the two coils to raise the  $\alpha/\epsilon$  ratio above that of the raw processed stock.

## E. DEVICE TESTING

### 1. Preliminary Testing

To check the operation of heliotrope models, preliminary thermal vacuum tests were performed on three models. These tests were conducted informally in a bell jar vacuum setup. The object was to identify 'bugs' which might occur in final testing so that modifications could be made and procedures identified. The preliminary tests were inexpensive and helped prevent delays and downtime when final testing was performed in a controlled environment.

a. Summary of Tests. Three models were tested, and in short, the results are as follows. The seasonal adjuster oriented itself to the light source from an arbitrary 40 degrees off-angle in 90 seconds to four minutes, depending on coil reflector configuration. Error angle was visibly less than 5 degrees. This device would provide adequate seasonal tracking for a solar array. The planetary gear device oriented itself to the light source from an off-angle of 90 degrees and provided tracking motion, as designed. Tracking motion was somewhat erratic because of an undersized coil. The stored energy device functioned as designed. It provided orientation capability from any degree of initial off-angle and 10 degree incremental sun tracking.

b. Test Setup. The experimental test setup for preliminary testing is illustrated in Fig. 41. A 36-inch diameter bell jar provided a vacuum environment of  $8 \times 10^{-5}$  to  $2 \times 10^{-4}$  torr. Pumpdown time was about 35 minutes. A cylindrical copper cooling shroud 16 inches in diameter was placed with its axis horizontal and at a 45-degree angle, with the 12-inch observation ports. Two colortran B10-32 lamps with parabolic reflectors were used as a sun simulator. The lamps were water cooled and provided a partially collimated light source. Intensity was checked in the test plane by a constant temperature secondary standard solar cell and related directly to lamp current. Simulator current was monitored throughout the tests and variation in the test area was within 10 percent. These lamps radiate more infrared energy than the solar source, so the intensity was possibly thermally higher than one sun. A DC gear-motor was used to allow in situ positioning of test specimens. The motor drove each model



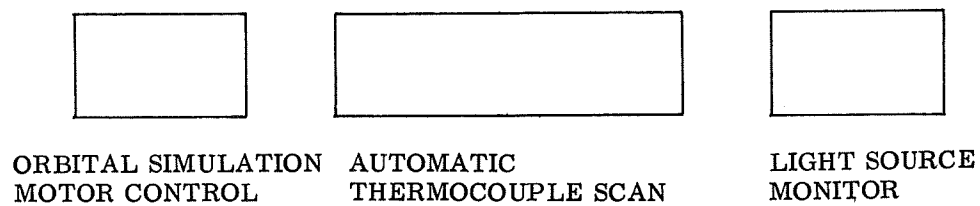
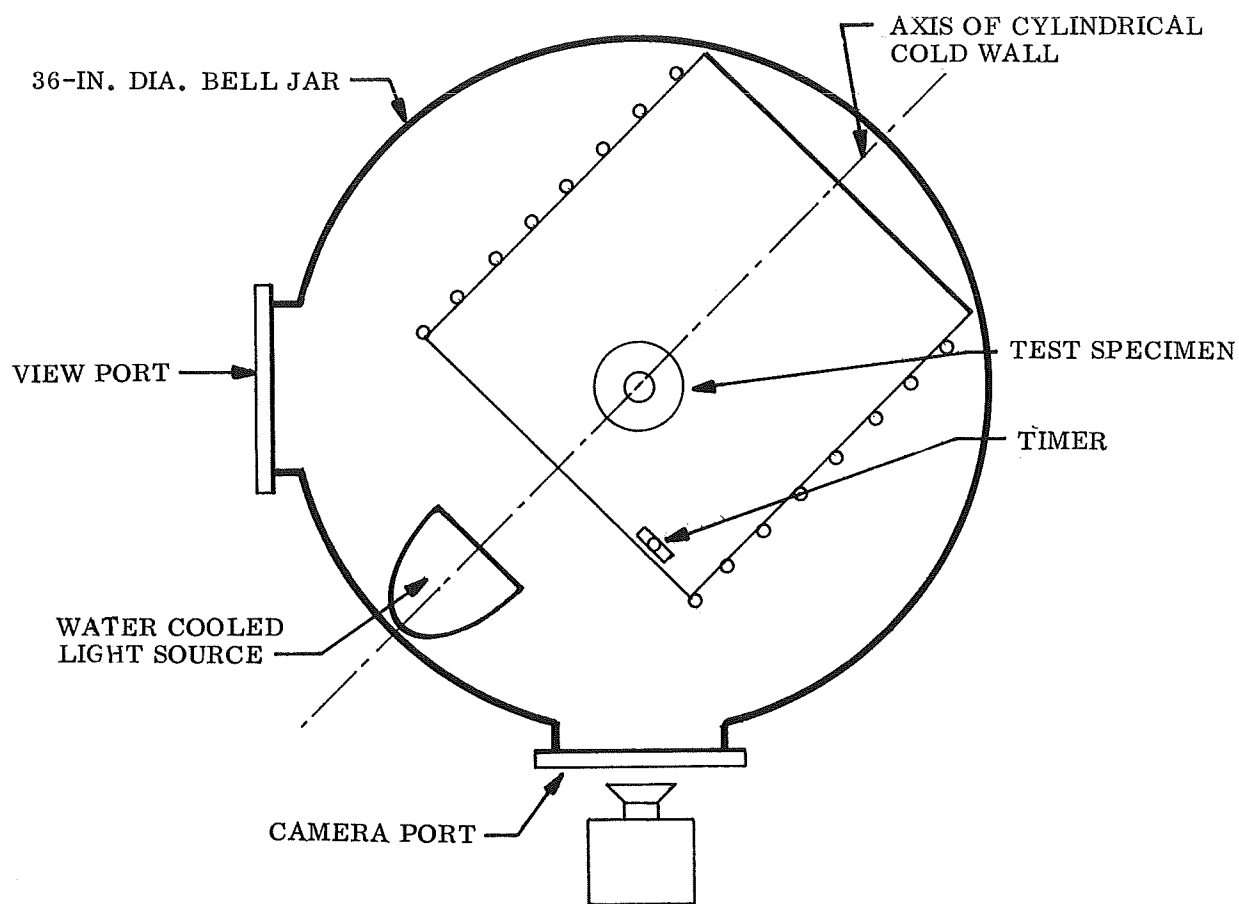


Fig. 41 Preliminary Test Setup

through a flex shaft arrangement and could be used to simulate an accelerated orbital rate (7 degrees per minute - synchronous rate is 0.25 degree per minute and 8100 nm orbiting vehicle is about 0.7 degree per minute). The motor had copper cooling straps to the  $\text{LN}_2$  shroud to prevent overheating should it be used continuously. A pocket watch was installed in the chamber so that it provided a time reference in the test movie. Four thermocouples on each model, one on the motor, and one on the cooling shroud, were scanned continuously by a Honeywell Electronik-16 recorder. Time lapse photography was used to document specimen position versus time.

c. Model Tests.

Seasonal Adjuster Test. Prior to the first Seasonal Adjuster test, the device was installed in the chamber as shown in the photograph, Fig. 38. One mounting screw also served as an anchor for the stationary sun gear. Since this screw was not securely tightened, the sun gear was free to rotate, and the device would not move relative to the light source. Camera documentation shows only movement due to the positioning motor. Temperature records were obtained, however, and visual observation indicated a need for a shade extension to prevent illumination of both bimetal coils simultaneously. This situation would cause engagement both coils and greatly hinder tracking due to binding. For the second seasonal adjuster test, the sun gear was properly fastened and the shade modified to prevent illumination of both coils. A foil reflector was placed behind one coil to study its effect on coil heating rate. The reflector may be seen in photograph, Fig. 38, prior to test and Fig. 42a. Initially, the device was misoriented an angle of 40 degrees, as shown in Fig. 42b. Upon illumination, the tracker oriented itself within 90 seconds of elapsed time. The device was then allowed to cool and motor driven to the position shown in Fig. 42c. The simulator was turned on, and the device oriented itself fully in about 5 minutes (1.7 minutes to start rotation and 4 more minutes to fully orient). Film coverage was not available for the second test.

Planetary Gear Device. The device shown in Fig. 39 was placed in the chamber with an initial misorientation of 90 degrees. The device oriented itself in less than 60 seconds. The orbit simulation motor was then started, and the device tracked the light

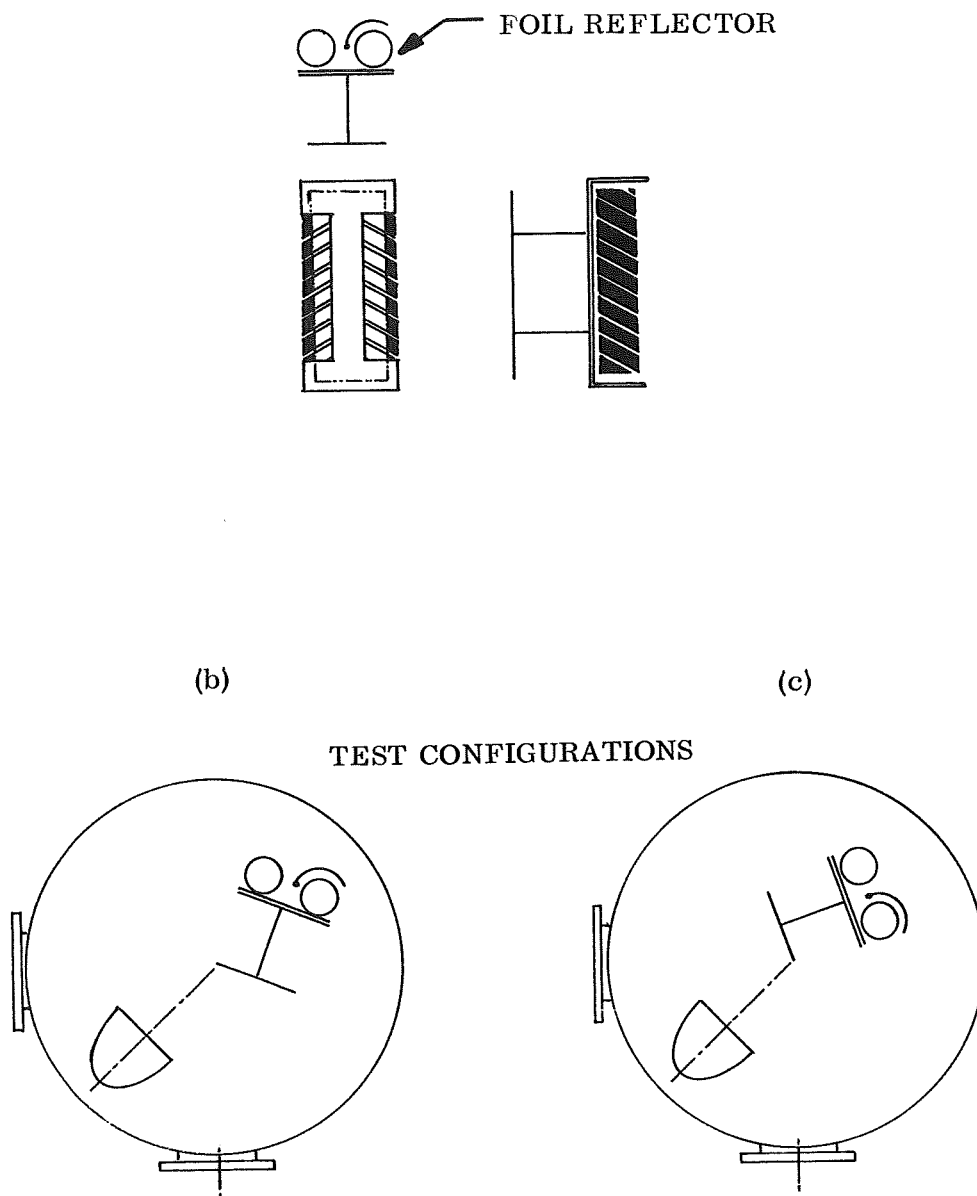


Fig. 42 Preliminary Seasonal Adjuster Tests

source. Tracking action on this device, as witnessed by time lapse photography, was erratic because of an undersized bimetal coil. The torque capability of the thin coil was not adequate to provide smooth tracking, so a thicker coil was incorporated for the final testing. No thermocouples were attached to this model during the preliminary tests.

Stored Energy Device. The stored energy device shown in Fig. 36 was initially mis-oriented 270 degrees from the light source. The simulator was turned on and a sunseek function occurred in 10-degree increments for 60 degrees of rotation, at which point the test was terminated. Heat input from the simulator caused the small cooling shroud to warm from  $-295^{\circ}\text{F}$  to  $0^{\circ}\text{F}$  during the test period of 70 minutes. This reduced sensor coil cooling rate and affected tracker response. A second test was run on the device after modifying the shroud slightly and a 60-hour vacuum soak at  $10^{-4}$  torr. (See Fig. 43 for simulated altitude.) The device was misoriented 60 degrees before the simulator was started. Initial orientation rate was about 2-degrees of arc per minute for this particular model in the partial coldwall environment. The

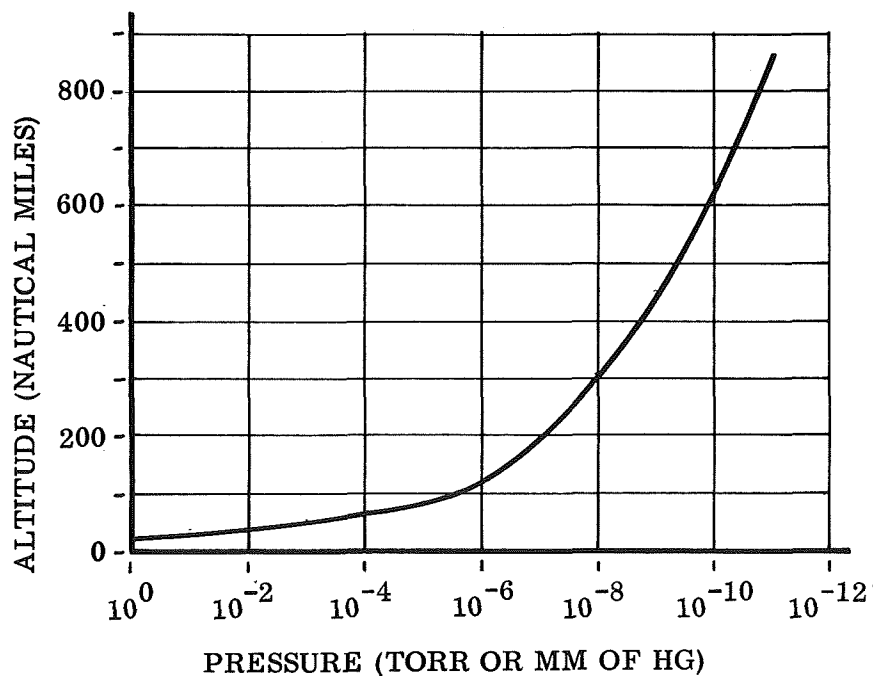


Fig. 43 Vacuum Chamber Simulated Altitude

device oriented itself 60 degrees and locked on the light source. At this point, the drive motor was started at an accelerated rate of seven degrees per minute to simulate array misorientation ("turn" zone on Fig. 44). The device again started tracking. During all of the test operation, temperatures are monitored. One readout is plotted in the figure.

On Fig. 44, the letter C indicates a closing of the shade assembly and 0 indicates an opening. The temperature plots are for thermocouples on the motor coil, sensor coil, outer shade, and coldwall shroud. Note the increase in shroud temperature caused by simulator heat input. Lamp current was varied to help control the effect of an imperfect cold wall. The motor coil performed as designed, providing a winding motion to the negator spring with temperature variations.

d. Test Configurations

Model	Seasonal Adjuster	Planetary Gear	Stored Energy
Coil Coating	A, B	A, B	E
Structure Coating	F	None	C
Shade Configuration	H	I	J
Reflector Configuration	J	None	None
Instrumentation	K	L	K, L

- A. Yellow Zinc Chromate Primer, MIL-P-8585A (air dry)
- B. 3M Velvet Coating, No. 101-C10 Black (baked on)
- C. 2A-100 White Thermatrol, PB-105-101 (air dry)
- D. Sonic Cleaning in MEK and Alcohol
- E. LMSC Oxidization Treatment
- F. Bare Sanded Aluminum
- G. Foil Reflector Behind Coil
- H. Closed Shade Support
- I. Centered Shade
- J. Concentric Cylinders
- K. 4 Thermocouples on Model
- L. Photo Coverage

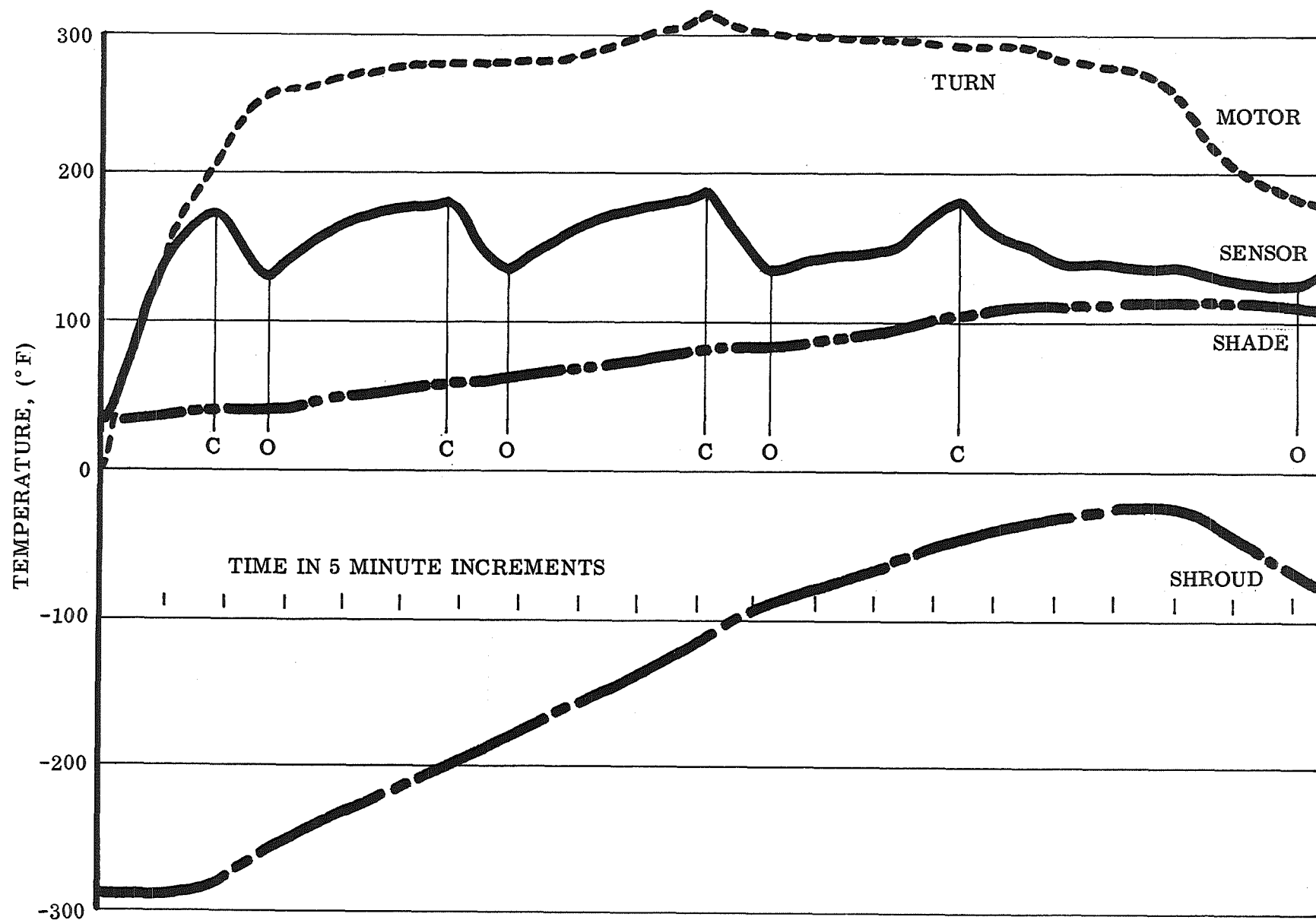


Fig. 44. Temperature Plot for Stored Energy Device

## 2. Final Testing

In addition to the three models examined during the preliminary testing, a fourth, the 2-coil continuous tracker, was tested during the final runs. These tests were performed in an accurately controlled vacuum cold wall environment.

a. Summary of Tests. Figures 45 through 48 show a summary of the final test results. The stored energy device was tested first after being set to actuate at temperature different from those on the preliminary tests; however, the setting was found to be still too high. After simulator adjustment to account for this, the device performed as designed with temperature traces as illustrated in Fig. 45. The seasonal adjuster performed perfectly at four different initial temperatures (Fig. 46). Operation of the Planetary Shade tracker was also successful with several tracking and reset cycles taking place (Fig. 47). The 2-coil continuous tracker provided ideal thermal data and initial tracking (Fig. 48). The orbit simulation motor, however, was too fast to allow complete ratchet reset, and thus the output sensor was not always oriented.

b. Test Setup. The final tests were held in the Palo Alto Search Chamber facility. The chamber and simulator are shown in Fig. 49 during the test. A Honeywell data system recorded temperatures of test specimens at finite scan intervals and printed them out via a teletype unit. The chamber has full  $\text{LN}_2$  coldwalls and ends and vacuum of  $10^{-6}$  torr. Models were generally mounted the day before a test and an overnight chamber pumpdown and vacuum soak performed. Nitrogen cooling was initiated about 2 hours before testing. Sun simulation was provided by a Genarco ME4W carbon arc simulator with calorimeter disks supplying intensity readouts. This simulator has a test area well over the entire specimen envelope. Photo documentation was available by viewing through a sideport in the chamber wall slightly in front of the test plane.

### c. Model Tests

Stored Energy Tracker. Referring again to Fig. 45, several items of interest were noted. On the sensor coil trace, the first inflection point is a change in simulator

intensity. Due to the coil adjustment, it was necessary to increase intensity above 1-sun in order to reach actuation temperature. This problem could be remedied by further adjustment of the coil or altering the thermal coating. Use of an anodized titanium flash on the coil will increase  $\alpha/\epsilon$  ratio several times and thus raise the upper equilibrium temperature considerably above that necessary to actuate the sensor-escapement assembly. Note a valley just prior to the first temperature peak in Fig. 45; this was caused by movement of a shade slat in front of the incoming solar flux, thus shading the sensor coil. The movement was simulated orbit motion provided by a D.C. gearmotor rotating the entire test assembly. This valley does not adversely affect operation of the tracking device but could be reduced by having smaller shade slats (more increments of tracking per orbit). As the first peak is reached with the shade assembly in the open position, the escapement was actuated by the sensor coil, thus providing 10 degrees of tracking and closing the shades. Cooling of the sensor again actuated the escapement and another 10 degrees of tracking took place. This cycle repeated several times until the device was oriented from its initial off angle of 60 degrees. After orientation, tracking took place at the average orbital rate (in this case, 1 degree/minute).

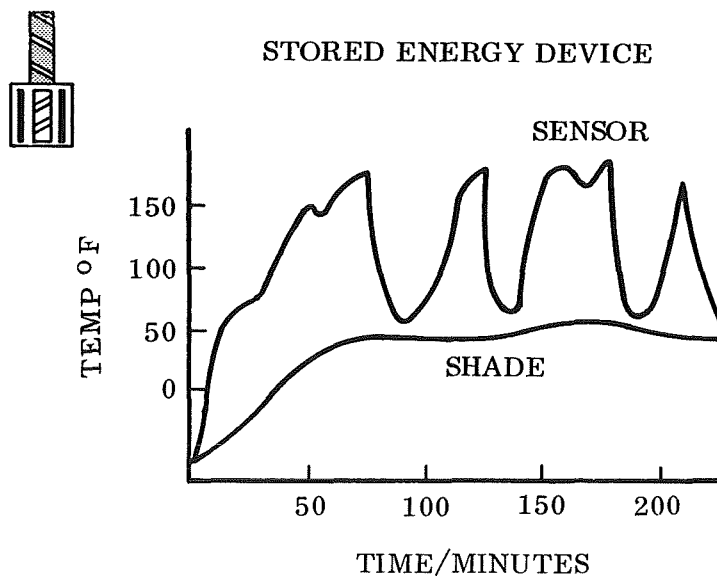


Fig. 45 Stored Energy Device



### 3. Seasonal Adjuster

The seasonal adjuster was modified slightly from the preliminary test configuration by including a foil shield between the outer shade and the base to prevent both coils from being illuminated at the same time. The device was instrumented with thermocouples and tested four times, each from a different initial temperature. Fig. 46 shows the temperature plot of the active (A) and passive coils. From an initial misorientation of 45 degrees, the active coil increased in temperature rapidly while the passive coil remained constant. The active unit engaged the walking tear system and oriented the device. After orientation, the active coil reached equilibrium and the passive coil became slightly illuminated during the lock-on phase. This explains the slight increase in passive coil temperature. The orientation cycle was repeated three more times to study the effect of different operating temperatures. The assembly ran extremely cold ( $-50^{\circ}\text{F}$  the highest temperature reached) but performed well and provided the same shape temperature trace for any operating temperature thus indicating that this device is not sensitive to operating temperature. Orientation time was typically in the order of three minutes for an angle of  $45^{\circ}$  degrees.

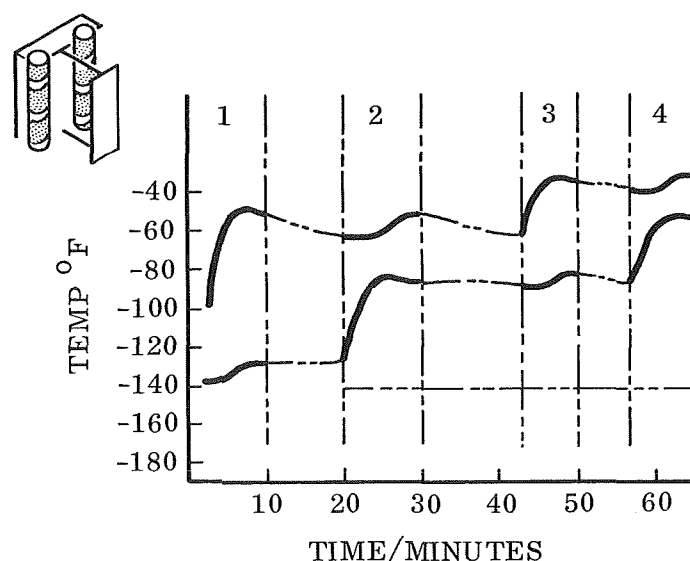


Fig. 46 Seasonal Adjuster

#### 4. Planetary Shade Tracker

Addition of a thicker coil and a reflective shade element were considered necessary for final testing of this unit. The coil itself was instrumented for temperature in order to monitor reset which was difficult to notice by eye or camera. Figure 47 is a plot of the coil temperature from an initial misorientation of 100 degrees of arc. The device oriented in less than six minutes and remained facing the simulated solar source while being rotated by the orbit simulation motor at 1 degree/minute. After initial orientation, multiple tracking-reset cycles occurred as evidenced by the temperature plot. It should be noted that this device also is rather insensitive to operating temperature. Each negative slope portion on the plot represents a portion of coil reset through the ratchet, and each positive slope portion is a small tracking increment. Accuracy of orientation was visibly within 5 degrees of arc.

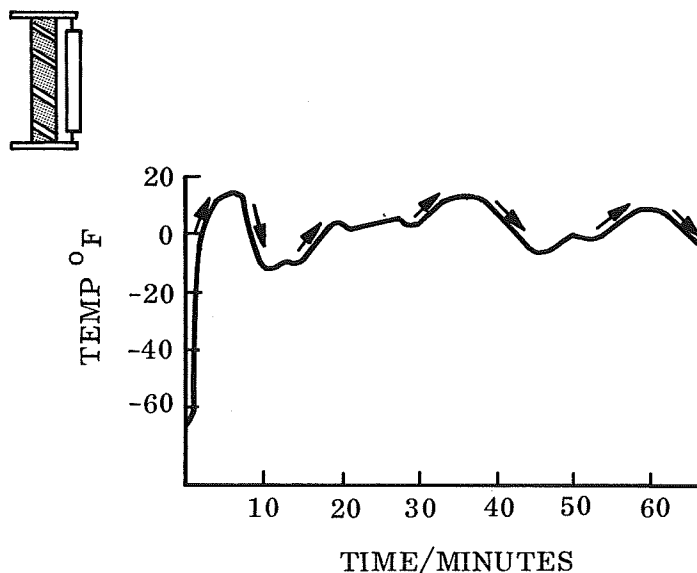


Fig. 47 Planetary Shade

## 5. 2-Coil Continuous Tracker

The 2-coil device was placed in the chamber with the sensor initially misoriented 10 degrees of arc. Initiation of the simulated solar flux oriented the sensor within 3 degrees of normal, and tracking occurred as expected. Figure 48 shows the temperature plot for each of the two coils; one is the helical coil (H), and the other is the zero-angle coil (Z). Both coils performed well. The plot shown is extrapolated after several identical cycles.

The orbit-simulation motor was operated at several speeds, the slowest rate being 1 degree/minute. Tracking initially took place, but the device was not given enough time to reset the cooling coil (orbit motor too fast). This could be easily remedied by either lengthening the coils 10%, changing the sprocket drive slightly, or allowing the orbit motor to operate more slowly (synchronous rate would be 0.25 degrees/minute, but the test would have taken four days). After the test, the gear ratio was changed. Results of the test indicated successful operation of both coil types in conjunction with the feedback shade system. Temperature cycles were identical for every orbit revolution. The coils operated within the temperature range for optimizing bimetal work.

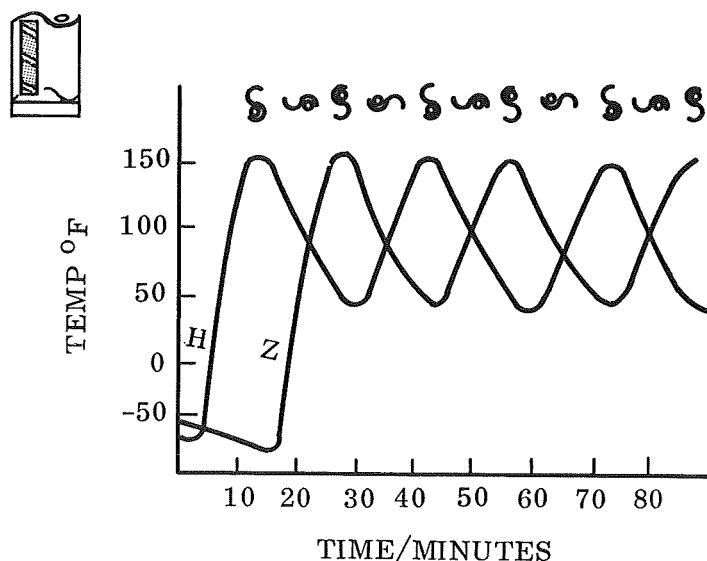
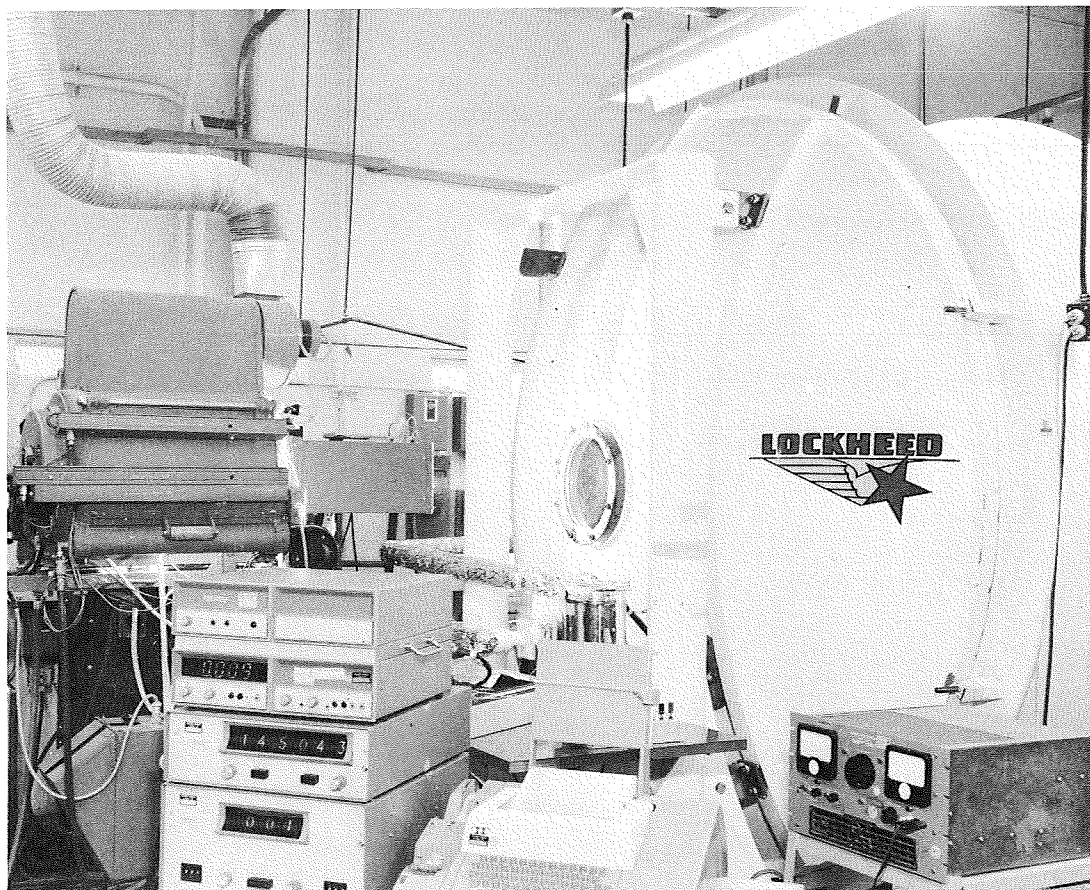


Fig. 48 Coil Continuous



ENVIRONMENTAL TEST FACILITY USED FOR OPERATIONAL  
TESTS ON THERMAL HELIOTROPE DEVICES

- o GENARCO ME4W CARBON ARC SUN SIMULATOR
- o FULL LN<sub>2</sub> COLDWALL VACUUM CHAMBER,  
8 BY 16 FT
- o HONEYWELL AUTOMATIC DATA SYSTEM
- o PHOTO DOCUMENTATION PORTS

Fig. 49 Test Facility



### SECTION III

#### NEW TECHNOLOGY

During the contract study period, six items of new technology were developed. The stored energy tracker is a continuous tracker that incorporates the use of two bimetal helices, one as a motor coil that winds a negator spring assembly and one as a sensor coil that activates an escapement. The escapement allows spring assembly/array rotation in discrete increments as a function of alternate illumination and shadowing via concentric cylindrical slotted shades. The 2-coil continuous tracker is another continuous device but provides tracking without incremental motion. One coil supplies tracking power during half an orbit while the other resets from a previous tracking cycle. The bidirectional 2-coil device is an incremental tracker capable of tracking the sun in either direction about the axis of rotation. A controlled escapement prevents rapid incremental movements. Still another continuous tracking device was designed called the planetary shade tracker. This device is a single coil tracker with a rotating shade for reset functions. A synthetic sunflower, the true (or mechanical) heliotrope, was devised consisting of series mounted curved bimetal strips in a triform configuration. This device seeks solar flux in any axis within a given range of adjustment. A method for eliminating axial motion from helical coils was developed also. The new coil design is called the non-helical helix and allows smaller winding diameters and better volume packing considerations. Each of these items are described in detail in Section II of this report.



## SECTION IV

### CONCLUSIONS AND RECOMMENDATIONS

#### A. CONCLUSIONS

##### 1. Earth Orbiting Applications

- Counter clockwise, unidirectional tracking will satisfy the majority of earth orbit tracking rotation requirements.
- Low orbit rates associated with earth orbiting applications result in very low array inertia torque requirements for thermal trackers. The predominate torque requirement is to overcome the friction of the bearing and power transfer systems used with a specific design.
- Single axis tracking appears more compatible than full two axis tracking for Thermal Heliotropes.

##### 2. Thermal Heliotrope Design

- Thermal torque capacity of a bimetal helix varies directly with temperature change, element width and the square of the element thickness. Thermal response varies directly with element thickness, a thinner coil being more responsive.
- Coil thermal response can be optimized through the use of appropriate thermal coatings. Better cooling or resetting response occurs from the device being at a high equilibrium temperature, this resulting from use of coatings that have high absorptivity and low emissivity.
- A variety of both continuous and reset Thermal Heliotrope trackers are feasible based on those designs evolved in this contract.
- Where high torque requirements exist, stored energy trackers and torque multiplier concepts are available.



## B. RECOMMENDATIONS

- Based on the progress achieved in this contract, additional investigations should be conducted to optimize thermal coatings.
- Pertinent data can be obtained by performing inertia simulation and life tests.
- The work accomplished on Thermal Heliotropes has demonstrated their feasibility. They should next be considered for earth orbit or lunar based experiments in flight configurations

SECTION V  
BIBLIOGRAPHY, REFERENCES, AND ACKNOWLEDGEMENTS

A. REFERENCES

1. A Passive Solar Panel Orientation Servo Mechanism  
R. L. Samuels  
3rd Aerospace Mechanisms Symposium Proceedings  
May 24, 1968, p 14-1
2. Thermal Heliotrope: A Passive Sun Tracker  
R. C. Byxbee and D. R. Lott  
4th Aerospace Mechanisms Symposium Proceedings  
May 23, 1969, p 13-1
3. Slip Ring Proposal  
Electro-Tec Corp,  
Blacksburg, Va.  
Inquiry No. 41-22510-E  
May 12, 1967
4. Mechanics-Dynamics  
J. L. Meriam  
Wiley & Sons, N.Y., 1959  
p 283
5. Fundamentals of Thermostat Metals  
R. M. Sears  
Materials Research and Standards, Vol 3, No. 12, p 981  
ASTM, 1963
6. Analysis of Bimetal Thermostats  
S. Timosheuko  
J of American Optical Soc., Vol 3, p 233  
Sept 1925
7. Method of Test for Flexivity of Thermostat Metals  
ASTM Standards, Part 3, B106  
1961
8. Maximum-Work Bimetals  
C. F. Alban, etal  
Machine Design, April 16, 1959, p 143

9. Bulletin TRU-40  
Texas Instruments Inc.  
Metals & Controls Division
10. Bimetal Rotary Heat Engine  
J. L. Adams  
Machine Design, June 12, 1969, p 128

#### Design Catalogs

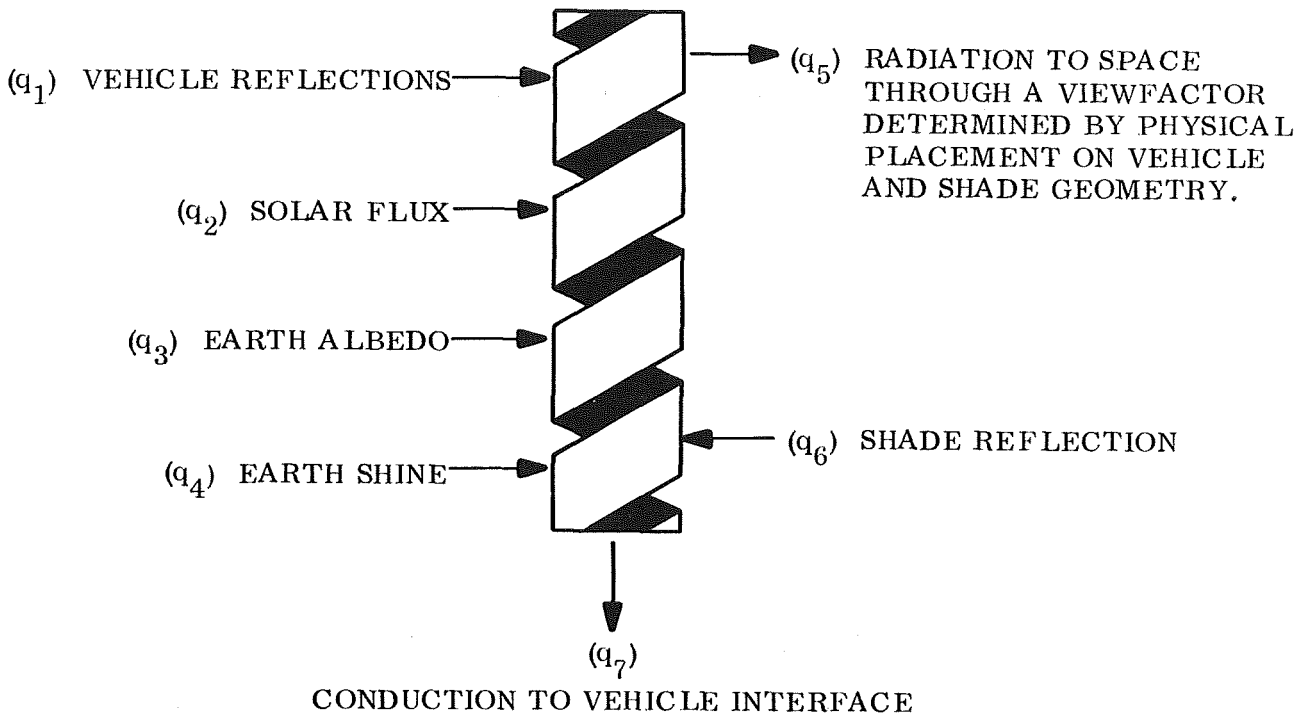
11. Truflex Thermostat Metals,  
Catalog TRU-1, 1957  
Metals and Controls Inc.  
Division of Texas Instruments Inc.
12. Wilco Thermometals  
Data File  
Engelhard Industries Inc., Newark, New Jersey
13. Thermostatic Bimetals  
Design Catalog  
W. M. Chace Co., Detroit, Michigan

#### B. ACKNOWLEDGEMENTS

The following personnel provided support to NAS5-11637:

Dan R. Lott – Project Leader  
R. Crawford Byxbee – Principal Investigator  
Leonard A. Haslim – Thermal Coatings  
Gene Troendle – Test Models  
Carl A. Jernberg – Test Support  
Lee A. Child – Test Support

Appendix A  
THERMAL ANALYSIS



The heat fluxes shown above were simplified to consider only solar flux input and radiation to space zero sink output (q<sub>2</sub>, q<sub>5</sub>) for the purposes of calculation. The simplified equations give an indication of the relative merit of various  $\alpha$  and  $\epsilon$  values associated with thermal coatings.

A more realistic feeling for thermal response will be obtained by model testing, which can form the basis for a more rigorous thermal model of any given tracker if required.

The basic radiation heat transfer equation

$$Q = \sigma A \epsilon \left( T_c^4 - T_s^4 \right) \quad (A-1)$$

was equated to the transient heat flow equation

$$Q = m c \frac{dT}{d\tau} . \quad (A-2)$$

As sink temperature ,  $T_s$  , is ideally zero the expression for cooling time becomes

$$\tau = \frac{m c}{3 \sigma A \epsilon} \left( \frac{1}{T_f^3} - \frac{1}{T_i^3} \right) . \quad (A-3)$$

$T_i$  was taken as the upper equilibrium temperature with a one-sun solar flux input:

$$T_i = \left( \frac{\alpha}{\epsilon} \frac{S A_p}{A_t} \right)^{1/4} \quad (A-4)$$

Cooling time from the equilibrium temperature for a given temperature drop  $\Delta T$  is given by

$$\tau = \frac{k t c}{\alpha \epsilon} \left( \frac{1}{(T_i - \Delta T)^3} - \frac{1}{(T_i)^3} \right) \quad (A-5)$$

Figure A-1 shows the computer program listing to obtain the data in Fig. A-2.

Figure A-2 gives cooling time in minutes for a given temperature drop (DELTAT) as a function of  $\alpha$  and  $\epsilon$  from the upper equilibrium temperature. The equilibrium temperature is listed in degrees rankine below each time listing. The curve shape noted in the final plot (Fig. 14) is explained as follows:

## Curve Shape Determination

Equation (A-5)

$$\tau = \frac{K_{ptc}}{\sigma e} \left( \frac{1}{(T_i - \Delta T)^3} - \frac{1}{(T_i)^3} \right)$$

Where

$$T_i = \frac{\alpha}{e} \left( \frac{SA_p}{\sigma A_t} \right)^{\frac{1}{3}}$$

For any given  $\alpha$ ,  $T_i$  is a constant "B"

The term outside the paren in (A-5) is constant "A"

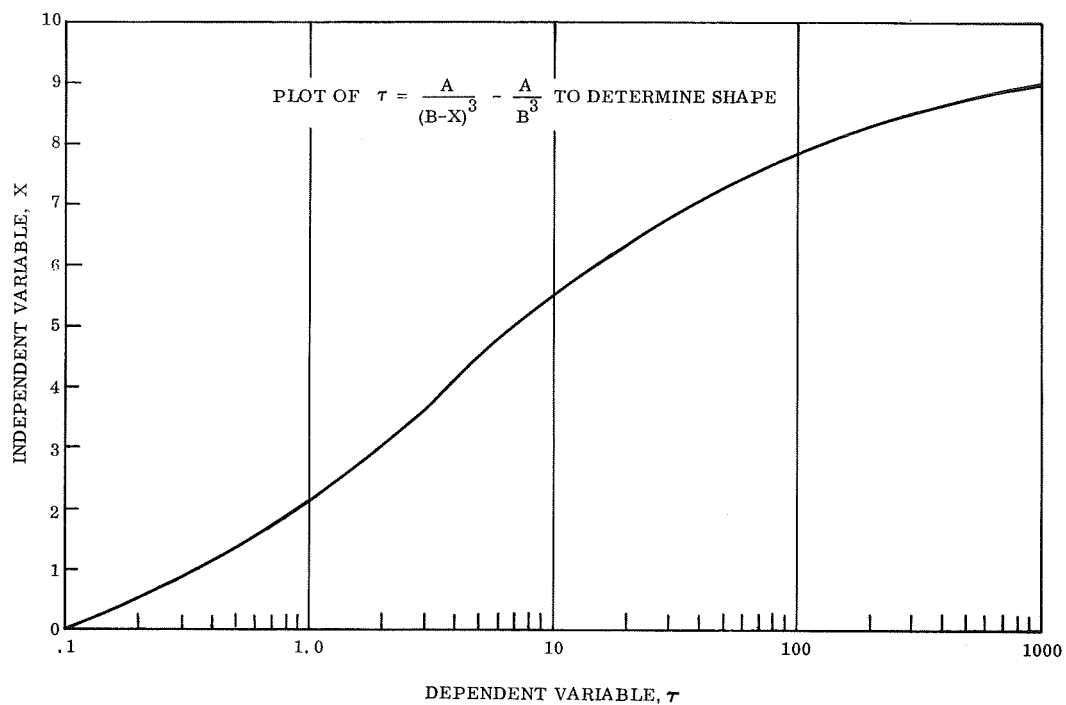
$$\therefore \tau = \frac{A}{(B - x)^3} - \frac{A}{B^3}$$

Letting constant  $\left. \begin{array}{l} A = 1000 \\ B = 10 \end{array} \right\} \text{Arbitrary Choice}$

and plotting:

X	B - x	$(B - x)^3$	$\frac{\Delta}{(B - x)^3}$	$\tau$
0	10	1000	1	0
1	9	729	1.38	.38
2	8	512	1.96	.96
3	7	343	2.92	1.92
4	6	216	4.64	3.64
5	5	125	8.00	7.00
6	4	64	15.6	14.6
7	3	27	37.0	36.0
8	2	8	125	124
9	1	1	1000	999

A plot of  $x$  vs  $\tau$  confirms the curve shape related to Equation A-5 :



For valid results in the equation

$$\frac{1}{(B - x)^3} > \frac{1}{B^3} \quad \text{For positive } \tau$$

or  $x$  must be +

Also  $B > X$  which is to say  $T_i > \Delta T$

This is obvious since the temperature drop cannot be larger than the initial temperature (can't drop below absolute zero).

```

1.  C    IDEAL RADIATIVE COOLING TIME CALCULATIONS FOR BIMETAL COIL VS.
2.  C    THERMAL COATING PROPERTIES
3.  C    NOTATION TAU=TIME, MINUTES THICK=STOCK THICKNESS, INCHES ABSOR=
4.  C    ABSORBTIVITY EMISS=EMISSIVITY AREAR=AREA RATIO (PROJECTED TO
5.  C    TOTAL)
6.  DIMENSION THICK(20), EMISS(20), ABSOR(20), DELTAT(20), TAUC(20), TE(20)
7.  TEQUIB (AB, SOLAR, EM, SIGMA, AREAR) = (AB/EM*SOLAR/SIGMA*AREAR)**.25
8.  SOLAR = 444.
9.  AREAR = .319
10. SIGMA = 1.714 E -9
11. RHO = .28
12. CP = .12
13. F = 2880.
14. DATA IMAX, JMAX, KMAX, LMAX/5, 11, 11, 11/
15. 4     FORMAT (17X, 11F10, 3)
16. 5     FORMAT (1X, 6HEMISS=, F4.2, 6X, 11F10, 3)
17. 6     FORMAT (10X, 7HABSOR=, 11F10, 3//)
18. 7     FORMAT (1X, 3X, 7HDELTAT=, F5.1)
19. 99    FORMAT (10X, 11F6, 4)
20. 98    FORMAT (10X, 11F5, 0)
21. 8     FORMAT(1H1, 6HTHICK=, F4, 3)
22. READ(5, 99) (THICK(I), I=1, IMAX)
23. READ(5, 99) (ABSOR(L), L=1, LMAX)
24. READ(5, 99) (EMISS(K), K=1, KMAX)
25. READ(5, 98) (DELTAT(J), J=1, JMAX)
26. DO 11 I=1, IMAX
27. WRITE (6, 8) THICK(I)
28. DO 22 J=1, JMAX
29. WRITE (6, 7) DELTAT(J)
30. WRITE (6, 6) (ABSOR(L), L=1, LMAX)
31. DO 33 K=1, KMAX
32. DO 44 L=1, LMAX
33. AB=ABSOR(L)
34. EM=EMISS(K)
35. FACTOR = F/SIGMA*RHO/EMISS(K)*THICK(I) *CP
36. TAU=((1./((TEQUIB(AB, SOLAR, EM, SIGMA, AREAR)-DELTAT(J))**3)-(1./TEQUI
37. B(AB, SOLAR, EM, SIGMA, AREAR)**3))*FACTOR
38. TAUC(L)=TAU
39. TE(L)=TEQUIB(AB, SOLAR, EM, SIGMA, AREAR)
40. 44    CONTINUE
41. WRITE (6, 5) EMISS(K), (TAUC(L), L=1, LMAX)
42. WRITE (6, 4) (TE(L), L=1, LMAX)
43. 33    CONTINUE
44. 22    CONTINUE
45. 11    CONTINUE
46. END

```

END OF LISTING.      0 \*DIAGNOSTIC\* MESSAGE(S).

Fig. A-1 Coil Cooling Time Program





THICK=.015  
DELTA= 25.0  
ABSOR=,

EMISS= .05	16.926	8.331	4.111	2.723	2.033	1.622	1.348	1.153	1.007	.894	1.000
EMISS= .10	536.155	637.600	758.238	839.129	901.702	953.434	997.898	1037.105	1072.311	1104.355	1133.831
EMISS= .20	17.249	8.463	4.165	2.755	2.056	1.638	1.361	1.164	1.017	.902	.811
EMISS= .30	450.851	536.155	637.600	705.620	758.238	801.739	839.129	872.098	901.702	928.648	953.434
EMISS= .40	17.647	8.624	4.231	2.794	2.083	1.659	1.377	1.177	1.028	.912	.819
EMISS= .50	379.119	450.851	536.155	593.353	637.600	674.180	705.620	733.344	758.238	780.897	801.739
EMISS= .60	17.922	8.736	4.277	2.821	2.101	1.673	1.388	1.186	1.035	.918	.825
EMISS= .70	342.573	407.390	484.471	536.155	576.136	609.190	637.600	662.651	685.146	705.620	724.453
EMISS= .80	18.140	8.823	4.312	2.842	2.116	1.683	1.397	1.193	1.041	.923	.829
EMISS= .90	318.800	379.119	450.851	498.949	536.155	566.915	593.353	616.666	637.600	656.654	674.180
EMISS=1.00	18.323	8.897	4.342	2.860	2.128	1.693	1.404	1.199	1.046	.928	.833
	301.502	358.549	426.389	471.877	507.064	536.155	561.159	583.207	603.005	621.025	637.600
	18.484	8.961	4.368	2.875	2.138	1.700	1.410	1.204	1.051	.931	.836
	288.068	342.573	407.390	450.851	484.471	512.266	536.155	557.221	576.136	593.353	609.190
	18.627	9.018	4.391	2.888	2.148	1.707	1.416	1.209	1.054	.935	.839
	277.178	329.622	391.989	433.807	466.156	492.900	515.886	536.155	554.356	570.922	586.160
	18.757	9.070	4.412	2.901	2.156	1.714	1.421	1.213	1.058	.938	.842
	268.078	318.800	379.119	419.564	450.851	476.717	498.949	518.552	536.155	552.178	566.915
	18.876	9.118	4.431	2.912	2.164	1.720	1.426	1.217	1.061	.940	.844
	260.299	309.549	368.118	407.390	437.769	462.884	484.471	503.506	520.598	536.155	550.465
	18.988	9.162	4.449	2.922	2.171	1.725	1.430	1.220	1.064	.943	.846
	253.532	301.502	358.549	396.799	426.389	450.851	471.877	490.417	507.064	522.217	536.155
DELTA= 50.0 ABSOR=,	.050	.100	.200	.300	.400	.500	.600	.700	.800	.900	1.000

EMISS= .05	37.514	18.140	8.823	5.801	4.312	3.428	2.842	2.426	2.116	1.875	1.683
EMISS= .10	536.155	637.600	758.238	839.129	901.702	953.434	997.898	1037.105	1072.311	1104.355	1133.831
EMISS= .20	39.072	18.757	9.070	5.946	4.412	3.502	2.901	2.474	2.156	1.910	1.714
EMISS= .30	450.851	536.155	637.600	705.620	758.238	801.739	839.129	872.098	901.702	928.648	953.434
EMISS= .40	41.068	19.536	9.378	6.126	4.535	3.594	2.973	2.533	2.206	1.953	1.751
EMISS= .50	379.119	450.851	536.155	593.353	637.600	674.180	705.620	733.344	758.238	780.897	801.739
EMISS= .60	42.502	20.089	9.595	6.252	4.621	3.658	3.023	2.574	2.240	1.982	1.777
EMISS= .70	342.573	407.390	484.471	536.155	576.136	609.190	637.600	662.651	685.146	705.620	724.453
EMISS= .80	43.667	20.534	9.768	6.353	4.689	3.709	3.063	2.607	2.268	2.005	1.797
EMISS= .90	318.800	379.119	450.851	498.949	536.155	566.915	593.353	616.666	637.600	656.654	674.180
EMISS=1.00	44.670	20.915	9.915	6.438	4.747	3.751	3.097	2.634	2.290	2.025	1.814
	301.502	358.549	426.389	471.877	507.064	536.155	561.159	583.207	603.005	621.025	637.600
	45.562	21.251	10.044	6.512	4.797	3.789	3.126	2.658	2.310	2.042	1.829
	288.068	342.573	407.390	450.851	484.471	512.266	536.155	557.221	576.136	593.353	609.190
	46.373	21.555	10.161	6.579	4.843	3.822	3.152	2.680	2.328	2.057	1.842
	277.178	329.622	391.989	433.807	466.156	492.900	515.886	536.155	554.356	570.922	586.160
	47.121	21.833	10.267	6.640	4.884	3.853	3.176	2.699	2.345	2.071	1.854
	268.078	318.800	379.119	419.564	450.851	476.717	498.949	518.552	536.155	552.178	566.915
	47.819	22.092	10.365	6.696	4.922	3.881	3.198	2.717	2.360	2.084	1.865
	260.299	309.549	368.118	407.390	437.769	462.884	484.471	503.506	520.598	536.155	550.465
	48.476	22.335	10.457	6.749	4.958	3.907	3.219	2.733	2.373	2.096	1.876
	253.532	301.502	358.549	396.799	426.389	450.851	471.877	490.417	507.064	522.217	536.155
DELTA= 75.0 ABSOR=,	.050	.100	.200	.300	.400	.500	.600	.700	.800	.900	1.000

EMISS= .05

62.810

14.251

9.296

5.445

4.502

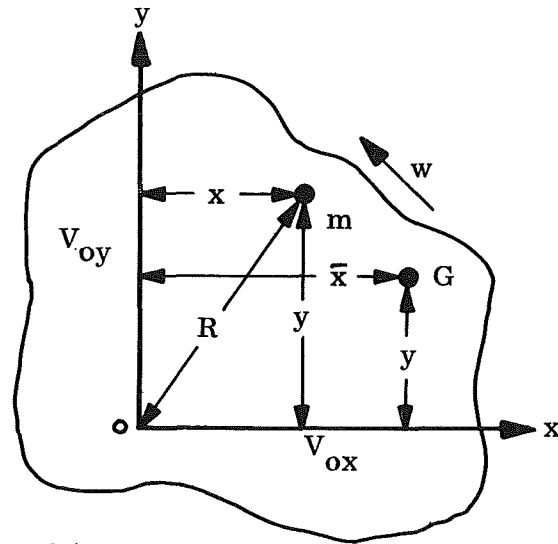
3.338

2.954

2.648

Fig. A-2 Cooling Time Printout

Appendix B  
ROTATIONAL INERTIA NOMENCLATURE



- R = distance O to m
- w = angular velocity
- G = center of mass
- m = particle of mass
- v = velocity of m
- O = reference point
- x = distance to m along x axis
- y = distance to m along y axis
- $\bar{x}$  = distance to G along x axis
- $\bar{y}$  = distance to G along y axis
- $\bar{I}$  = moment of inertia about G
- M = total mass

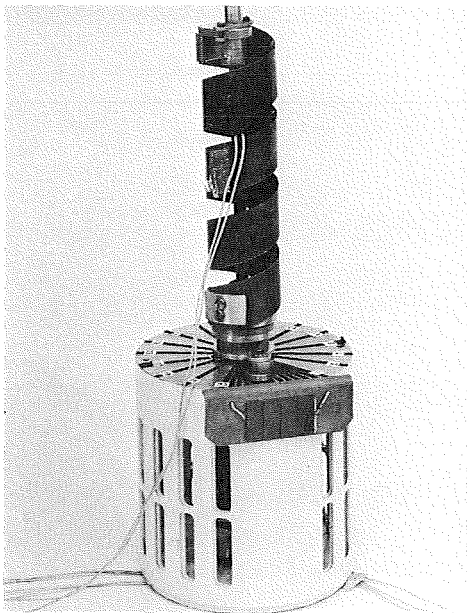
$$H_O = \sum m R^2 w + \sum m V_{oy} X - \sum m V_{ox} y$$

and with the definition of moment of inertia about O.

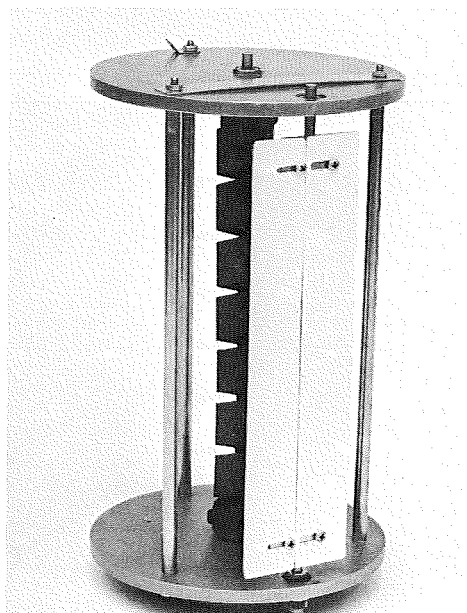
$$H_O = I_O w + \bar{x} M V_{oy} - \bar{y} M V_{ox}$$

Appendix C

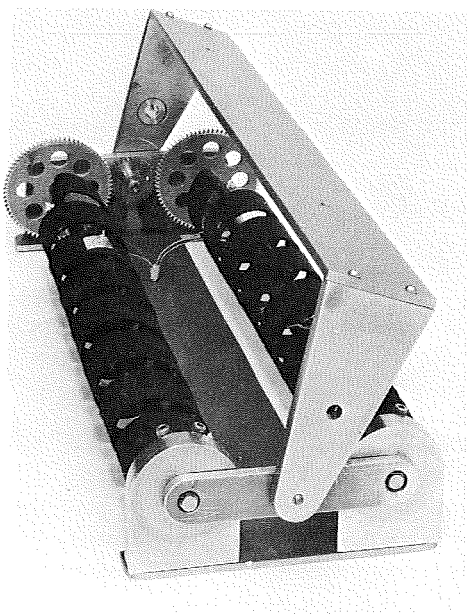
THERMAL HELIOTROPE DEVICES DEVELOPED UNDER NAS 5-11637  
(OPERATIONAL TEST MODELS)



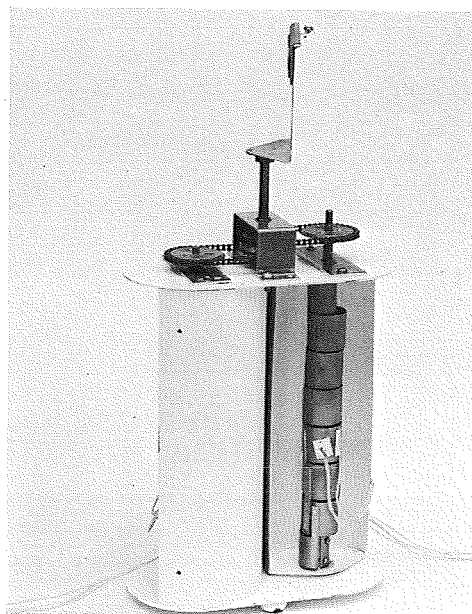
Stored Energy Device



Planetary Shade Tracker



Seasonal Adjuster



Two-Coil Continuous Tracker